# Impact of Exhaust Gas Recirculation on NOx emissions in non-premixed combusted Gas Turbines using CRN

Abdulrahman Dastagir

Technische Universiteit Delft

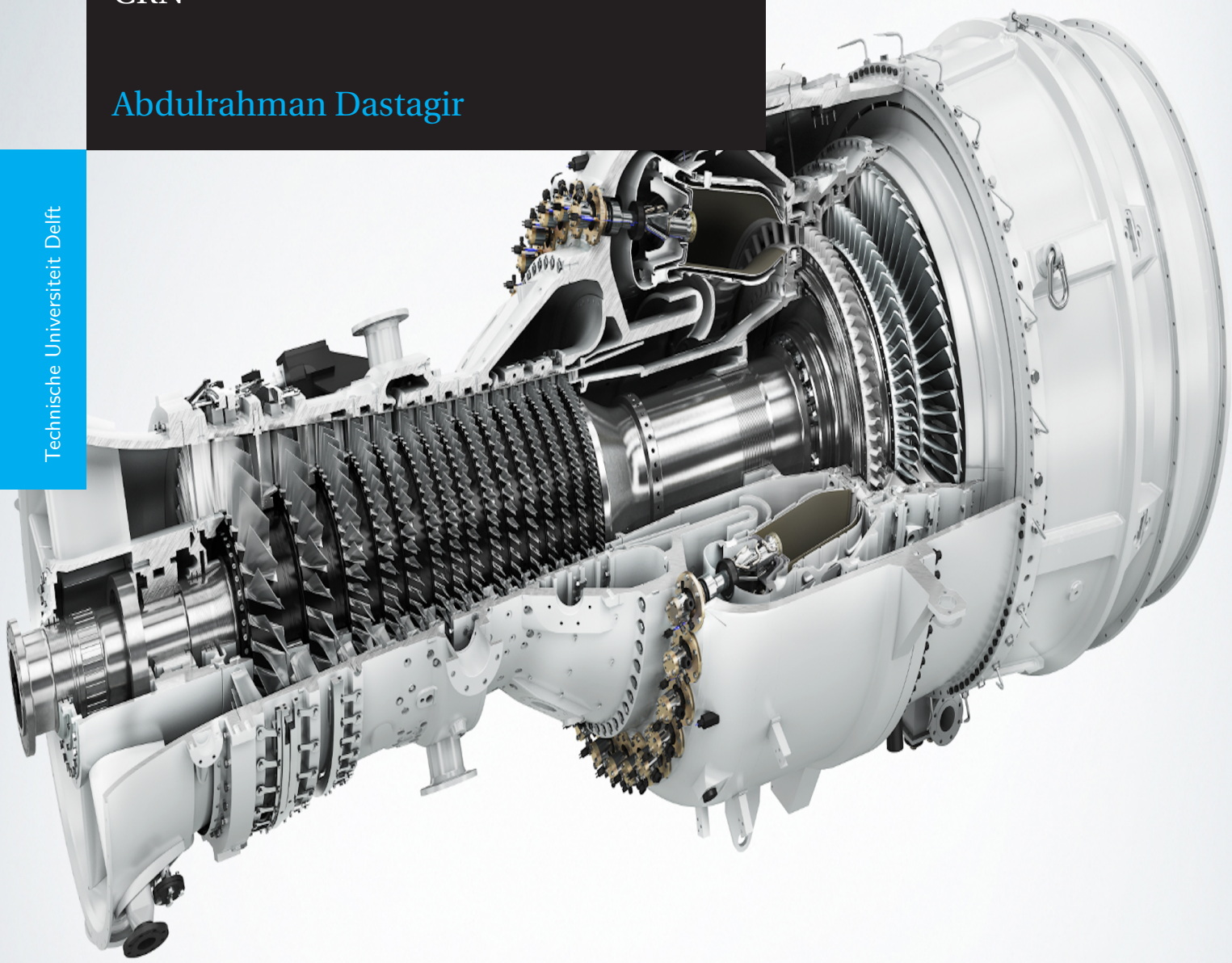

TU Delft Delft University of Technology

Challenge the future

# Impact of Exhaust Gas Recirculation on NOx emissions in non-premixed combusted Gas Turbines using CRN

by

**Abdulrahman Dastagir**

in partial fulfillment of the requirements for the degree of

**Master of Science**
in Mechanical Engineering

at the Delft University of Technology,
to be defended publicly on Friday September 28th, 2018 at 13.30.

| | | |
|---|---|---|
| Chairman: | Prof. Dr. Ir. S. A. Klein, | TU Delft |
| Thesis committee: | Prof. Dr. Ir. D. J. E. M. Roekaerts, | TU Delft |
| | Prof. Dr. Ir. B. J. Boersma, | TU Delft |
| | Dr. Ir. J. S. Steimes, | TU Delft |

*This thesis is confidential and cannot be made public until September 28th, 2018.*



TU Delft Delft University of Technology

# Acknowledgment

This thesis research has been quite a journey which tested my mind, knowledge and skills. This research pushed me beyond my limits which I'm really proud of. I'd like to give my gratitude and appreciation to my thesis supervisor Prof. Dr. Ir. S.A. Klein for his advise, thoughts, guidance, and encouragement throughout this project. His enthusiasm and his faith in me inspired me and gave me zest to achieve my goals. I'd also like to thank Dr. Ir. J.S. Steimes for helping me throughout this research with his ideas and support.

I would like to thank God for keeping my mind and health in the best condition to complete this research. I'd like to thank my mother Mrs. Naseem Dastagir for her prayers and always telling me that I can complete anything if I put my mind to it. I'd like to thank my siblings Mr. Mohammed Faisal Dastagir and Ms. Fauziya Dastagir for their continuous support and cheering me on whenever I felt low during this course. I'd not be able to complete this thesis without the final support of my friend Mr.Vickram Srinivas. I want to extend my heartfelt appreciation to my friends and classmates who have helped me to understand concepts and give their own input in my research even when they were busy with their own.

This thesis and this master's journey in Netherlands wouldn't have come together completely without the love and support of my girlfriend Ms. Nquan Johsnon. She kept it together for both of us and supported me every step of the way. She endured all the long hours of technical and research talks even when it was nothing close to her domain of study. With her help and love, I was able to successfuly complete my studies and my thesis work. This thesis wouldn't be mine without the input and help from everyone.

# Abstract

The major challenges in the world today is to reduce pollutant emissions from gas turbines while still being able to retain the maximum efficiency in the gas turbine. Especially due to stringent norms on emissions, the research on gas turbines have increased to reduce NOx levels. Most of the gas turbines have been using non-premixed combustion for power generation and since the early 90s research on premixed combustion was sought after. Aircraft engines and many other CHP power plants still currently use non-premixed combustion. Even though there have been a lot of technologies and researches on facilitating gas turbines with premixed combustion, there are still gas turbines that use non-premixed combustion. Changing the combustors to accommodate premixed combustion would require a lot of investment and would drive a steep loss especially when the gas turbine has not even reached half of it's life cycle. So, research has been undertaken to find means and ways to improve the existing technology with some upgrades to improve the NOx emissions levels. Exhaust gas recirculation (EGR) was one of the major part load operations in a gas turbine which was determined to improve part load efficiency and at the same time reduce NOx emission levels.

This thesis research would give an overview on how to model non-premixed combustion in a gas turbine and how different parameters effect NOx emissions. The model was made using a chemical reactor network with cantera which was loaded with a GRI-mech 3.0 mechanism. The two main reactors that were used are perfectly stirred reactor(PSR) and a plug flow reactor(PFR). The combustor volume was divided equally between perfectly stirred reactor and plug flow reactor. The half of the combustor where the mixing between the fuel and oxidizer and the combustion reactions occur are modelled by three perfectly stirred reactors which contain flame sheet reactor (FSR), post-flame PSR and PSR recirculation. The volume of FSR was determined by modelling the stoichiometric mixture fraction. This is done by determining the scalar dissipation rate which tells the rate of mixing between the fuel and oxidizer at the stoichiometric interface. Understanding mixture fraction gradients when fuel and oxidizer intensively mix when they come in contact with each other inside the combustion chamber can assist in calculating the scalar dissipation rate. The model uses the amount of oxidizer required for stoichiometry combustion at FSR and the rest of the oxidizer is equally divided between the two PSRs with a feedback loop between post-flame PSR and PSR recirculation. This was done to accommodate the swirl function which diffuses the incoming fuel and oxidizer, thus creating the recirculation flame zone. The model was then validated using different technical studies on non-premixed combustion. The model validated an industrial furnace and also cases which utilized gas turbine combustors.

Parametric analysis was performed with this model using EGR as oxidizer and compared with results that were obtained when using air as oxidizer. It was seen that thermal NOx which was the most amount of NOx released during the combustion was reduced when EGR was used as an oxidizer. It was thus proved that replacing oxygen with carbon dioxide led to a reduction of NOx but maintained a favourable turbine inlet temperature. It was also found that the CO levels were increased when using EGR but still remained below the level when air was used as an oxidizer. This was due to insufficient residence time inside the combustor. When using EGR as a part load operation and at high pressures in gas turbine, the NOx emissions were lower. The results from the pressure analysis showed that at lower pressures the amount of NOx that was reduced was more when using EGR, but at high pressures the amount of NOx that was reduced was quite less even though it was EGR-oxydizer compositon. It was observed that the NOx and CO levels were still lower while using EGR compared to using inlet guide vanes as a part load operation(IGV). While using a fuel mixture of $H_2$ and natural gas, it appeared that the NOx levels were higher with EGR and air as an oxidizer than just using only natural gas as fuel. At the same time CO emission levels showed that it was low for both EGR and air when fuel mixture of $H_2$ and natural gas was used.

**Keywords:** Gas turbine, NOx, CO, exhaust gas recirculation, flame sheet reactor, mixture fraction, scalar dissipation rate, air, stoichiometry.

# Contents

# List of Figures

# List of Tables

# List of symbols

**GREEK LETTERS**

$\tau_{chemical}$ - Chemical time scale (sec)
$\rho$ - Density (kg/m$^3$)
$\delta(x)$ - Dirac delta function
$\nu_{turb}$ - Eddy viscosity
$\phi$ - Equivalence ratio
$\nabla$ - Gradient
$\delta_{99\%}$ - Half-width of the jet
$\tau_{mixing}$ - Mixing time (sec)
$\tau_{res}$ - Residence time (sec)
$\chi$ - Scalar dissipation rate (s$^{-1}$)
$\omega$ - Source term
$\nu_i$ - Stoichiometric co-efficient of species 'i'
$\eta_{th}$ - Thermal efficiency of a gas turbine
$\epsilon$ - Turbulent diffusion rate (m$^2$/sec$^3$)

**PARAMETERS**

D - Diffusion co-efficient/Diffusivity rate (m$^2$/sec)
H - Enthalpy (kJ/kg)
g - Gravitational acceleration (m/sec$^2$)
$L_F$ - Length of the flame (metres)
Y - Mass fraction
$\dot{m}_F$ - Mass flow rate of fuel (kg/sec)
$\dot{m}_O$ - Mass flow rate of oxidizer (kg/sec)
$m_i$ - Mass of all molecules of species 'i'
Z - Mixture Fraction
$W_i$ - Molecular weight of species 'i'
$F_{st}$ - Stoichiometric Fuel/Air ratio
u - Velocity (m/sec)
P - Power (Watts)
p - Pressure (bar)
R - Radius (metres)
Cp - Specific heat capacity (J/(kg.K))
T - Temperature (Kelvin)
k - Turbulent kinetic energy
V - Volume (m$^3$)

**ABBREVIATIONS**

ad - Adiabatic
B.C - Boundary condition
$CO_2$ - Carbon dioxide
CO - Carbon monoxide
CRN - Chemical reactor network
EGR - Exhaust gas recirculation
Fr - Froude number
FSR - Flame Sheet Reactor

F - Fuel
in - Inlet
IGV - Inlet guide vane
$LHV_F$ - Lower heating value of fuel
$CH_4$ - Methane
MW - Molecular weight
NG - Natural gas
$N_2$ or 'N' - Nitrogen
NOx - Nitrogen oxides
NO - Nitric oxide
$NO_2$- Nitrogen dioxide
out - Outlet
O - Oxidizer
$O_2$ or 'O' - Oxygen
PSR - Perfectly stirred reactor
PFR - Plug flow reactor
st - Stoichiometric
(i.e.) - That is
TiT - Turbine inlet temperature
turb - Turbulent

# 1

# Introduction

One of the reasons that there has been a steep increase in the level of technology especially in the past century is due to the need for humans to have a better life and also an adventure of curiosity. The advancement of technology has been always there to make lives of humans easier and better. In the modern world today, the need of advancement grows hand in hand with the rapid growth of technology. As this need increases there are also constraints determined by the government on the amount of pollutant levels that can be produced. This is done so that we don't achieve this technology growth in the cost of the future of this world.

As research and development moves in the path of effectively using renewable sources of energy, there are still researches conducted to reduce pollution caused by non-renewable sources of energy. The government enforces severe laws to force the industries to reduce the emission levels. In order to make sure that the emissions are kept below the required level can be a difficult task to implement. By just changing a component in a lean manufacturing industry, it takes a lot of investment from the company to bring the emissions lower than the expected level. There has always been a fine line between achieving high power generating efficiency and producing low pollutant emissions. So, there has been a lot of research on improving the system to reduce the high pollution levels and at the same time also retaining it's maximum efficiency.

The world's demand for energy has increased tenfold due to the increase in the world population in the past few decades. Figure 1.1 shows the demand for energy between Organisation for Economic Co-operation and Devlopment (OECD) countries and non-OECD countries. It has been foretold by the International energy Outlook that the world's energy consumption will increase by 56% between 2010 to 2040 (i.e.) from 153 quadrillion Watt hour to 240 quadrillion Watt hour [1].

## 1.1. Environmental impact due to emissions

Due to the rapid growth of technology and demand of energy, there has been a global warming wall struck by the world population and the technology industry. Global warming is a serious concern in modern times, as there has been a noticeable shift in the climate change. One of the main reasons behind climate change is due to an increase in what is called the greenhouse effect. Figure 1.2 gives an outlook of how the greenhouse effect works. The steady increase in greenhouse gases such as oxides of nitrogen, methane, and carbon dioxide is due to the advancement in technology. This caused less amount of infrared rays to pass through the atmosphere into space due to the presence of more amount of greenhouse gases. Most of it is reflected back to the earth's surface heating up the surface above it's nominal temperature. This heat is trapped in the earth's surface making it warmer than the required temperature for the earth to sustain itself. This change in earth's temperature leads to other undesired outcomes such as climate change.

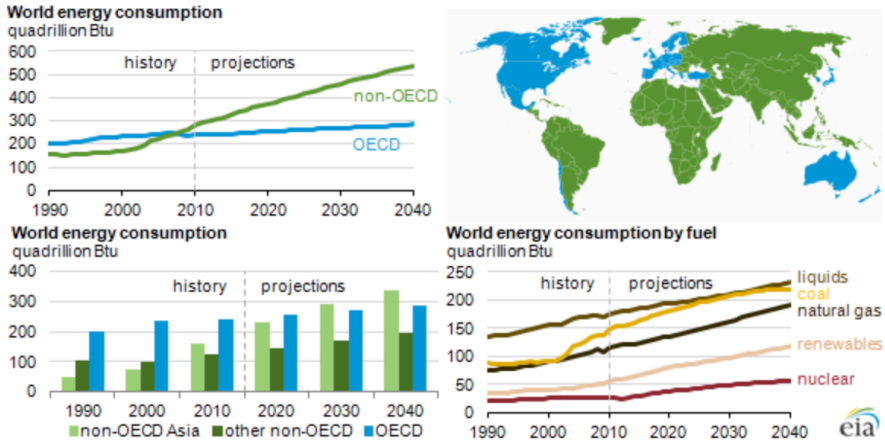


Figure 1.1: World energy consumption [1]

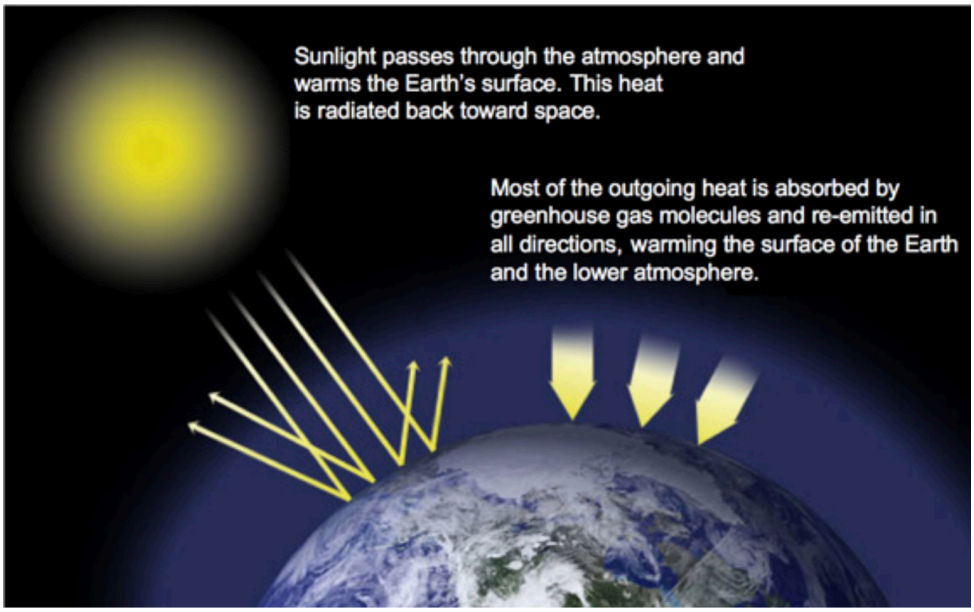


Figure 1.2: Green house gases attracting the sun's radiation, Source:[NASA]

The major two greenhouse gases $CO_2$ and NOx are emitted by gas turbines. Apart from these gases, there are other harmful pollutant emissions that are caused by gas turbines. Table 1.1 describes the harmful effects of the polluted gases which are emitted by our global industries. A group of 1,300 independent scientific experts from countries all over the world under the United Nations, the Intergovernmental Panel on Climate Change, in it's Fifth Assessment Report concluded there's a more than 95 percent probability that human activities over the past 50 years have warmed our planet [29].

From this it was clear that changes had to be done to make sure there is a continued survival of every species. Leading up to this the Paris agreement was forged in 2015 by countries from all over the world. They came to an agreement of intensively reducing carbon emissions for a sustainable future. The agreement's long term goal is to keep the increase in global average temperature to well below 2°C above pre-industrial levels; and to limit the increase to 1.5°C, since this would substantially reduce the risks and effects of climate change [30]. There was a directive that was created due to this paris accord showcasing the maximum emission limiting value that an existing medium combustion plant( 1 MWth to 50 MWth) can emit [31]. For gas turbines, the number to limit NOx emissions were from 150 to 200 mg/Nm$^3$. This limitation for existing plants operating below 5 MW should be implemented by 1st January 2025 and plants operating above 5 MW by 1st January 2030 [31].

Table 1.1: Harmful effects of the pollutants caused by gas turbines

| Pollutant | Impact on health and environment |
|---|---|
| **Greenhouse effect causing pollutants** | |
| Carbon dioxide ($CO_2$) | Causes an increase in greenhouse effect<br>Increases the pH levels of the ocean making it more acidic |
| Nitrogen oxides (NOx) | Causes acid rain by forming $HNO_3$<br>Photochemical smog, greenhouse gas causing climate change |
| **Other pollutants** | |
| Carbon monoxide (CO) | Toxic gas<br>Reduced capacity of $O_2$ absorption by blood |
| Unburnt hydrocarbons (UHC) | Toxic in nature<br>Combines with NOx to form photochemical smog |
| Sulphur oxides (SOx) | Toxic and corrosive gas<br>Acid rain forming reactant |
| Soot/Smoke | Poor visibility<br>Allergy, Asmathic problems, Nausea |

## 1.2. Gas Turbines

Gas turbines have been the pinacle of thermal machinery development since the late eighteenth century. Gas turbines have actively been researched upon and developed since the 1930s/40s. A thermal machine which could convert the energy released from combusting a fuel into useful work. This developing technology is setting the world standard in two major industrial applications in the mobility sector(Eg:Jet engines) and the electric power generation business(Eg:combined cycle power plants)[2]. Figure 1.3 shows the application of gas turbines at various sectors and how useful gas turbines are in the modern industries. Gas turbines find applications in diverse variety of different sectors. Micro gas turbines are used for combined heat and power plants which give out about 50-250kW and for heavy applications, CHP gas turbines find a wide application in the industries providing power ranging from 50 kW to 150 MW.

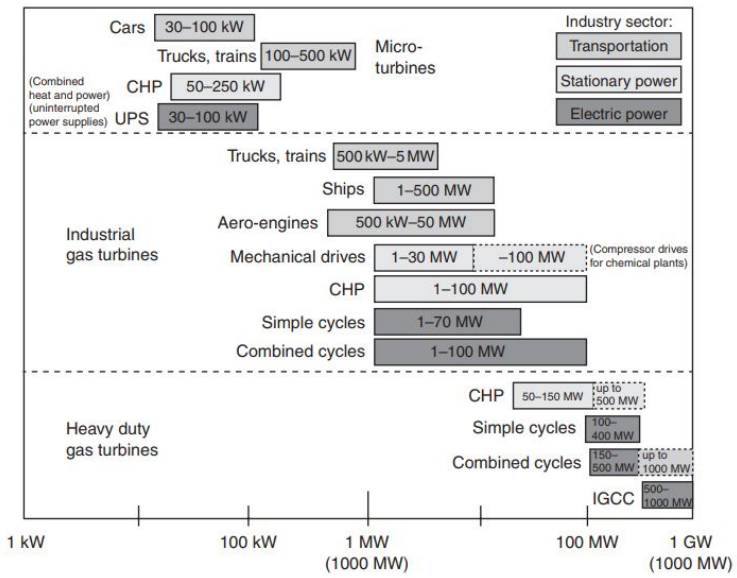


Figure 1.3: Gas turbine application vs power output [2]

### 1.2.1. Part load operations

Gas turbines have always been operated in full load in the past few decades. Since, the increase in the use of renewable sources for energy, gas turbines have been commissioned to operate on part loads due to less demand in power and also due to economical reasons. However, while using gas turbines in part load operations, the efficiency of the gas turbine reduces as well due to the reduction in the flame temperature. Figure 1.4 shows the change in load vs efficiency for gas turbines.

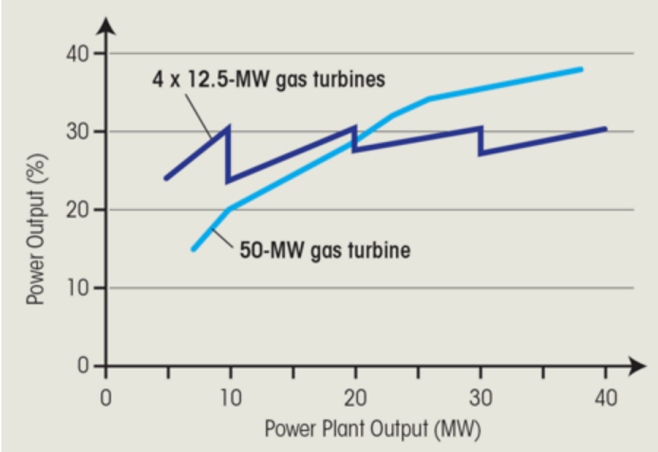


Figure 1.4: Efficiency vs load comparison for a 50MW gas turbine(light blue line) and four 12.5MW gas turbines(dark blue line) in open cycle at 40°C ambient temperature [3]

### 1.2.2. Exhaust Gas Recirculation

Exhaust gas recirculation is an innovative technique in part load operation, especially assisting in reducing NOx emissions. A portion of the combusted exhaust gas is recirculated back to the inlet of the compressor. This is done to dilute oxygen in the incoming air stream and convert the gases to be inert to combustion and act as absorbents of combustion heat. This also increases the specific heat capacity(increasing the $CO_2$% content) and thus lowering the flame temperature (reducing NOx levels). Figure 1.5 illustrates a basic layout of EGR for a gas turbine CHP plant.

Steimes, Klein and Persico [4] mentioned in their paper that EGR has a potential in reducing emissions and enabling efficient part load operation in gas turbines. Especially when compared to traditional techniques such as Inlet guide vanes (IGV), decreasing Turbine inlet temperature, and compressor air recirculation. EGR goes through a heat exchanger to reduce the heat before supplying it to the combustor. If in case it stays uncooled, the inlet temperature of the gas turbine will rise resulting in a lower mass flow through the installation. Also lower power production at a higher efficiency due to stack losses reduction.

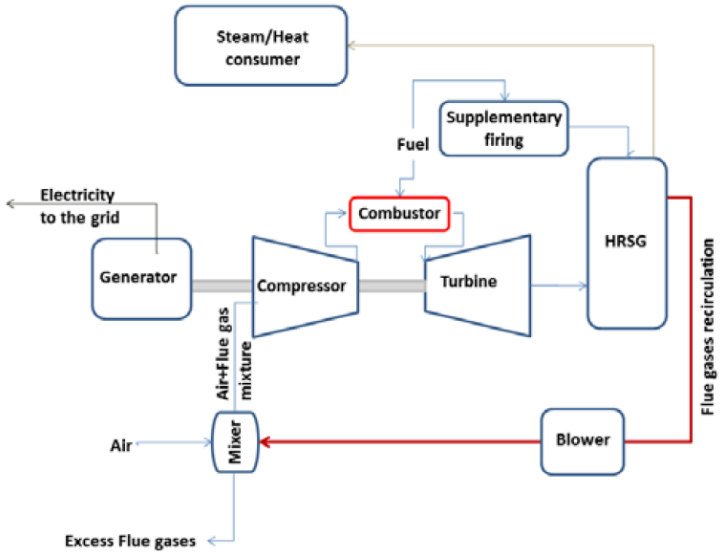


Figure 1.5: Flue Gas Recirculation for a gas turbine CHP plant [4]

## 1.3. Motivation of the thesis

Before widespread research into premixed combustion started in the 1990s effectively, all gas turbines were using non-premixed combustion. Non-premixed combustion occurs in most of the gas turbines to produce power (aircraft engines, CHP power plants etc.) even today. Even though premixed combustion is the future solution in reducing the emission level, there are still many gas turbines in use in the industries which have a life expectancy of at least 30 years and combust under non-premixed combustion.

Modifying or upgrading the combustion chamber to accommodate premixed combustion in a gas turbine will result in a huge investment in the industry. This is the reason there has been continuing research on improving the gas turbine with non-premixed combustion on giving high thermal efficiency while reducing the emission levels too.

Understanding the characteristics of NOx especially when implementing EGR can result in an overview of how NOx or any other pollutants can be controlled by changing the input parameters. Due to the increase of the role of renewables, the burden of using gas turbines at different load operations to reduce the emission levels has been of such high priority. Exhaust gas recirculation can be a stepping stone to maintaining a higher turbine efficiency, while also increasing the $CO_2$ content which can result in effective carbon capture as well. A few of the factors that make EGR as an efficient technology to be used can be seen in Figure 1.6.

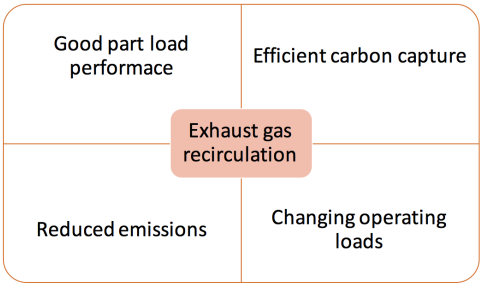


Figure 1.6: Factors of EGR that contribute to a growing technology.

## 1.4. Research questions and philosophy

Understanding the influence of exhaust gas recirculation (EGR) on the chemical mechanisms of NOx formation in a non-premixed combustion, can help in reducing those emissions in a gas turbine. Thus, to give a clear view of that, the following questions must be answered:

- **How can non-premixed combustion in a gas turbine be modelled using a Chemical Reactor Network?**
- **What are the emission(NOx and CO) characteristics in a non-premixed combustion in a gas turbine with Exhaust Gas Recirculation?**
- **How sensitive are the emissions (NOx and CO) to parameters such as amount of $CO_2$ in the oxidizer, pressure, blend of $H_2$ and natural gas?**

Unfolding answers to these questions can lead to a better understanding of how to control NOx emissions. A chemical reactor network can be modelled in such a way that the result gives an overview of the NOx emission characteristics. The objective of this research overall is to understand the impact of EGR (i.e.) if it is only a measure to improve part load efficiency of a gas turbine or that it can also reduce NOx emissions.

# 2

# Literature review

Combustion is a very broad and complex topic which requires extensive research and work to give a basic understanding. The basic theory of combustion relates to three major phenomena.

- Transport phenomena
- Thermodynamics
- Chemical kinetics

Number of experiments and research is performed to understand it's process and theory. Combustion can be described as most simply an exothermic reaction of a fuel and an oxidant. During combustion, many chemical reactions form the final products in a very short time. It is hard to segregate between the chemical reactions and understand the product formation. This lead to the creation of several chemical mechanisms to follow these combustion related kinetics.

## 2.1. Application of combustion in gas turbines

Combustion of fuels provides ample energy to be used as work in a thermodynamic cycle. Gas turbines are used to convert the energy that is produced from combustion into useful work like wide scale electricity generation. In gas turbine applications, the fuel may be gaseous or liquid, but the oxidant is always air. Figure 2.1 shows a typical gas turbine cycle. The incoming oxidizer is compressed by the compressor before it is combusted along with the fuel. The energy ouput is achieved by the expansion of these combusted products in the turbine. The combusted products are given to the turbine which converts to mechanical work and generates power.

Equation 2.1 expresses this thermal power output in terms of the amount of fuel and oxidizer that flows into the combustor. The exit temperature ($T_{out}$) is known as the turbine inlet temperature at constant specific heat capacity. The higher the turbine intlet temperature, the higher the power is generated and turbine thermal efficiency. As, will be explained later in this chapter(Section 2.7.1), higher the temperature more NOx emission is given out. So, it is always a balance between the power output and the impact to the environment due to emission. This combusted power output can be expressed as:

$$P = (\dot{m}_F + \dot{m}_O) * Cp_F * (T_{out} - T_{in}) \tag{2.1}$$

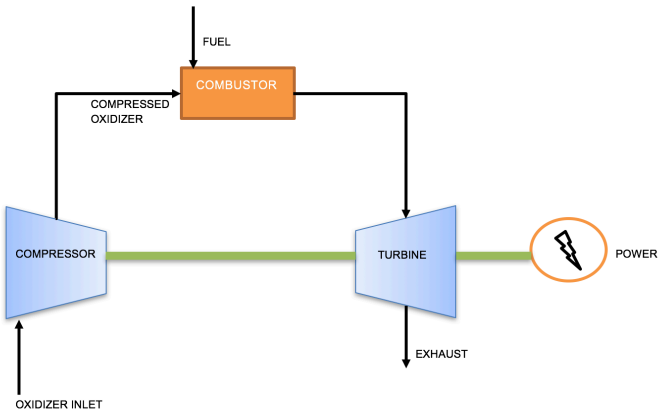


Figure 2.1: Gas turbine cycle

## 2.2. Types of combustion

Combustion occurs in many forms, not all of which are accompanied by flame or luminescence. This research studies non-premixed combustion in a gas turbine. Premixed and non-premixed are classification of flames in the most fundamental studies of flame combustion. They depend on whether the fuel and air are mixed before combustion, or mixed by diffusion in the flame zone. A brief overview on how these flames are represented in gas turbine can be seen in Figure 2.2

- **Premixed combustion:** In premixed combustion, fuel and oxidizer are mixed together before they enter the combustion chamber to be combusted. The major chemical transformation that occurs is primary in a thin interfacial region which separates the burned and the unburned gases. Once, the combustion is initiated the process is self sustained to form a sTable combustion.
- **Non-premixed combustion:** In non-premixed combustion, the fuel and oxidizer enter the combustion chamber separately and are then combusted. The fuel and oxidizer are mixed at molecular stoichiometric proportion inside the combustion chamber where the flame is formed at the stoichiometric interface.

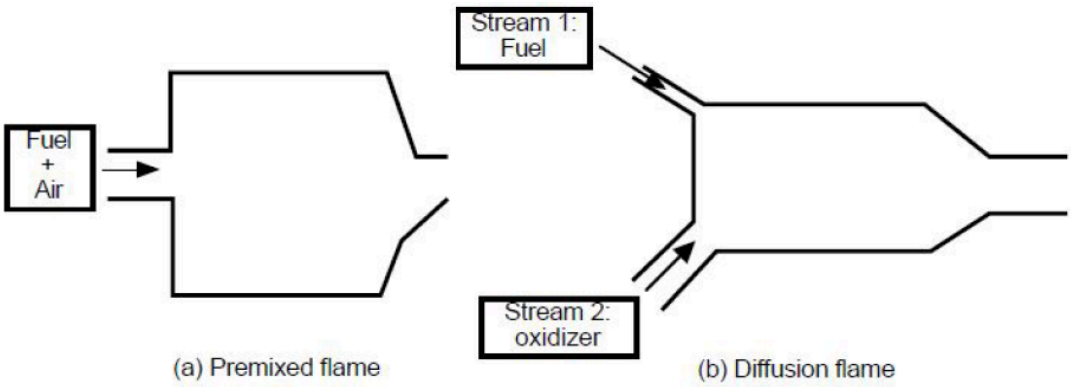


Figure 2.2: Representation of a premixed and a non-premixed combustion [5]

When the flame has been initiated at some point in the mixture (by means of a hot surface, an electric spark, or some other ignition source), it will propagate throughout the entire volume of combustible mixture. The speed at which it propagates and the factors affecting its rate of propagation are of special interest to the designer of practical combustion systems. Turbulence is of prime importance because most flowing fuel–air mixtures are turbulent and turbulence is known to enhance flame speeds considerably especially for non-premixed combustion [32]. For small diffusion flames, the rate of inter-diffusion of air and fuel is considered as the rate-controlling step. For large turbulent diffusion flames, the rate of large-scale mixing, are the rate-controlling steps [32].

## 2.3. Non-premixed combustion

Laminar flames in premixed systems, the chemical reaction rates can be rate controlling. In systems which employ non-premixed combustion, the fuel and oxidant come together in a reaction zone through molecular and turbulent diffusion[32]. The fuel can be in the form of a gaseous or a liquid(droplet) fuel. If both the fuel and the oxidant are initially gaseous, then the flame is referred to as a diffusion flame.

When the fuel and oxidizer come into play inside the combustion chamber, the chemical reactions between them occurs at a fast rate. This means that the chemical time scales are smaller or shorter than all the other flow-characteristic times (i.e.) chemical reactions occur faster than the diffusion and the flow time scales. This is also called the equilibrium assumption[5]. When the two streams come into the combustion chamber, the fuel and oxidizer mix at molecular level and wherever there is stoichiometric mixing, the structure of the flame is formed emitting the highest temperature. The mixing that takes place here is due to the convection and diffusion of the fuel and oxidizer species. There are two types of diffusion flame that can be understood co-flow diffusion flame and counter-flow diffusion flame:

### 2.3.1. Co-flow diffusion flame

The fuel and the oxidizer are supplied from the same side into the combustion chamber to mix at the ignition point and generate combustion. Upon combustion the flame can be curved depending on the stoichiometry of the the mixture and the co-efficient of reaction. Over here there is mostly species mixing and not momentum mixing. A simple example of this type of diffusion flame is the *bunsen burner*.

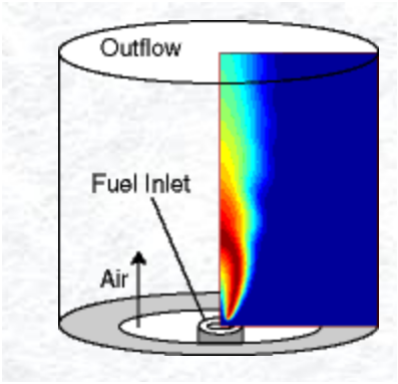


Figure 2.3: Co-flow diffusion flame, Source:[Center for computational sciences and engineering]

### 2.3.2. Counter flow diffusion flame

The fuel and oxidizer are supplied into the combustion chamber in opposite direction in different velocities. The resultant diffusion flame would be flat and the stagnation point will be created mostly in the middle of the combustion chamber to form a pure diffusion flame. An example for this type of diffusion flame can be seen Figure 2.4.

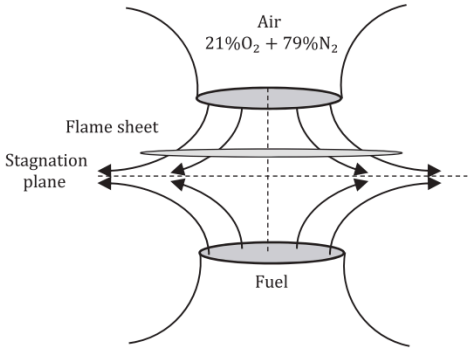


Figure 2.4: Counter flow diffusion flame [6]

## 2.4. Burke-Schumann flame solution

### 2.4.1. Burke-Schumann flame

Burke-Schumann anointed the term diffusion flame as a type of flame aroused due to non-premixed combustion. Burke-Schumann analyzed the theory of mechanism of diffusion flame due to non-premixed combustion. They were able to predict the flame shape and the flame height by using their analysis of infinite fast chemistry. This was done by considering two concentric pipes with the outer pipe having infinite length and the inner pipe is of semi-infinite length. The configuration of the experiment can be seen in Figure 2.5.

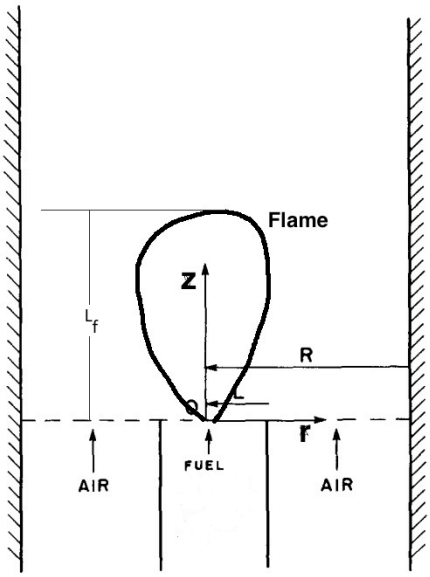


Figure 2.5: Configuration of diffusion flame formation [7]

When discussing about the species involved in the combustion, the species can either be fuel or the oxidizer. Flame shape depends on the axial convection of the species and also the radial diffusion of the species, whereas flame height can be determined from the flame shape by adapting the Schvab-Zeldovich formulation [8]. Burke-Schumann adopted the following assumptions [8] to solve the diffusion flame:

- The velocity of the incoming species is parallel to the duct's axis(z-direction) $U_z$=u$e_z$, and the velocity in the radial direction is ignored $U_r$=0.
- The mass flux in the axial direction is constant, $\rho u_F = \rho u_O$. Therefore there is no change in density, so the fuel and oxidizer are mixed with different diluents to achieve equal density.
- The effects of gravity is neglected.
- Diffusion in the axial direction is also negligible when compared to radial diffusion (i.e.) $\frac{\partial^2 y_i}{\partial z^2} << \frac{\partial^2 y_i}{\partial r^2}$, where $y_i$ is the mass fraction of the species. Axial diffusion can be assumed at low Peclet number and neglected at high Peclet number [8]. Peclet number is ratio of rate of advection to that of rate of diffusion. So, at higher Peclet numbers, advection dominates more than diffusion thus neglecting axial diffusion.
- The flame sheet assumption where this corresponds directly to infinite-rate chemistry or infinite kinetics or mixed-is-burnt approach.

By analyzing the Burke-Schumann flame approach, the mixture between fuel and oxidizer at the point of combustion can be understood.

### 2.4.2. Mixed-is-burnt approach

The flame sheet assumption means that the reactants react instantaneously when they mix in stoichiometric proportions. This means that there is going to be a contour where fuel and oxidizer are mixed. The flame is going to form a sheet that is coincident with the stoichiometric contour of the mixing field. We consider only the species conservation Equation of fuel and oxidizer(Schvab-Zeldovich formulation) given by the Equation:

$$\nabla.[(\rho\vec{u})Y_i - \rho D\nabla Y_i] = \omega_i \tag{2.2a}$$

$$\nu'_F F + \nu'_{O_2} O_2 -> \nu''_{CO_2} CO_2 + \nu''_{H_2O} H_2O \tag{2.2b}$$

where,

- $\rho$ is the density of the species.
- $\vec{u}$ is the velocity vector of the incoming species.
- $\omega_i$ is the chemical source term of species i which is determined from the reaction rate and Arrehenius law.
- D is the molecular diffusion co-efficient.
- *i* can either be oxidizer 'O' or fuel 'F'.
- $\nu_i$ is the stoichiometric co-efficient of fuel or oxidizer.
- $Y_i$ is the mass fraction of the species.

Since, Equation 2.2a is a single step reaction of $\nu_f F + \nu_o Ox$ =Products, so $\nu_i^{''} = 0$ and therefore the mass fraction of a species 'i' can be written as

$$Y_i = \frac{m_i}{W_i(\nu_i^{''} - \nu_i^{'})} = -\frac{m_i}{W_i \nu_i^{'}} \tag{2.3}$$

where, $m_i$ is the mass of all molecules of species 'i' and $W_i$ is the molecular weight of the species 'i'. Expressing Equation 2.2a in terms of Fuel 'F' and Oxidizer 'O', we get:

$$\nabla.[(\rho\vec{u})Y_F - \rho D\nabla Y_F] = \omega \tag{2.4a}$$

$$\nabla.[(\rho\vec{u})Y_O - \rho D\nabla Y_O] = \omega \tag{2.4b}$$

where, $\omega = \frac{\omega_i}{W_i(\nu_i^{'} - \nu_i^{''})}$.

Now, if we take a conserved scalar quantity which in this case mixture fraction Z = $Y_F$ - $Y_O$. Subtracting Equation 2.4b from 2.4a we can express it as one homogeneous linear Equation in terms of *Z*.

$$\nabla.[(\rho\vec{u})Z - \rho D\nabla Z] = 0 \tag{2.5}$$

These fundamental equations are used to understand the flame shape and height. Combustion is understood based on it's convection, diffusion and reactions. With the above equations the chemical reactions aren't considered and only convection and diffusion is considered making the combustion problem a bit easier to solve. Assuming cylindrical polar co-ordinates with $\vec{U} = u.\hat{e_z}$ and $\frac{\partial^2 Z}{\partial z^2} << \frac{\partial^2 Z}{\partial r^2}$, Equation 2.5 becomes

$$\frac{u}{D}\frac{\partial Z}{\partial z} = \frac{1}{r}\frac{\partial}{\partial r}(r\frac{\partial Z}{\partial r}) \tag{2.6}$$

Equation 2.6 is now the simplified governing Equation from which the mixture fraction is expressed in axial direction and as a laplacian of the ***r***-component in cylindrical polar co-ordinates. Now applying the boundary conditions to Equation 2.6. Second order of the mixture fraction with respect to r needs 2 B.Cs and the first order of the mixture fraction with respect to z needs 1 B.C. The domain has to be first realized before applying the B.Cs. From Figure 2.5 the domain chosen is from r=0 to R and from z=0 to ∞. The following are the boundary conditions that are realized with respect to the domain:

- For all z>0 and at r=0, $\frac{\partial Z}{\partial r} = 0$ which is the symmetry boundary condition. The partial derivative of the mixture fraction is indirectly the partial derivative of the mass fraction. The physical meaning of the partial derivatives of the mass fraction amounts to diffusion fluxes. From this boundary condition there are no diffusion across the centre line because of symmetry.
- For all z>0 and at r=R, $\frac{\partial Z}{\partial r} = 0$ which is the wall boundary condition. There is no diffusion or mass flux across the wall as there is only inviscid convective flow.

There are two Neumann B.Cs observed here. At z=0 which is at the lip of the burner, there should be another B.C. which can be a Dirichlet B.C to make the solution more unique.

- So, for z=0; $mixture\ \ fraction, Z = \begin{cases} -(\frac{m_F}{W_F\nu_F}) & 0 < r < L \\ (\frac{m_O}{W_O\nu_O}) & L < r < R \end{cases}$

From r=L to R, there is a jump in the mixture fraction, making it discontinuous. This is due to the mixing of the fuel and the oxidizer. As the mixture flows through the domain towards the positive z-direction, the discontinuities are smoothened out as a consequence of diffusion.

### 2.4.3. The Mixture Fraction Coordinate

The mixture fraction can be derived for a homogenoeus system without taking diffusion into account[8]. The global reaction Equation for the combustion of a hydrocarbon fuel is as follows:

$$\nu_F^{'}F + \nu_{O_2}^{'}O_2 -> \nu_{CO_2}^{''}CO_2 + \nu_{H_2O}^{''}H_2O \tag{2.7}$$

where, $\nu_F^{'}$ and $\nu_{O_2}^{'}$ are the stoichiometric coefficients. The reaction equation relates to each other the changes of mass fraction of oxygen $dY_{O_2}$ and fuel $dY_F$ by[8]:

$$\frac{dY_{O_2}}{\nu_{O_2}^{'}W_{O_2}} = \frac{dY_F}{\nu_F^{'}W_F} \tag{2.8}$$

where $W_i$ denotes the molecular weight of the species and the homogenoeus system of this equation may be integrated to:

$$\nu Y_F - Y_{O_2} = \nu Y_F - Y_{O_2} \tag{2.9}$$

The mass fractions $Y_F$ and $Y_{O_2}$ are the local mass fractions of fuel and oxygen respectively in the initial unburnt mixture.

Considering a two-feed system, the fuel stream which has a mass flux $\dot{m}_F$ and the oxidizer stream with mass flux $\dot{m}_O$ entering the system. Then the mixture fraction is defined as the local mass fraction of all elements within the mixture originating from the fuel feed[8].

$$Z = \frac{\dot{m}_F}{\dot{m}_F + \dot{m}_O} \tag{2.10}$$

Now, if we consider that the subscript '1' denotes pure fuel stream and subscript '2' denotes pure oxidizer stream. The local unburnt mass fraction of the fuel is the same as in the original fuel stream,

$$Y_F = Y_{F,1} Z \tag{2.11}$$

$Y_{F,1}$ is the mass fraction of the fuel in the fuel stream and the mass fraction of the oxidizer stream in the unburnt mixture can be represented by 1-Z. The local mass fraction of oxygen is as follows:

$$Y_{O_2} = Y_{O_2,2}(1 - Z) \tag{2.12}$$

where $Y_{O_2,2}$ is the mass fraction of oxygen in the oxidizer stream. Now substituting Equations 2.12 and 2.11 into Equation 2.9, the mixture fraction(Z) for any state of combustion can be obtained:

$$Z = \frac{\nu Y_F - Y_{O_2} + Y_{O_2,2}}{\nu Y_{F,1} + Y_{O_2,2}} \tag{2.13}$$

A stoichiometric mixture can be defined by $\nu Y_F = Y_{O_2}$ and it's mixture fraction can be defined by:

$$Z_{st} = \left[1 + \frac{\nu Y_{F,1}}{Y_{O_2,2}}\right]^{-1} = \frac{1}{1 + (A/F)_{st}} \tag{2.14}$$

where for pure fuel $Y_{F,1}=1$, and $(A/F)_{st}$ is the stoichiometric Air-to-Fuel ratio. The mixture fraction is a quantity than can be conserved during combustion and it can also be related to the fuel-air equivalence ratio. When considering infinitely fast chemistry, the reaction zone will be an infinitely thin layer at which the mixture fraction of the unburnt mixture will the the same as that of stoichiometric mixture fraction (i.e.) $Z=Z_{st}$. Outside of this infinitely thin layer the temperature will be a piecewise linear function of Z. When the profiles of temperature and mass fractions are plotted as a function of mixture fraction, one can relate it to the Burke-Schumann solution. Figure 2.6 describes the mixing and equilibrium lines for a given fuel and oxidizer. It is noticed that there is excess of air for values below the stoichiometric mixture fraction point and there is excess fuel for values above stoichiometric mixture fraction point. The enthalpy release is the highest at the stoichiometric mixture fraction point which is $Z=Z_{st}$ at constant specific heat capacity and one-step chemistry (no heat losses).

$$T(Z) = T_u(Z) + \frac{(-\Delta H) Y_{F,1}}{c_p \nu'_F W_F} Z, \quad Z \leq Z_{st} \tag{2.15a}$$

$$T(Z) = T_u(Z) + \frac{(-\Delta H) Y_{O_2,2}}{c_p \nu'_{O_2} W_{O_2}} (1 - Z), \quad Z \geq Z_{st} \tag{2.15b}$$

$$T_u(Z) = T_2 + Z(T_1 - T_2) \tag{2.15c}$$

where $T_u$ is the temperature of the unburnt mixture and $-\Delta H$ can be defined as the heat of reaction as the reaction enthalpy is negative for exothermic reactions. The specific heat($c_p$) and $-\Delta H$ can be assumed as constant and the maximum temperature is achieved when $Z=Z_{st}$, so:

$$T_{st} = T_u(Z_{st}) + \frac{(-\Delta H) Y_{F,1}}{c_p \nu'_F W_F} Z_{st} \tag{2.16a}$$

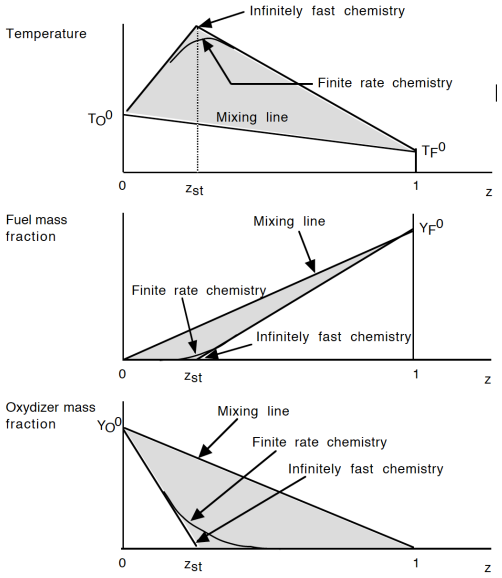


Figure 2.6: Evolution of z diagrams when chemistry evolves from infinitely fast to finite chemistry [5]

$$T_{st} = T_u(Z_{st}) + \frac{(-\Delta H)Y_{O_2,2}}{c_p \nu'_{O_2} W_{O_2}}(1 - Z_{st}) \tag{2.16b}$$

The mass fractions of the reactants can also be piecewise linear functions of Z:

$$Y_{O_2} = Y_{O_2,2}\left(1 - \frac{Z}{Z_{st}}\right), \quad Z \leq Z_{st} \tag{2.17a}$$

$$Y_F = Y_{F,1}\frac{Z - Z_{st}}{1 - Z_{st}}, \quad Z \geq Z_{st} \tag{2.17b}$$

The mass fractions for the product species can also be expressed the same as in Equation 2.17. Figure 2.7 shows that at stoichiometric combustion the mass fraction of oxidizer and fuel reach zero. The point where they reach zero is known as the stoichiometric mixture fraction point. $T_2$ and $T_1$ denote the temperature change in oxidizer and fuel respectively and $T_u$ is the temperature of the unburnt species. At stoichiometric combustion, the maximum temperature ($T_{st}$) will exactly be the point of stoichiometric mixture fraction ($Z_{st}$) whuch can be seen from Figure 2.7.

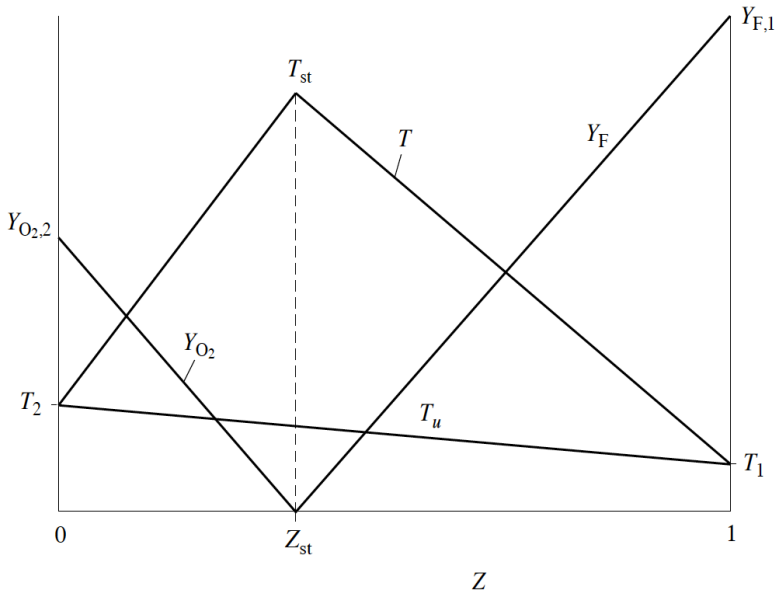


Figure 2.7: The Burke-Schumann solution as a function of mixture fraction [8]

### 2.4.4. Order of magnitude w.r.t. Flame length

The axial convection rate is proportional to radial diffusion. Axial convection time is the residence time of reactants in the flame $L_F/u_f$, where $u_F$ is the fuel flow velocity. The diffusion time scales with $\sim L^2/D$, where L as mentioned earlier is the radius of the fuel duct. If the residence time scales with the diffusion time then the flame length scales with ratio of the volumetric flow rate to that of the diffusion co-efficient (i.e) $L_F \sim (uL^2)/D \sim \frac{Volumetric\ \ flow\ \ rate\ \ of\ \ fuel}{Diffusion\ \ co-efficient}$. Figure 2.8 shows how the flame length changes with respect to the flow velocity of the fuel. The flame length($L_F$) reduces when there is a transition from laminar to turbulent.

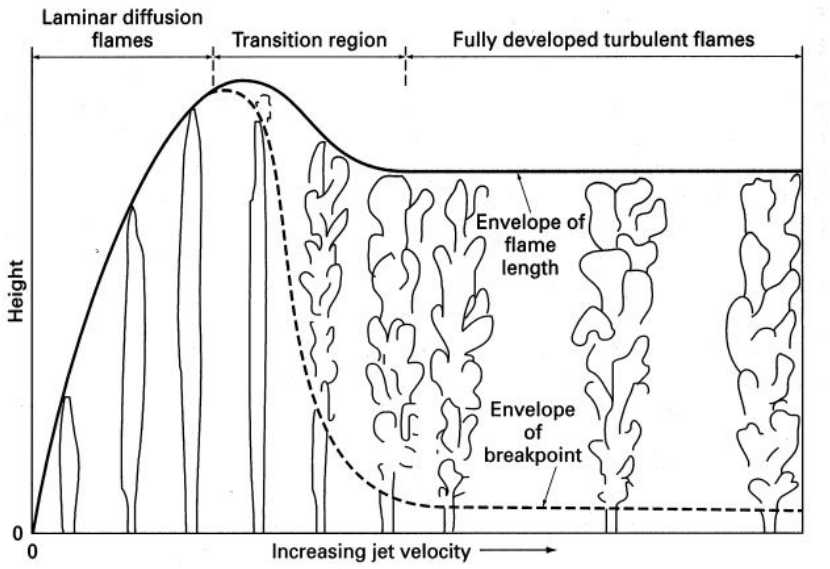


Figure 2.8: Flame length Vs Velocity [9]

## 2.5. Non-premixed Turbulent Combustion

Non-premixed turbulent flames are used in a lot of practical combustion systems like gas turbines, aircraft propulsion systems etc., as such flames are easily controlled[33]. Due to turbulence, the fuel and oxidizer mix intensely inside the combustion chamber. In non-premixed turbulent flames the rate at which the chemicals react to equilibrium is the same. To design an efficient combustor system that employs turbulent combustion, the flame shape and size is one of the main criteria that is taken into account along with flame stability, heat transfer and pollutant emissions[33].

### 2.5.1. Reaction rate for the flame

By considering mass fraction of fuel to be a function of the mixture fraction, a relationship with the amount of fuel consumed to reach the stoichiometric point can be understood. By taking the usual Schvab-Zeldovich assumptions, the unsteady conservation Equations for mass fraction of fuel can be written as:

$$\rho\frac{\partial Y_F}{\partial t} + \rho u.\nabla Y_F - \nabla.(\rho D\nabla Y_F) = \dot{\omega}_F \tag{2.18}$$

where the subscript F denotes fuel species. The first term on the l.h.s describes the local rate of change of the fuel; the second term on the l.h.s describes the convection term; and the third term on l.h.s describes the diffusion of the fuel species. The term on the r.h.s is the source term which signifies the rate of consumption of fuel. Bilger [34] defines the mixture fraction as a conserved scalar quantity, so the unsteady conservation equation with respect to the mixture fraction can be written as:

$$\rho\frac{\partial Z}{\partial t} + \rho u.\nabla Z - \nabla.(\rho D\nabla Z) = 0 \tag{2.19}$$

As understood earlier, the mass fraction of the fuel($Y_F$) reduces as it reaches the stoichiometric mixture fraction point, and at stoichiometry(Z=$Z_{st}$) the mass fraction of fuel is zero. So the composition of fuel is a unique function of the mixture fraction:

$$Y_F = Y_F(Z) \tag{2.20}$$

Then, from Equation 2.18 the following is derived:

$$\dot{\omega}_F = -\rho D\frac{\partial^2 Y_F}{\partial Z^2}(\nabla Z)^2 \tag{2.21}$$

Mixture fraction Z is a conserved scalar quantity and the mass fraction of fuel is defined as a function of the mixture fraction. This can be only done when the species is alone a unique function of the conserved scalar quantity. As scalar dissipation rate defined in Equation 2.30, the above equation can be re-written as following:

$$\dot{\omega}_F = -\frac{1}{2}\underbrace{\rho\chi}_{Mixing}\underbrace{\frac{\partial^2 Y_F}{\partial Z^2}}_{Reaction} \tag{2.22}$$

From the above Equation it is clear that the rate of consumption of fuel depends on two factors:

- The mixing field of the species which is defined mainly by the turbulent scalar dissipation rate.
- The reaction of the species in the mixture fraction space of the combustion field.

The rate of consumption of the fuel also depends on the change in the mass fraction of the fuel. Figure 2.7 displays how the change of mass fraction can be plotted with respect to mixture fraction. From Z=$Z_{st}$ to Z=1, the mass fraction of fuel seems to behave like a step function. This will lead to getting a dirac delta function. Dirac delta function is a generalized mathematical function whose integral over the entire real line of a specific function which is equal to zero is one.

At $Z_{st}$, the fuel mass fraction ($Y_F$) will be completely consumed during combustion. At Z=1, $Y_F$ will also be 1 which represents 100% fuel which is before the combustion begins. The slope of $Y_F$ from $Z_{st}$ to Z=1 will be $\frac{dY_F(Z)}{dZ}$ which would make $Y_F$ as a step function. Thus, representing the second derivative of the mass fraction of fuel as a dirac delta function whose integral will yield (1-$Z_{st}$). So, we can relate the change in mass fraction of fuel at stoichiometry by using the dirac delta function and get a final relation as follows:

$$\frac{\partial^2 Y_F}{\partial Z^2} = \frac{1}{1 - Z_{st}} \delta(Z = Z_{st}) \tag{2.23}$$

where, $\delta(Z)$ is the dirac delta function. So, finally Equation 2.22 can be expressed as:

$$\dot{\omega}_F = -\frac{1}{2} \rho \chi \frac{1}{(1 - Z_{st})} \delta(Z = Z_{st}) \tag{2.24}$$

### 2.5.2. Turbulent transport Equation of the mixture fraction

The mixture fraction co-ordinate has been discussed in section 2.4.3 which plays an important quantity for the theory of non-premixed combustion. The mixture fraction (Z) can be defined as the solution of a convective diffusive Equation [9]:

$$\rho \frac{\partial Z}{\partial t} + \rho \vec{u} . \nabla Z = \nabla . (\rho D \nabla Z) \tag{2.25}$$

and the reactive diffusive structure of the flame is determined by the temperature Equation[9]:

$$\rho c_p \frac{\partial T}{\partial t} + \rho c_p \vec{u} . \nabla T = \nabla . (\rho c_p D_T \nabla T) - \sum_{i=1}^{n} h_i \dot{m}_i + q_R + \frac{\partial p}{\partial t} \tag{2.26}$$

where, $\sum_{i=1}^{n} h_i \dot{m}_i$ is the heat release rate in which $\dot{m}_i$ is the chemical source term. The heat capacity $c_p$ is assumed to be constant, $q_R$ is the radiative heat loss which can be calculated by thin gas approximation [9].

Equation 2.25 defines the transport equation of mixture fraction Z to be given in the flow field as a function of space and time. As mentioned in section 2.4.3 the stoichiometric mixture can be determined by $Z=Z_{st}$ and this is shown in Figure 2.9 for a turbulent jet flame. The fuel and oxidizer inter-diffuse at the lip of the nozzle [9]. In turbulent combustion the instantaneous flame location is not taken into account much and more considered in the form of mean quantities. This makes the Equation 2.25 for the Favre mean mixture fraction [9]:

$$\overline{\rho} \frac{\partial \widetilde{Z}}{\partial t} + \overline{\rho}\ \vec{v} . \nabla \widetilde{Z} = \nabla . (\overline{\rho} D_T \nabla \widetilde{Z}) \tag{2.27}$$

where $D_T$ is the turbulent diffusivity which is much larger than the molecular diffusivity D and hence it has been neglected.

The Favre variance $\widetilde{Z''^2}$ is modeled by standard procedures as follows:

$$\overline{\rho} \frac{\partial \widetilde{Z''^2}}{\partial t} + \overline{\rho}\ \vec{u} . \nabla \widetilde{Z''^2} = \nabla . (\overline{\rho} D_t \nabla \widetilde{Z''^2}) + 2 \overline{\rho} D_T (\nabla \widetilde{Z})^2 - \overline{\rho} \widetilde{\chi} \tag{2.28}$$

Here, the first term on the l.h.s represents the rate of change of the mixture fraction variance, second term represents the convection term. The first term on the r.h.s represents the turbulent diffusion of the mixture fraction, second term on r.h.s represents the production terms and $\widetilde{\chi}$ is the mean dissipation rate which is an important factor when it comes to turbulent combustion. It defines the dissipation of turbulent fluctuations.

$$\widetilde{\chi} = 2 D_T (\nabla \widetilde{Z''})^2 = c_\chi \frac{\tilde{\epsilon}}{\tilde{k}} \widetilde{Z''^2} \tag{2.29}$$

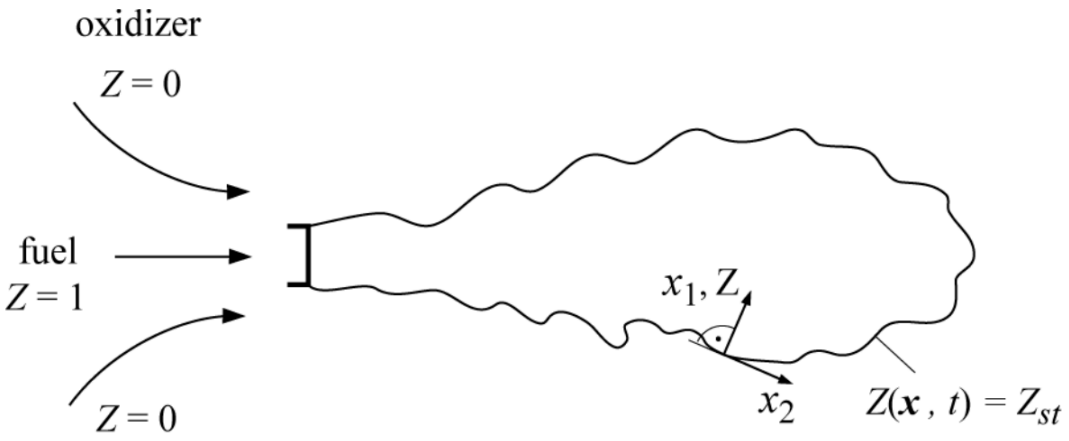


Figure 2.9: Surface of stoichiometric mixture in turbulent jet [9]

where, $c_\chi$=2.0, $\tilde{\epsilon}$ is the turbulent diffusion rate and $\tilde{k}$ is the turbulent kinetic energy. The above equation represents the mean scalar dissipation at any given position in a mixture fraction space and time. Scalar dissipation rate when capturing in the stoichiometric contour of the flame surface is defined at the mixture fraction position($Z=Z_{st}$) at a direction normal to the surface of the flame. So, the scalar dissipation rate at stoichiometric mixture fraction ($Z(x,t) = Z_{st}$) can be represented as:

$$\chi_{st} = 2D_T \left(\frac{\partial Z}{\partial x}\right)^2_{st} \tag{2.30}$$

where $\chi_{st}$ is the instantaneous scalar dissipation rate at stoichiometric conditions. For turbulent non-premixed combustion it must be replaced by a conditional average value(average of the large eddies) $\widetilde{\chi_{st}}$ and has dimension 1/s (inverse characteristic of diffusion time).

### 2.5.3. Scalar Dissipation rate

The dissipation rate of mixture fraction in non-premixed combustion is a fundamental parameter to understand if the flame during combustion is controlled by mixing. For infinitely fast and irreversible chemistry, the fuel and oxidizer is independent of scalar dissipation rate. This is because the fuel and oxidizer cannot coexist when taking it under the assumption of infinitely fast and irreversible. While assuming finite rate chemistry, the fuel and oxidizer composition may overlap in the reaction zone depending on the scalar dissipation rate [5]. This makes the modelling of diffusion flame structures a bit less complex. Understanding scalar dissipation rate assists in modelling the diffusion flame structure at the overlap region. At the region where fuel and oxidizer overlap, the scalar dissipation rate can be used to find the rate of mixing at stoichiometry. For large scale, turbulent mixing is what drives the fuel and oxidizer to mix at molecular level. It contributes to this molecular scalar mixing only indirectly by increasing the scalar variances and thereby increasing the scalar gradients [10]. Removing these scalar variances, molecular mixing occurs in the smallest turbulent scales and the rate of this mixing is defined by the scalar dissipation rate. The departure of the chemical equilibrium is described by the scalar dissipation rate at the stoichiometric mixture fraction.

Pitsch et al [10] modeled the diffusion flamelet and studied the scalar dissipation rate for a sandia D flame using Large Eddy Simulations. A sandia D flame is a specific type of jet flame which is designed and researched by the Sandia laboratory[35]. Figure 2.10 shows the instantaneous distribution of the unconditionally filtered scalar dissipation rate. From the figure, it is seen that at the point of ignition which is at the core of the flame the scalar dissipation rate is the highest and as the flame is quenched the scalar dissipation rate is the lowest. The Figure also indicates the stoichiometric contour of the flame. From this the importance of scalar dissipation rate is understood. It can be used in modelling the stoichiometric contour of the flame where the fuel and oxidizer overlap.

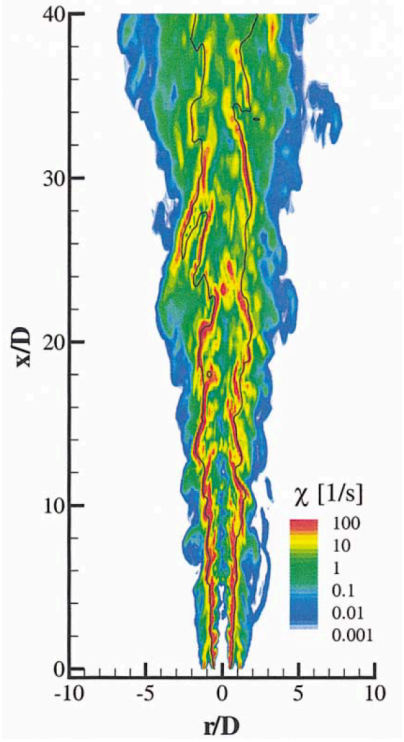


Figure 2.10: Instantaneous scalar dissipation rate distribution, [10].

## 2.6. Stoichiometric Fuel-to-Air ratio

The Equation($F_{st}$) used to calculate the stoichiometric fuel-to-air ratio is simple and depends on the amount of air/oxygen required to completely burn 1 mole of each fuel species contained in the fuel. For example if methane is considered as the fuel used for combustion. To burn 1 mole of $CH_4$, 9.52 moles of air is required which can be seen from the Equation 2.31.

$$\mathrm{CH_4} + 2\,(\mathrm{O_2} + 3.76\,\mathrm{N_2}) \longrightarrow \mathrm{CO_2} + 2\,\mathrm{H_2O} + 3.76\,\mathrm{N_2} \tag{2.31}$$

The following Equation is used to calculate the $F_{st}$:

$$F_{st} = \frac{MW_F}{MW_O * total\ \ air\ \ requirement(mol/mol)} \tag{2.32}$$

where, $F_{st}$ is the stoichiometric Fuel-to-Air ratio and $MW_i$ is the molecular weight of the species. So, in the case of methane, the following will be the stoichiometric (F/A) ratio .

$$F_{st} = \frac{16(g/mol)}{29(g/mol) * 9.52} = 0.057 \tag{2.33}$$

The air or fuel required to combust is known from the equivalence ratio at which the combustion takes place. Equivalence ratio is defined as following:

$$\phi = \frac{\dot{m}_F/\dot{m}_O}{F_{st}} \tag{2.34}$$

## 2.7. Emissions in non-premixed systems

The chemical kinetics that are involved in the formation of NOx is the same in premixed and non-premixed combustion. In non-premixed combustion there is an additional physical process of mixing and evaporation that can lead to a production of local compositions of fuel-oxidizer mixture which span over a wide range of stoichiometries [15]. If we take for instance combustion in a Burke-schumann flame, at some locations there are stoichiometric combustions, while at other locations the combustions can be either rich or lean. Due to the creation of rich and lean zones inside the combustion chamber, the formation of emissions is substantially complex in non-premixed systems[15].

**Oxides of Nitrogen (NOx)**

In simple turbulent jet flames, formation of NOx was broadly studied and an overview on how the NOx was formed is given by Turns et al and Driscoll et al [33, 36]. It can be produced by five different mechanisms:

- Thermal NOx or Zel'dovich mechanism
- Prompt NOx or Fenimore mechanism
- NNH Mechanism
- $N_2O$ or Nitrous oxide mechanism

Experiments were conducted to understand OH imaging by J.Seitzman [37] as OH is one of the radicals that breaks and oxidizes nitrogen to form NOx. It was reviewed that NO is formed in thin laminar like flamelet regions in the lower-to-mid regions of the flame. In jet flames that involve hydrocarbons as fuel, the NOx formation mechanism mostly observed were thermal NOx and prompt NOx among others as well [15]. Most of the nitric oxide (NO) formed in combustion subsequently oxidizes to $NO_2$. For this reason, it is customary to lump NO and $NO_2$ together and express results in terms of NOx, rather than NO. The formation of NOx behaviour is not linear and depends on different parameters such as temperature, pressure and residence time.

### 2.7.1. Thermal NOx or Zel'dovich mechanism

Thermal NOx is produced by the oxidation of atmospheric nitrogen in high-temperature regions of the flame and in the post flame gases[32]. This is endothermic and it proceeds at a significant rate only at temperatures above around 1850 K[32]. Most of the proposed reaction schemes for thermal NO utilize the extended Zeldovich mechanism [32]:

$$O_2 \rightleftharpoons 2\,O \tag{2.35a}$$

$$N_2 + O \rightleftharpoons NO + N \tag{2.35b}$$

$$N + O_2 \rightleftharpoons NO + O \tag{2.35c}$$

$$N + OH \rightleftharpoons NO + H \tag{2.35d}$$

Thermal NO formation is found to usually peak on the fuel-lean side of stoichiometric [32].This is a consequence of the competition between fuel and nitrogen for the available oxygen. Although the combustion temperature is higher on the slightly rich side of stoichiometric, the available oxygen is then consumed preferentially by the fuel.

### 2.7.2. Prompt Nitric Oxide or Fenimore Mechanism

Under certain conditions, prompt nitric oxide is found very early in the flame region, a fact that is in conflict with the idea of a kinetically controlled process. According to Nicol et al in 1994 [38], the initiating reaction is:

$$N_2 + CH \rightleftharpoons HCN + N \tag{2.36}$$

This occurs at low pressures and low temperatures. The balance of the prompt NO mechanism involves the oxidation of the HCN molecules and N atoms. Under lean-premixed conditions, the HCN oxidizes to NO mainly by a sequence of reactions involving HCN $\longrightarrow$ CN $\longrightarrow$ NCO $\longrightarrow$ NO. The N atom

reacts mainly by the second Zeldovich reaction. The influence of pressure is of special interest and importance because prompt NO can be a significant contributor to the NO emissions produced in lean premix (LPM) combustion [39]. For equivalence ratios less than about 1.2, the conversion of HCN into NO is according to the following steps [15].

$$HCN + O \rightleftharpoons NCO + H \tag{2.37a}$$

$$NCO + H \rightleftharpoons NH + CO \tag{2.37b}$$

$$NH + H \rightleftharpoons N + H_2 \tag{2.37c}$$

$$N + OH \rightleftharpoons NO + H \tag{2.37d}$$

### 2.7.3. NNH Mechanism

The one to introduce this mechanism was Bozzelli and Dean in 1995[40] which involves the reaction of NNH with the oxygen atoms due to the presence of abundace of oxygen radicals e.g. lean premixed combustion. The formation of NNH is through the reaction of nitrogen with 'H' radical at low flame temperatures. The following Equations illustrates the formation of NNH:

$$N_2 + H \rightleftharpoons NNH \tag{2.38a}$$

$$NNH + O \rightleftharpoons NO + NH \tag{2.38b}$$

$$NNH + O \rightleftharpoons N_2O + H \tag{2.38c}$$

$$NNH + O \rightleftharpoons N_2 + OH \tag{2.38d}$$

### 2.7.4. $N_2O$ or Nitrous oxide mechanism

Fuel reacts with $N_2$ molecule and the oxygen radical at low flame temperatures (T<1800K) giving rise to the species $N_2O$. The mechanism was first proposed by Malte and Pratt in 1974 [41] and the formation of nitrous oxide is given as a three reaction pathway and given as a third body reaction.

$$N_2 + O + M \rightleftharpoons N_2O(\cdot) + M \tag{2.39a}$$

$$N_2O(\cdot) + M \rightleftharpoons N_2O + M \tag{2.39b}$$

$$N_2O + M \rightleftharpoons N_2 + O + M \tag{2.39c}$$

here, M is the third body under the presence of which the reaction is carried out. With the presence of M as the third body, $N_2$ and O reacts with it to form an unsTable intermediate $N_2O(*)$ which subsequently forms $N_2O$. Nicol et al [38] stated that the above three step reaction pathway initiates the formation of NO. Due to the presence of nitrogen in the atmosphere, this mechanism is frequent under combustion. Understanding the generation of $N_2O$ is important as it leads to better grasp of the formation of enhanced NO. NO is produced after reacting with O radicals or H radicals or even CO which can be seen in the following Equations[32]:

$$N_2O + O \rightleftharpoons NO + NO \tag{2.40a}$$

$$N_2O + H \rightleftharpoons NO + NH \tag{2.40b}$$

$$N_2O + CO \rightleftharpoons NO + NCO \tag{2.40c}$$

### 2.7.5. Dependence of NOx on Residence time

The residence time of fuel and oxidizer inside the combustor can greatly influence NOx emissions. Anderson in 1975[11] researched on the influence of residence time on NOx emissions. He found that the NOx emissions increase with increase in residence time except for very lean mixtures ($\phi \cong 0.4$) which can be seen from Figure 2.11. This is because the rate of formation is so low that NOx emission becomes insensitive to time [32].

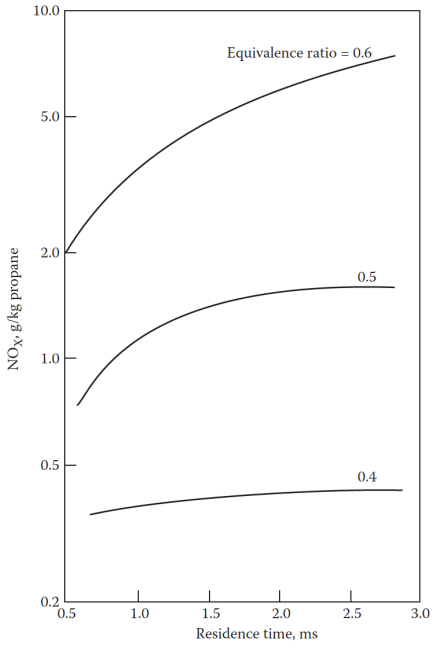


Figure 2.11: Effect of residence time on NOx, [11].

Lefebvre [32] mentioned that one of main factors that contribute to the increase in emission is the residence time in the primary zone. The larger the volume and residence time on the primary zone, there is an increase in the NOx emissions as well. But, increasing the primary zone/combustor volume assists in reducing the CO emission. So, there is always a balance that needs to be achieved to keep both NOx and CO emissions at bay while designing the combustion chamber.

### 2.7.6. Carbon Monoxide (CO)

Apart from NOx that is emitted due to combustion, carbon monoxide is the other pollutant which is formed in gas turbine combustors. The following are the reasons behind formation of CO as explained by Lefebvre and Ballal [32].

- **Improper mixing:** When the fuel and oxidizer aren't mixed properly, there are spatial and temporal unmixedness inside the combustor. This leads to various rich and lean pockets inside the combustor which favours the formation of CO.

- **Insufficient residence time or Incomplete combustion:** When the residence time is low, the fuel is not burnt completely which leads to incomplete combustion. In order to reach equilibrium values of CO, the flow must have an infinite residence time. Incomplete combustion can also occur due to lack of oxygen in the primary zone of the combustor.

- **Flame quenching:** Local quenching of flame can occur due to cooling air entrainment from the combustor liner which leads to high amounts of CO production.

CO is oxidation resistant and the conversion to $CO_2$ can be a rate determining step. The dissociation of $CO_2$ to give CO and $O_2$ can be understood from the following Equation [15]:

$$CO_2 \rightleftharpoons CO + 0.5\,O_2 \tag{2.41}$$

The overall oxidation of CO can be split into 4 steps [15]:

$$CO + O_2 \rightleftharpoons CO_2 + O \tag{2.42a}$$

$$O + H_2O \rightleftharpoons OH + OH \tag{2.42b}$$

$$CO + OH \rightleftharpoons CO_2 + H \tag{2.42c}$$

$$O_2 + H \rightleftharpoons OH + O \tag{2.42d}$$

The rate determining step is Equation 2.42a and acts as the initiation reaction. As, OH, O and H radicals are formed, this can accelerate the process of formation of $CO_2$ from oxidation of CO. Equation 2.42c is the main reaction that forms $CO_2$ by removing CO.

### 2.7.7. NOx reduction techniques

Figure 2.12 shows the various techniques that were reported by J. Bluenstein in 1992 [12] which involve combustion modifications and also post-combustion controls. This thesis focuses upon reducing thermal NOx through the use of Exhaust Gas Recirculation among other techniques. Combustion designers adopt preheating the incoming oxidizer to increase the thermal efficiency of the system. Reducing the oxidizer preheat leads to the reduction of combustion temperatures and thus subsequently reducing NOx emissions. EGR acts as diluents and how effective it is to reduce the emissions depend upon the quantity and temperature of the recirculated gas.

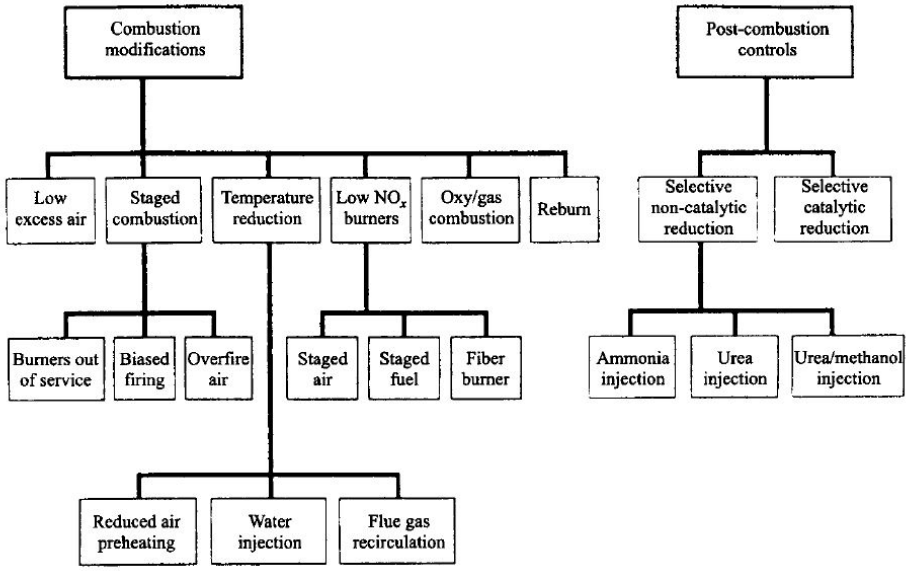


Figure 2.12: NOx control technologies for gas-fired industrial combustion equipment, [12]

### 2.7.8. Quantification of Emissions

The mechanism, production, and reduction of the emission has been discussed, but the emission levels need to have a common representation. By quantifying the emissions in a common scale, the emissions can be compared with other technical results that were obtained either from experiments or from the system measurements.

- **Emission Index:** The emission index (EI) is designed as the ratio of the mass of the pollutant in grams to that of the mass of fuel in kg. There is a difference in units to account for the order of magnitude difference between the two quantities [42]. EI in gas turbine is a common method used to quantify emissions and is given as following:

$$Emission\ \ Index = \frac{Mass\ \ of\ \ pollutant(g)}{Mass\ \ of\ \ fuel(kg)} \tag{2.43}$$

- **$O_2$ correction:** Oxygen is diluted at various degrees. To remove that a specific $O_2$ correction level is introduced so that the emission levels can be compared while still retaining a familiar mole-fraction-like variable. The unit of representation apart from the EI is parts per million by volume, dry (ppmv). After combustion, there are traces of $H_2O$ present in the product, to apply the $O_2$ correction level and represent the emission in ppmv, the concentrations should first be converted from wet to dry.

$$X_{dry} = \frac{X_{wet}}{1 - X_{H_2O,wet}} \tag{2.44}$$

  If the correction is required for 15%, then the correction formula that is used for air as an oxidizer that contains 21% oxygen(0.21 mole fraction $O_2$) is given as:

$$NOx_{15\%O_2} = NOx_{dry}\frac{0.21 - 0.15}{0.21 - X_{O_2,dry}} \tag{2.45}$$

## 2.8. Modelling the emissions

Chemical reactor network (CRN) was used to model non-premixed combustion in a gas turbine. The method used to derive this chemical reactor network can be understood from this thesis work. There are various chemical reactor networks that have been produced for modelling non-premixed combustion, to quote a few Lebedev et al [20], DeToni et al [18], and Broadwell and Lutz [16].

As quoted by Igor V. Novosselov in his PhD thesis [43], there aren't many computer models that can incorporate the full set of chemical kinetic reactions that is coupled with turbulent flow modeling. There have been attempts made to include such complex turbulent chemistry models, but such models are limited to rather simple systems. In order to model complex combustion systems, various simplified global kinetic mechanisms have been developed which contain all the chemical kinetic history that occurs inside a combustion process. However, these mechanisms are limited by their operating conditions and may fail to predict CO and NOx emissions accurately.

Modelling non-premixed combustion can also be done through computational fluid dynamics using simplified chemistry which can take weeks to converge and great amounts of computer time. If a CRN is modelled skillfully with a robust design, the model can provide quantitative behaviour of NOx and CO emissions leaving the combustor. These results can be very helpful in designing combustors and also modification stages and can also aid in the reducing the emission levels in the combustion system [43].

A parametric analysis is the main reason in this research for modelling non-premixed combustion using a CRN. This is done in CRN as the computation time compared to CFD is in several orders of magnitude lesser. CFD incorporates reduced chemistry which is a disadvantage, but at the same time it predicts the flow field and also the turbulence effects. CRN models can be designed using the information from the literature research gathered especially when it comes to the flow field of the fluid inside the combustion chamber. This gives a broader idea on how a fluid in combustion reaction acts and according

to that with a more detailed chemistry a CRN can be modelled. CRN models have been taken and implemented in their thesis project by V. Prakash [13], Rosati [44], and C.Merino Madrid [45]. According to Rosati, the methodology followed in CRN modeling is about spatially discretizing a combustor as a chain of chemical reactors connected in series. An outline of how CFD and PIV measurements can be used to create a CRN model has been shown by V.Prakash in his thesis [13] and can be seen in Figure 2.13. The flow field information along with velocity and temperature information can be obtained using CFD. This information along with the information obtained form PIV results can be given as an input to the CRN. The input from CFD and PIV measurements describes the various high temperature zones formed inside the combustion chamber and can be recreated using PSRs to obtain accurate emission results. This is known as the hybrid CFD-CRN method. A hybrid of CFD/CRN will always give a more elaborate result and a much more clear understanding of the pollutant emissions which has be shown in the works of Rishikesh Sampat in 2018[46].

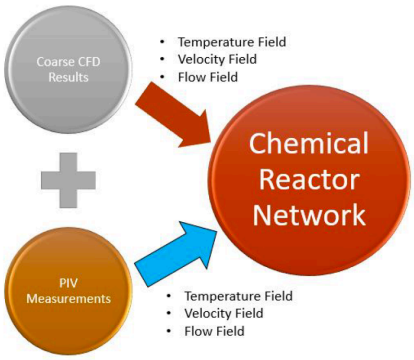


Figure 2.13: Pre-requisites for a CRN model development [13]

## 2.9. Chemical Reactor network modeling for combustion systems

Chemical reactor network modeling is used to understand the NOx emission and CO emission pathways in a combustion system depending on the CRN design. It gives the user an idea as to where the emission initiates or on how the formation of various radicals leads to the generation of those emissions. It is a valuable tool which uses less simulation time compared to that of CFD modeling and gives an evaluation of the pollutant formation and blowout performance of the combustion systems. The volume of the combustor inside a gas turbine can be divided into zones and represented by chemical reactors such as perfectly stirred reactors(PSR) and plug flow reactors(PFR) which are 0-Dimensional chemical reactors.

Chemical reactor network modelling uses simplified flow field and more importance is given to the different chemical kinetics that occur inside the reactions of a combustion system. Modelling through CRN gives an overview of the emissions faster.

### 2.9.1. Perfectly Stirred Reactors (PSR)

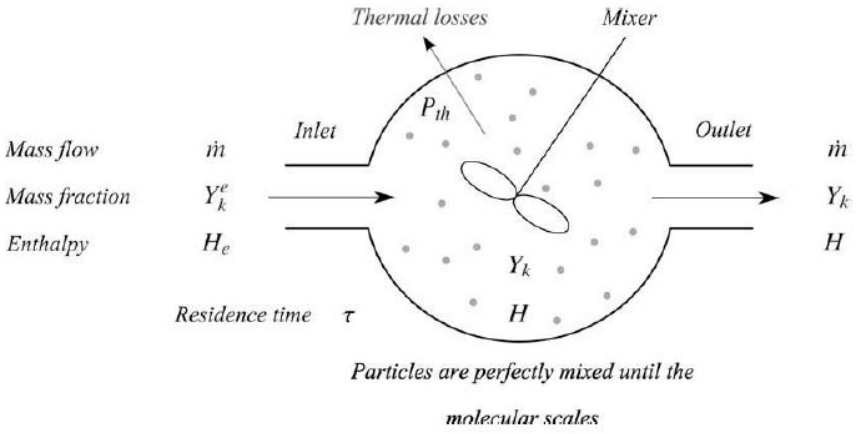


Figure 2.14: Schematic of a PSR under steady-state conditions [14]

These reactors are also known as a continuously stirred tank reactor and is assumed that mixing occurs in molecular scale and is instantaneous compared to the chemical reaction. These chemical reactions occur homogeneously in the reactor. In the reactor, whatever species enters, an instantaneous and perfect mixing is assumed.

The PSR hypotheses is valid in regions where turbulent eddy motion time scales are smaller compared to the chemical time scale. Since the formation of NOx keep occuring only after the flames in the products, it isn't crucial to describe what happens in thin local flamelets [14]. The governing Equations used by the chemical reactors in the software can be found in the Cantera website [47] and is given as follows.

**Mass Conservation**
Overall mass conservation in a control volume of the PSR is given by,

$$\frac{dm}{dt} = \sum \dot{m}_{in} - \sum \dot{m}_{out} + \dot{m}_{wall} \tag{2.46}$$

over here $\dot{m}_{wall}$ can be neglected as it isn't used for the modeling of the combustion system and there are absence of penetrable walls.

**Species Conservation**
The species conservation governing Equation of the chemical reactor is the rate at which the species k is generated and is as follows:

$$\dot{m}_{k,generated} = V\dot{\omega}MW \tag{2.47}$$

and the rate at which the mass is changed for each species is as follows:

$$\frac{d(mY_k)}{dt} = \sum \dot{m}_{in}Y_{k,in} - \sum \dot{m}_{out}Y_{k,out} + \dot{m}_{k,generated} \tag{2.48}$$

where, $Y_k$ is the mass fraction of species k, V is the reactor volume in $m^3$, MW is the molecular weight of the species k in kg/mol and $\dot{\omega}$ is the chemical source term in $mol/m^3sec$ The mean residence time that is used in the modeling the reactor networks is as follows:

$$\tau_{res} = \frac{\rho V}{\dot{m}} \tag{2.49}$$

where, $\rho$ is the density of the species, V is the combustor volume and $\dot{m}$ is the mass flow rate of the species through the reactor.

**Energy conservation**
Inside the PSR reactor, along with mass and species even energy is conserved as every species entering the reactor is destroyed and a new species is formed. The governing Equations for energy conservation is as follows:

$$U = m\sum_{k} Y_k u_k(T) \tag{2.50a}$$

$$\frac{dU}{dt} = u\frac{dm}{dt} + mc_v\frac{dT}{dt} + m\sum_{k} u_k\frac{Y_k}{dt} \tag{2.50b}$$

where, U is the total internal energy and m is mass in kg.

All the above Equations are given for an ideal gas reactor, that is used in this thesis for modeling the ideal gas mixtures, which was also recommended by Rosati[44] and Vaibhav Prakash [13] in their respective thesis.

## 2.9.2. Plug Flow Reactors:

In a plug flow reactor, the flow of the species entering the reactor is assumed to move as a plug and the chemical reaction is assumed to move one dimensionally. This means that radial diffusion is alone considered in a plug flow reactor and axial diffusion is completely neglected. This reactor is also a steady state reactor with a continuous flow and possesses uniform properties in the axial direction [13].This reactor is used mostly to model the exhaust of the combustor where the gases complete the combustion process and exit the exhaust of the combustor. Similar to PSR, PFR is also governed by mass, momentum, species and energy conservation which can be seen in Figure 2.15. As, the flow

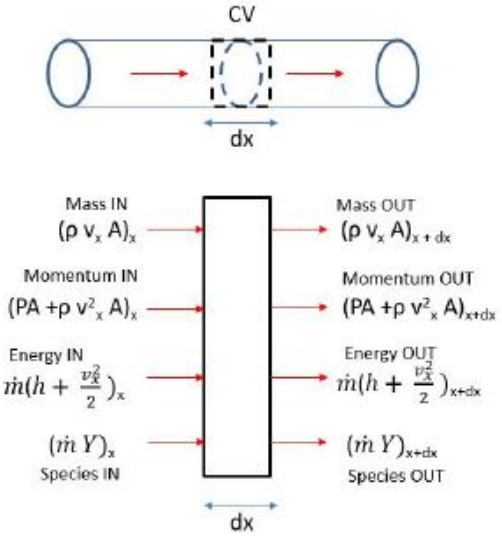


Figure 2.15: Schematic of a PFR under steady-state conditions [15].

is considered to be one dimensional (i.e.) only in axial direction, only the x direction of Equations is considered in the governing Equations and is given by:

$$\frac{d(\rho U_x A)}{dx} = 0 \tag{2.51a}$$

$$\frac{dY_i}{dx} = \frac{\dot{\omega} MW A}{\dot{m}} \tag{2.51b}$$

$$\frac{d(h + \frac{v_x^2}{2})}{dx} + \frac{\dot{Q}'' P}{\dot{m}} = 0 \tag{2.51c}$$

Equations 2.51a, 2.51b, 2.51c are mass conservation, species conservation and energy conservation Equations respectively. If Equation 2.51c is expanded an expression for the temperature derivative can be obtained. PFR can be modelled as a set of coupled PSRs in series.

## 2.10. Modelling tools

There are two major softwares that are used to understand the chemical kinetics of a combustion process which are Chemkin and Cantera from python. This research uses cantera which is an open-source suite of object-oriented software tools for problems involving chemical kinetics, thermodynamics, and/or transport processes [47]. This library can be called using Python 3.6 and was also used and recommended by Rosati[44] and V. Prakash[13] for their thesis. It allows the users to quickly and efficiently incorporate and execute fundamental thermodynamic, chemical kinetic and species transport calculations in their work.

**Chemical Mechanisms**

Cantera still needs to call several chemical mechanisms to identify the NOx kinetics in a combustion process. The global combustion reaction for a hydrocarbon fuel in air is given as:

$$C_xH_y + (x + (y/_4))(O_2 + 3.76\,N_2) \longrightarrow xCO_2 + y/_2H_2O + 3.76\,(x + (y/_4))N_2 \tag{2.52}$$

There are a lot of chemical reactions that occur when it comes to combustion along with complex chemistries. Therefore, combustion can not be considered as a single step reaction and is a sequence of different reactions together to form the final product. From dissociation of $CH_4$ to the formation of $CO_2$ there are number of chemical reactions and paths created in between. The library or a collection of all these chemical reactions is known as a chemical mechanism. When it comes to natural gas combustion, there are various chemical mechanisms that are available with different number of species and reactions.

- GRI-Mech 3.0
- Konnov Mechanism
- C2-NOx Mechanism
- C1-C3 Mechanism (Version 1412)

In this thesis, GRI-Mech 3.0 is used due to it's robustness, newer modifications on reactions rates. The main advantage behind using this mechanism is that it includes the kinetics of $C_2H_6$ and $C_3H_8$ which are some of the important constitutents of natural gas.

GRI-Mech 3.0 was first developed in 1999, by Smith et al. [48] of the Gas Research Institute and University of Berkeley. When modelling while using this mechanism, it simulates natural gas combustion along with NOx formation and reburn chemistry. GRI-Mech 3.0 consists of 325 reactions and 53 species.

## 2.11. Examples of CRN models used for diffusion flames

The idea of using a chemical reactor network to model a combustor with a PSR-PFR was first introduced by Bragg in 1953[49]. He proposed that the chemical time inside the PSR is assumed to be slower than the mixing time and thus chemistry would be the rate limiting step of a combustion process. He also mentioned that the combustor volume inside the combustor can be split into two distinct zones, with the flame contained in the PSR and the dilution zone as the PFR.

### 2.11.1. Flame sheet reactor modelling

Broadwell and Lutz [16] in 1998 proposed a two reactor model that can be seen in Figure 2.16. They modelled a turbulent jet chemical reaction to find the amount of NOx that was produced in the jet flames. They observed the flame sheets into the core of the flame from the experiments done by Chen et al in 1991. They understood that the fuel enters the flame sheet and the products are returned by diffusion [16].

This process was approximated by replacing the flame sheet at every axial location by a PSR. The core of the reactor is modelled by a PSR where the output from the FSR is given and the feedback from the core reactor is given back to the FSR as the diffusive reactions take place inside the core PSR reactor. They found that most of the NOx and CO are produced in the core especially in the region around flame tip. They concluded that the reactions that occur in the flame sheet reactor needs to be treated only approximately and that the two-reactor configuration is adequate.

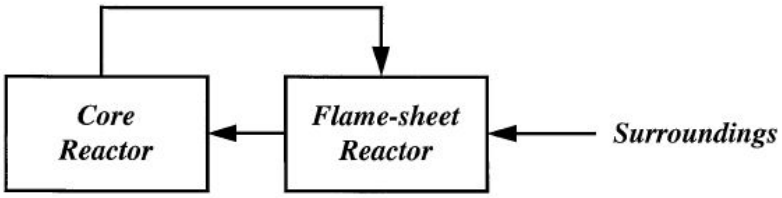


Figure 2.16: Sketch of a 2-reactor model designed by Broadwell and Lutz [16]

### 2.11.2. Recirculation zone modelling

Pedersen et al in 1997 [17] published their works explaining the residence time distributions in a confined swirling flames of a pulverised coal flame. As combustion systems are developing, the use of swirl gives rise to the reduction of NOx. The incoming oxidizer is swirled to create a recirculation zone which enhances the mixing of the oxidizer and the fuel to give a homogeneous mixture within a short time. Recirculation also heats up the incoming oxidizer which results in self-sustaining combustion reactions inside the combustion chamber. This helps in reducing the emissions and at the same time gives better combustion of fuels which results in more power.

Figure 2.17 shows the various models introduced by Pedersen et al to model a recirculation zone inside the furnace. According to the authors, the recirculation and dispersed zones can be modelled as stirred regions of the flame zones, while the central and the post-flame zone can be modelled using a plug flow reactor. This describes the distribution of residence time inside the combustor chamber of the furnace.

This theory introduced by Pedersen et al was adopted by DeToni et al in 2013 [18] to calculate the NOx emission from a BERL-300kW industrial gas burner. DeToni et al instead of using a PFR to model the post-flame zone, used a PSR. This was because the software Chemkin did not allow the recirculation of reagents between PFR and PSR. They used a PSR as a recirculation by taking the feedback from the post-flame zone which was modelled using a PSR as well. The author also introduced a PFR at the exhaust of the combustion chamber representing the dilution of the burnt mixture. Figure 2.18 shows the streamline flow in the furnace considering the symmetry which was adapted from Silva [19] and the CRN model that was developed by DeToni et al [18].

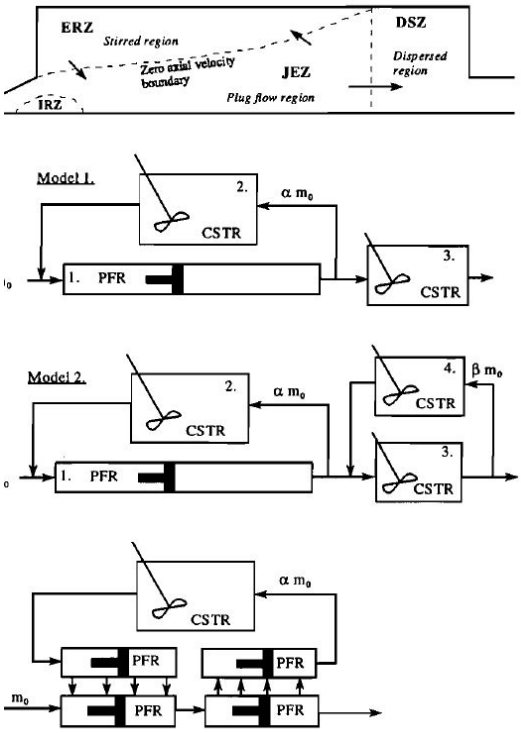


Figure 2.17: CRN based on the recirculation zones of the furnace(top) [17]

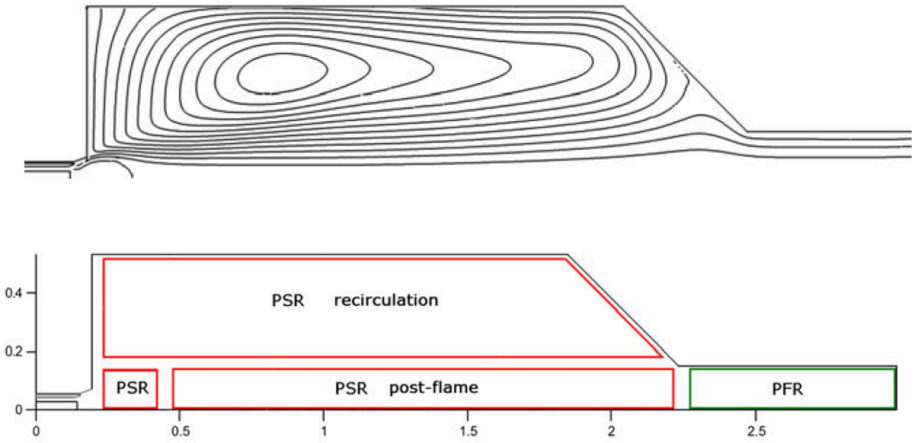


Figure 2.18: CRN [18] based on the streamlines of the furnace(top) [19]

### 2.11.3. Gas turbine modelling

The technical papers that were found describes how the authors designed a working CRN model for a non-premixed combusted gas turbine. The authors described the zones inside the combustor based on the mixture fractions gradients and the diffusive properties of the flame. These CRN designs were later used by the authors to perform parametric analysis and study the NOx emission characteristics.

- **A.B. Lebedev et al.:**

A.B. Lebedev et al in 2009[20] did a modelling study of a gas turbine combustor emission. Based on a 3-D CFD simulation, the authors designed a CRN model for a diffusion type gas turbine combustor. The combustor that was used in this model was a CIAM-M combustor from a research institute. The authors divided the whole combustor volume based on the mixture fraction gradients. They found regions with uniform values of the mixture fraction and divided those regions in the combustor volumes as domains.

The authors modelled the fuel rich regions as 1-PSR and then allowed that mixture to enter the flame front which was divided between two other-PSRs. The flame front consists of almost stoichiometric region, so fuel and air was accordingly divided and added to bring it to a stoichiometric region of combustion. Two PSRs were used to model the upstream flame front region and the downstream flame front region. The combustor volume was divided based on residence times, giving each flame front reactor a residence time and was evaluated by the following Equation [20]:

$$\tau_{res} = \frac{Flame\ \ front\ \ thickness}{Flow\ \ velocity} \tag{2.53}$$

where the flame front thickness was calculated using the following Equation:

$$Flame\ \ front\ \ thickness = \sqrt{\frac{D_T \Delta Z^2}{\chi}} \tag{2.54}$$

where, $D_T$ is the diffusion coefficient and $\Delta Z$ is taken to be 0.01 and is the difference in mixture fraction which determines if the region is above or below the stoichiometric mixture fraction (rich or lean). Figure 2.19 shows the schematic diagram of the CRN model that was designed by the authors to model the gas turbine emission. Using this CRN design they were able to validate the NOx values obtained form model with the experimental data.

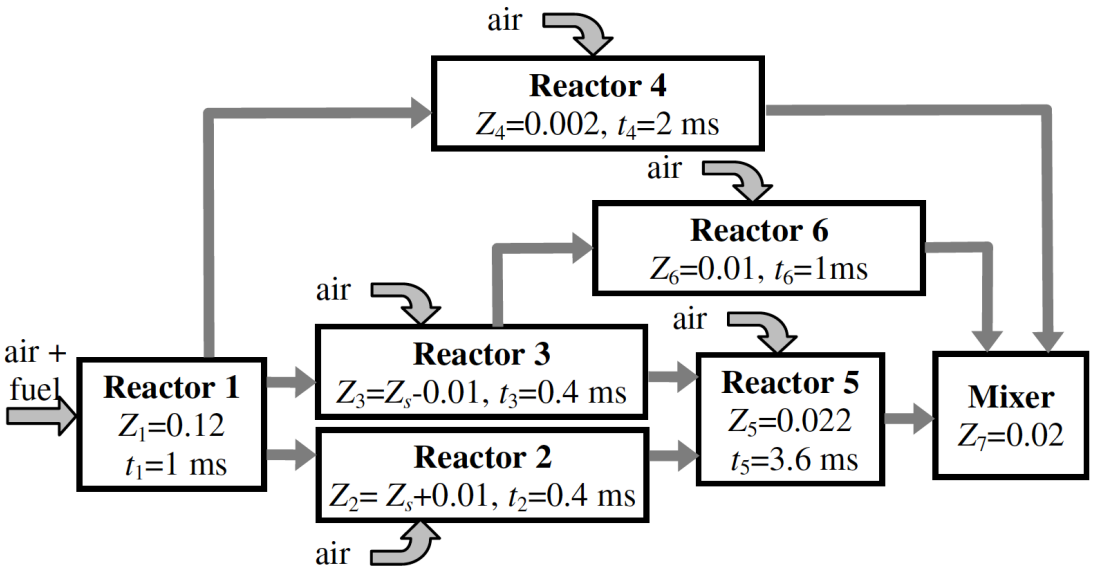


Figure 2.19: Schematic representation of a CRN model for a CIAM-M combustor [20]

- **Andreini and Facchini:**

  Andreini and Facchini in 2004[21] provided with a CRN model for a conventional diffusion flame combustors in a gas turbine. This CRN model was later then compared with the MS7001F gas turbine combustor. They used this design to understand and evaluate the NOx emissions of the gas turbine at different turbine inlet temperatures. They described that their primary zone model of the combustion chamber was derived from the idea of Broadwell and Lutz which was explained earlier in Section 2.11.1. They modelled the rest of the combustion chamber by dividing it into flame stablization zone and recirculation zone.

  The downstream flame stablization zone was modelled as a post-flame zone of PSR. This represents the axial propagation of the flame and a maximum temperature rise is developed understanding that the flame still is intact with it's diffusive properties. The authors used a PFR to model the flame zone and a PSR to model the outer-flame zone.

  As the gas turbine has a air cooling flow entry, the diffusive features of the flame are reduced and this forms the secondary zone of the combustion chamber. The authors used a PSR to model these secondary zones, and also understood that due to quenching effects caused by the reaction of small mass fractions near the combustor walls, these zones were simulated using specific PSR reactors. The authors then designed the analogous dilution zone which is towards the end of the combustor using a PFR which represents the best central flow. Figure 2.20 shows the schematic representation of the conventional diffusion flame combustor designed by the authors.

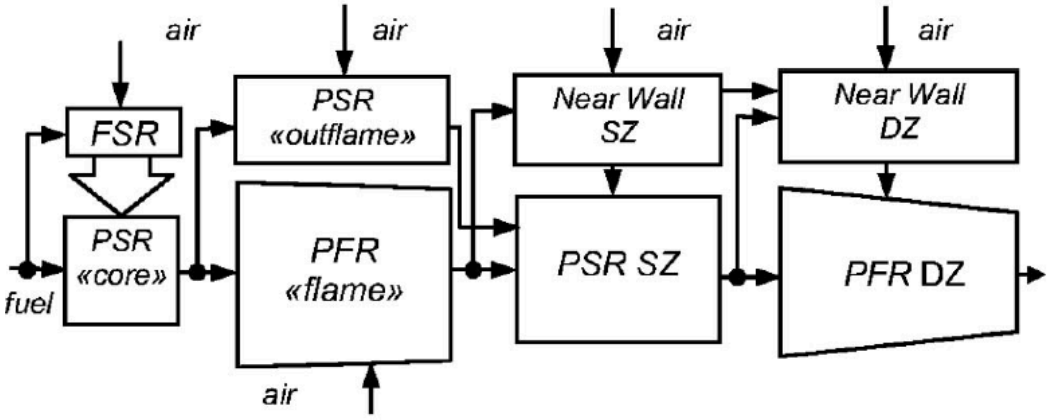


Figure 2.20: Schematic representation of a CRN model for a conventional diffusion flame combustor [21]

## 2.12. Summarizing the reviewed literature

The information that was found in this chapter lead to an understanding on how a non-premixed combustion occurs and how it can be modelled. The Burke-Schumann flame solution gave a descriptive overview on how important mixture fractions are when it comes to a diffusion flame. The mass fraction of fuel can be used as an unique function of the mixture fraction when describing a flame. At stoichiometry the fuel mass fraction is completely consumed and the rate of consumption of fuel is described by it's mixing field and the reaction field. The rate of mixing at stoichiometry is defined by the scalar dissipation rate. Scalar dissipation rate is the base parameter which is used to understand the mixing aspect of the fuel and oxidizer molecules during non-premixed combustion. Using this information the flame contour at stoichiometry can be modelled.

The emission mechanisms that occur during combustion is also understood and it assists in understanding the combustion profile better. Different methods to model the combustion process were also studied. It was understood that between CFD and CRN modelling, CRN modelling would have given an acceptable result with less computational time. Therefore, various CRN models were studied to know the design aspects of creating a successful CRN model. These CRN examples give an idea on how a non-premixed combustion can be modelled inside a gas turbine and implemented to understand the NOx emissions. These examples displayed CRN designs that models the stoichiometry contour of the flame, the recirculation zone of the flame and how mixture fraction and residence time can be used to model combustion for a gas turbine.

# 3

# Model development

From the previous chapter all the information was understood to develop a working CRN model. This chapter will discuss on how a turbulent non-premixed flame inside a combustor can be modelled using a CRN. This CRN model can capture emissions at different zones(flame zone, recirculation zone etc.) of the combustor. The CRN model takes into account different assumptions which will be discussed later in this chapter. The base of the model lies in creating the flame sheet reactor(FSR) volume. To develop a FSR volume, the theory behind it must first be understood.

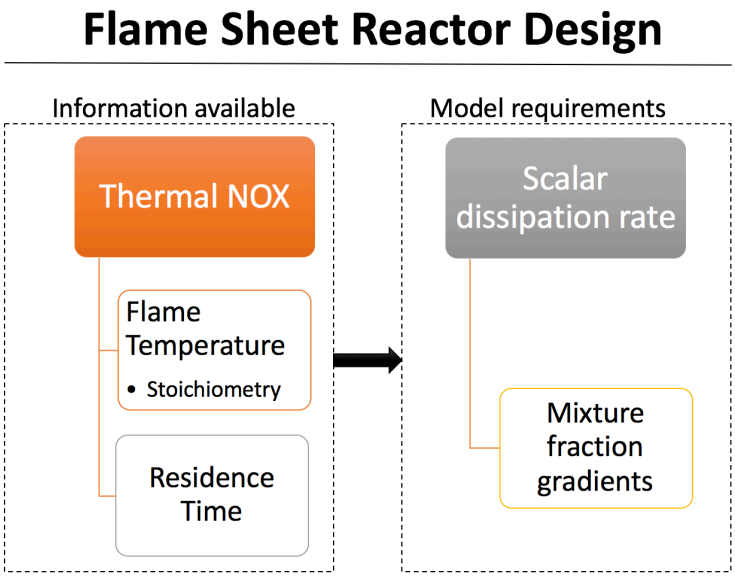


Figure 3.1: Outline of the model development.

Figure 3.1 describes on how the idea was formulated to develop the FSR design. It is a well known fact that the most common and highest NOx created is the thermal NOx in a gas turbine. Thermal NOx is described in section 2.7.1 and is released when the flame temperature is above 1850 K. When the fuel and oxidizer mixes at molecular level at stoichiometry that's where the highest flame temperature is formed in a non-premixed combustion. The time taken for the stoichiometric flame contour to be formed depends on the residence time inside the combustion chamber. Using this information that was available, lead to the parameters required to developing the model. Scalar dissipation rate provides the information of rate of mixing between the fuel and oxidizer at stoichiometry. This rate of mixing information is provided by the mixture fraction gradient (i.e.) when fuel and oxidizer molecules come

together and mix intensely inside the combustion chamber. At stoichiometric mixture fraction, the fuel and oxygen molecules are completely consumed. The diffusion of the fuel and oxidizer molecules at stoichiometric mixture fraction will give the highest flame temperature. So, using scalar dissipation rate the region where the highest flame temperature formed is computed. Using this structure, the final FSR design is developed and modelled.

## 3.1. Influence of Residence time

To design the FSR volume one of the main aspect was to understand the influence of residence time during combustion. Cantera has an inbuilt **combustor.py** program that was used to understand how the software worked and how the code was compiled. This code simulates a simple combustion where it takes two separate stream - one pure methane and the other air, both at 300 K and 1 bar to flow into an adiabatic combustor where they mix and burn. So, this program in cantera was used to understand the influence of residence time on $CH_4$, OH and NO. The program's oxidizer and fuel parameters were edited. The fuel that was defined was **Natural gas** and the oxidizer used was **AIR**. The combustor volume was specified in cantera and the following Equation was used to calculate the residence time and simulate in cantera:

$$\tau_{res}(sec) = \frac{\rho V}{\dot{m}} \tag{3.1}$$

where, $\rho$(kg/m$^3$) is the density of the products inside the PSR, V(m$^3$) is the combustor volume and $\dot{m}$(kg/sec) is the mass flow rate given to the PSR.

### 3.1.1. $CH_4$ dissolution vs Residence time

The impact of residence time on $CH_4$ was analyzed at different equivalence ratios. From the Figure 3.2 there are still some traces of $CH_4$ available after combustion for a rich fuel combustion compared to it's stoichiometric and lean combustion. As the equivalence ratio increases the amount of time required for the $CH_4$ to react and combust reduces. This is only until it reaches stoichiometric combustion as the fuel readily combusts with the exact amount of oxidizer. During rich combustion there is more fuel than oxygen which takes $CH_4$ longer to be completely consumed. During lean combustion the residence time is more for $CH_4$ to completely burn inside the PSR. So, $CH_4$ would require more time inside the PSR to burn completely.

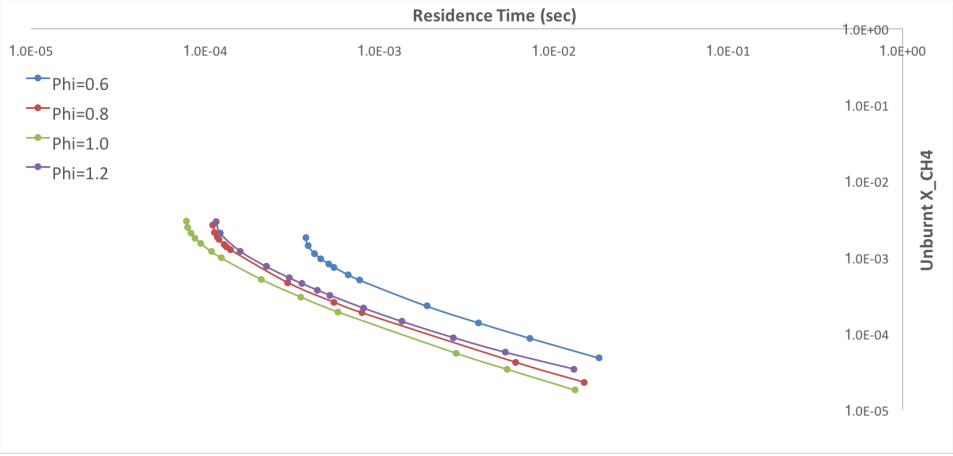


Figure 3.2: $CH_4$ vs Residence time for different equivalence ratios

### 3.1.2. OH formation and dissolution vs Residence time

OH radical plays an important role in the formation of NOx, as it acts as a bridge for nitrogen to react and form NOx. Figure 3.3 shows the formation and dissolution of the OH radical for different equivalence ratios. OH is formed earlier on during combustion and then due to increase in temperature, the OH radical bond is broken after the maximum amount of OH is formed. As the residence time increases, OH is then dissolved to 'O' and 'H' radical to go ahead and create other reaction pathways. So, at shorter residence time, it is less likely for NOx to be formed as the OH radical doesn't break.

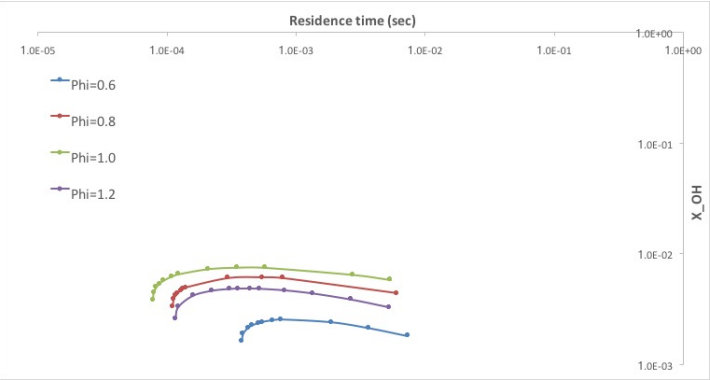


Figure 3.3: OH vs Residence time

### 3.1.3. Formation of NO vs Residence time

The impact of residence time on NO production was computed at various equivalence ratios. Figure 3.4 shows that as the residence time increases, the amount of NO formed also increases. For phi = 0.8, the NO production stops at 0.006 seconds and for phi = 1.2 it stops at 0.012 seconds. At phi = 1.0, the NO production is more than when combusting at phi = 1.2. This can be because of the stoichiometric flame temperature being more at phi=1.0 than at phi=1.2 which activates the thermal NOx mechanism. So at shorter residence times most of NO is formed after combustion. This figure also shows why lean-premixed combustion is a good technique to minimize NOx formation in a flame.

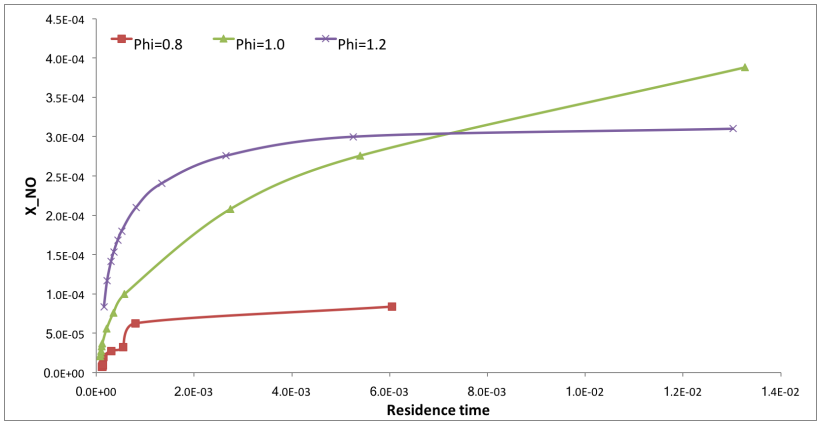


Figure 3.4: NO formation vs Residence time for different equivalence ratios

### 3.1.4. NOx vs Residence time with and without EGR at stoichiometric conditions

The influence of residence time on NOx when using EGR-oxydizer was computed. The composition that was used for EGR is- $CO_2$-1.3%, $O_2$-18.4%, $N_2$-80.1%, $H_2O$-0.2%, it is the same composition Evulet et al used to understand dry low NOx combustors using EGR [50]. Figure 3.5 shows the formation of NOx when using air and when using EGR-oxydizer. At shorter residence time there was a steep rise in NOx as the combustion is initiated. After the introduction of EGR-oxydizer, the amount of NOx that was released was less compared to taking air as an oxidizer. Due to the replacement of oxygen with EGR, the oxides of nitrogen formed were also less. This concludes that at the same residence time, EGR-oxydizer produces less NOx compared to when using air.

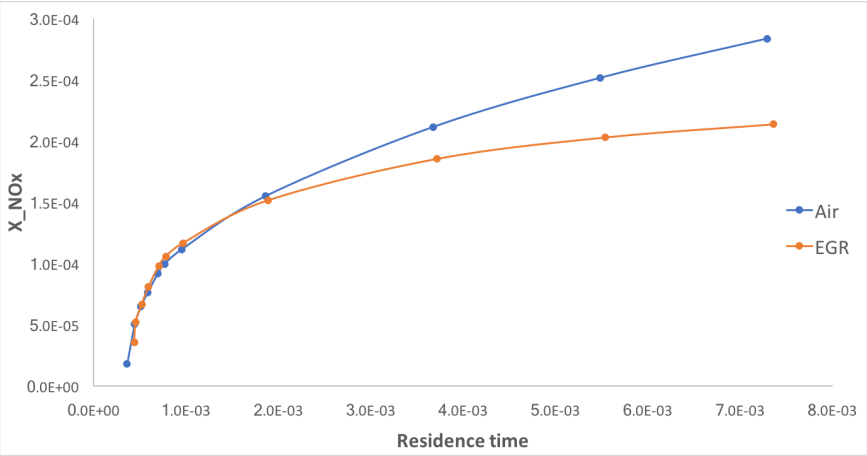


Figure 3.5: NOx vs Residence time at phi = 1

## 3.2. Reactor network model for non-premixed combustion

In a system where either the mixing rates are high or the chemical reaction rates are slow, the chemical kinetics constrains the burning rates in the mixture, and the residence time is the most important parameter of the reactor [15]. Figure 3.6 shows how a CRN model is created inside a combustor to capture the NOx emission. The flame sheet reactor is used to catch the stoichiometric flame zone (where fuel and oxidizer are combusted at stoichiometric interface), which afterwards the output of the FSR is given as an input to the the subsequent PSRs. Finally the emissions are calculated at the exit of the combustor. All the emissions simulated from each PSR is given to PFR which is created at the exhaust of the combustor. As explained in section 2.5.3, when assuming infinitely fast chemistry, the fuel and oxidizer react instantaneously thus making it independent of scalar dissipation rate. Assuming finite rate chemistry (i.e.) assuming that the chemistry is the rate-limiting step assists us in modelling the CRN using PSRs and using the scalar dissipation rate as well. In large scale modelling of combustion, this assumption does not make sense, as large scale mixing occurs. Since we model small scale mixing inside the combustion chambers using the PSRs, then this assumption becomes valid.

As the PSRs are placed away from the inlet of the combustor, the equivalence ratio decreases to a lean combustion as the combusted products from FSR is diluted with the oxidizer. By the end of the combustor, the final PSR is considered as the PSR dilution. The combusted products inside PSR dilution are at the equivalence ratio at which the user would like the combustion to take place. The reactor network was coded using python 3.4 which was loaded with cantera 2.3.0.

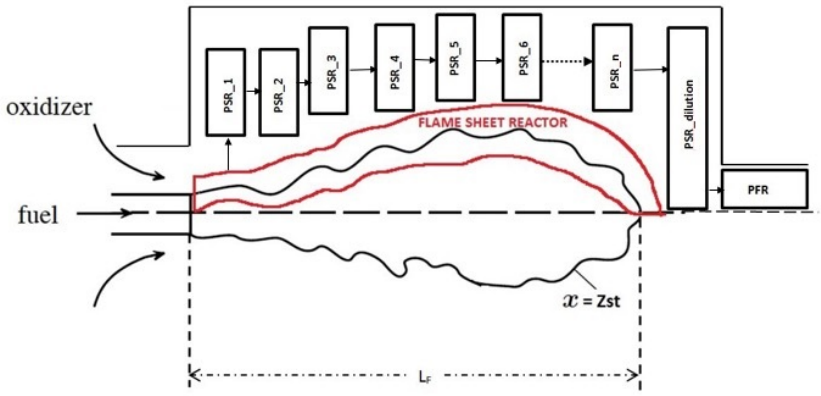


Figure 3.6: Reactor network inside the combustor

## 3.3. Determining the Flame sheet reactor volume

The finalized layout is based on the works done by Pedersen et al[17] and De Toni et al[18]. They suggested that only one recirculation PSR is required where the combusted product information can be passed on from the post-flame PSR. According to the authors the recirculation and dispersed zones are the stirred regions, while the central or the post-flame flow is more like a PFR. The final layout which was employed from the works of Pedersen et al[17] and DeToni et al[18] was more simple and gave a more accurate result. The validation of this model will be discussed more in detail in chapter 4. The final layout can be seen in Figure 3.7. It is the CRN model that is used to perform a parametric and sensitivity analysis.

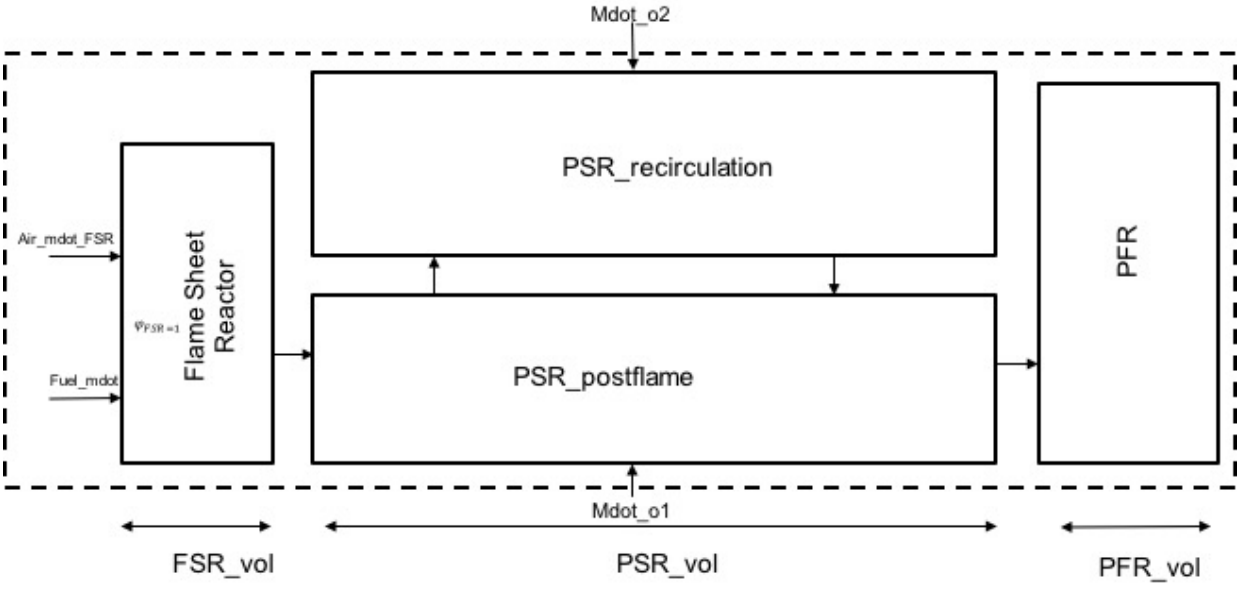


Figure 3.7: The Final CRN model

### 3.3.1. Determining the scalar dissipation rate

Sections 2.5 and 2.5.3 discusses how scalar dissipation rate is an important factor in turbulent non-premixed combustion. As mentioned scalar dissipation explains the rate of mixing that happens when the mixture of fuel and oxidizer is diffused within each other and is given as follows [5]:

$$\chi_{st} = 2D_T(\frac{\partial Z_{st}}{\partial x})^2 \tag{3.2}$$

where $D_T$ is the turbulent mass diffusion rate, and $\frac{\partial Z}{\partial x}$ is the mixture fraction gradient in the flame. The following parameters that are defined are used to construct the model.

- **Turbulent diffusion rate:** Although turbulent diffusion rate needs to be known to calculate the scalar dissipation rate, some assumptions given by Turns [15] is taken to equate turbulent diffusion rate to eddy viscosity. For an axisymmetric turbulent jet flow, Stephen R. Turns[15] derives the value for eddy viscosity as $\nu_{turb} = 0.0285 * U_{turb}R_F$. By assuming Schmidt number, Lewis number and Prandtl number to be unity, one can substitute turbulent momentum diffusivity for turbulent mass diffusivity and thermal diffusivity [15] (i.e.)

  $$D_T = \nu_{turb} = 0.0285 * U_{turb}R_F \tag{3.3}$$

  where $U_{turb}$ is the incoming turbulent fuel velocity and $R_F$ is the radius of the fuel nozzle.

- **Mixture fraction gradient:** The flow information of the species is contained in the scalar dissipation rate. Applying all the empirical information and experiment found by Schlicting et al in 2000[22] which shows that for an axisymmetrical turbulent jet, dZ/dx = dZ/dr = $1/\triangle r = 1/\delta_{99\%} = 1/(2.5r_{1/2})$. Where $\delta_{99\%}$ is the half-width of the jet that is measured from the centerline to the radial location where maximum axial velocity has decayed by 1%. Also, $r_{1/2}$ is the jet radius where the axial velocity has fallen to half of it's value. Figure 3.8 shows the measurements that were taken to understand the relationship between $r_{1/2}$ and the maximum axial velocity.

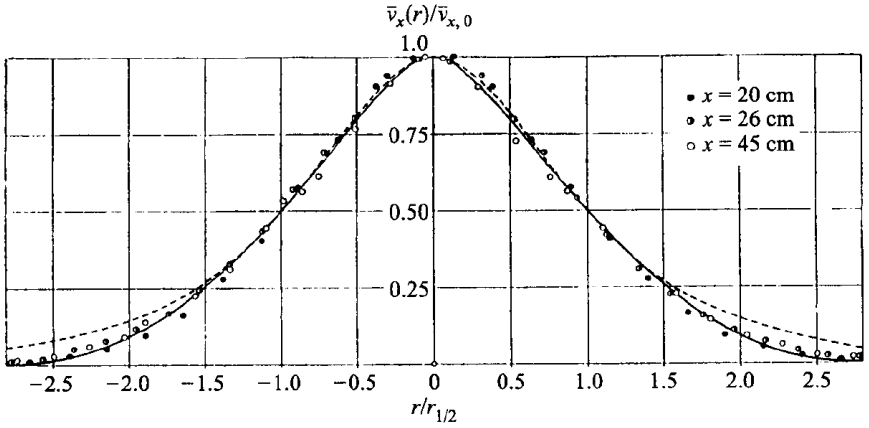


Figure 3.8: Radial profile for an axial velocity for a turbulent jet [22].

The turbulent jet's velocity decay and spreading rate does not depend on the Reynold's number unlike the laminar diffusion flames [15] as long as the jet is a fully developed turbulent flow. Assuming that the jet spreading rate contains the information of the mixture fraction gradient, and according to Turns,[15] the jet spreading rate for an axisymmetric turbulent jet is :

$$r_{1/2}/x = 0.08468 \tag{3.4}$$

Where, x is the axial distance from the centre of the jet. Evaluating the equation closer to the lip of the nozzle where the maximum diffusion takes place when fuel and oxidizer come in contact with each other(10% of the length of the flame), then the final half-width of the jet would become:

$$\delta_{99\%} = 2.5 * 0.08468 * 0.1 * L_F \tag{3.5}$$

**Flame Length:** Different definitions were found in the literature to understand the length of the flame. Investigators performed experiments on turbulent diffusion flames/jet flames to understand this definition. The definition used by these investigators for flame length in non-premixed combustion is that it is the axial location when the mean mixture fraction is at it's stoichiometric point on the flame axis. Froude number is one of the important dimensionless number while understanding the length of the flame. Froude number describes a relation between the initial jet momentum flux to that of the external buoyant forces that is incurred during combustion. The factors that affect the flame length can be characterised as follows [15]:

- Importance of initial jet momentum flux and buoyant forces acting on the flame, Froude number.
- Stoichiometry in which the flame is combusted ($F_{st}$).
- Ratio of nozzle fuid to ambient gas density, $\rho_F/\rho_\infty$.
- Initial jet diameter, $d_j$.

Flame length can finally be calculated by the following Equation:

$$L_F = \frac{L^* d_j^*}{F_{st}} \tag{3.6}$$

$L^*$ is a dimensionless flame length. If Froude number $\geq 5$ then $L^* = 23$, if it is less than 5:

$$L^* = \frac{13.5 * Fr^{2/5}}{(1 + 0.07Fr^2)^{1.5}} \tag{3.7}$$

$d_j^*$ is the momentum diameter and is calculated by:

$$d_j^* = d_j * (\frac{\rho_F}{\rho_O})^{1/2} \tag{3.8}$$

Calculating the jet flame length first depends on the Froude number [15]

$$Fr = \frac{U_F * (f_{st})^{3/2}}{(\frac{\rho_F}{\rho_O})^{1/4}[\frac{T_{ad} - T_{in}}{T_{in}} * g * d_j]^{1/2}} \tag{3.9}$$

where, $U_F$ is the velocity of the incoming fuel; $\rho_F$ and $\rho_O$ is the density of the fuel and the oxidizer respectively; $d_j$ is the incoming jet nozzle exit diameter; $T_{ad}$ is the adiabatic flame temperature; and $F_{st}$ is the stoichiometric fuel-to-air ratio. From Figure 3.9 different flame lengths are observed for different fuels used. These correlations formed can be used to extract the dimensionless flame length.

From Figure 2.7, it is evident that the fuel mass fraction reaches it's stoichiometric mixture fraction when there is no more fuel left to burn. Equation 3.5 can be used to represent the mixture fraction gradient at stoichiometry. The scalar dissipation rate which is Equation 3.2 can be re-written as follows:

$$\chi_{st} = 2 * 0.0285 * U_{turb} * R_F * (\frac{1}{2.5 * 0.08468 * 0.1 * L_F})^2 \tag{3.10a}$$

$$\chi_{st} = \frac{1.27 * U_{turb} * R_F}{(0.1L_F)^2} \tag{3.10b}$$

where $U_{turb}$ is the incoming turbulent fuel velocity and $R_F$ is the radius of the fuel nozzle.

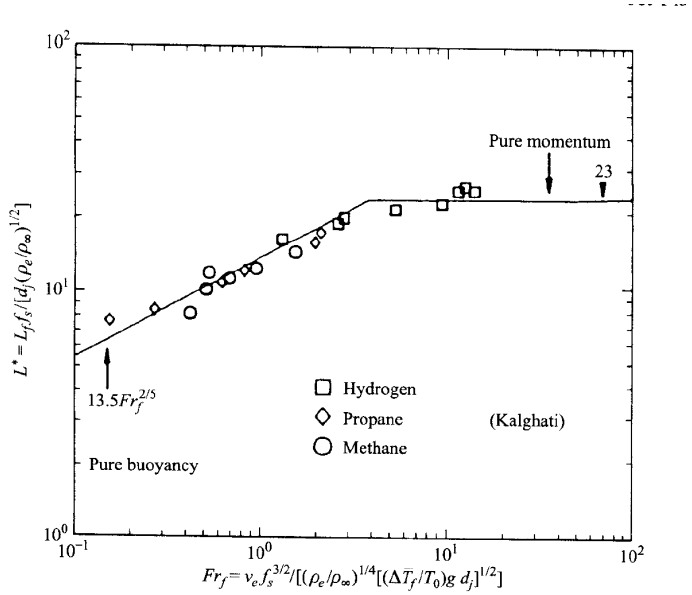


Figure 3.9: Flame lengths for jet flames correlated with Froude number, [23].

### 3.3.2. Flame sheet reactor volume

The flame sheet reactor is defined by using scalar dissipation rate which contains the information of rate of mixing of fuel and oxidizer. Scalar dissipation rate at stoichiometry is what is used to create the FSR volume. For calculating the amount of consumption of the fuel species at $Z_{st}$, Equation 2.24 is integrated across the volume of the field where the stoichiometric reaction occurs (i.e.) at Z = $Z_{st}$.

$$\dot{m}_F = \int \frac{1}{2}\rho_{(z=z_{st})}\chi_{(z=z_{st})}\frac{1}{1-Z_{st}}\delta(Z=Z_{st})dV \tag{3.11}$$

The volume of the FSR depends on the mass flow rate of the fuel as well as it's density which is evident from Equation 3.11. Therefore, the volume of FSR at stoichiometry depends on the mixing and the reaction field and is given by:

$$V_{FSR} = \frac{2\dot{m}_F(1-Z_{st})}{\rho_{(z=z_{st})} * \chi_{(z=z_{st})}} \tag{3.12}$$

## 3.4. Constructing the CRN model

### 3.4.1. Flow Chart

Figure 3.10 describes how the program would calculate and display the emission results. It starts with defining all the parameters which are the combustor dimensions, fuel and oxidizer composition, input flow rates and finally the temperature and pressure at which the fuel and oxidizer is combusted. The program would take all these parameters and calculate the stoichiometric equivalence ratio and the equivalence ratio. The program will then take the combustor dimensions and use the information to calculate the scalar dissipation rate and thus calculating the FSR volume.

With all this information the program divides the FSR, PSR and PFR volume accordingly and also divide the oxidizer flow rate for FSR and each PSR. FSR and the PSRs are defined as the reactor network.The program then iterates this reactor network until the FSR reaches it's steady state and then gives the information as an input to the PFR. All the emissions are calculated at the output of the PFR.

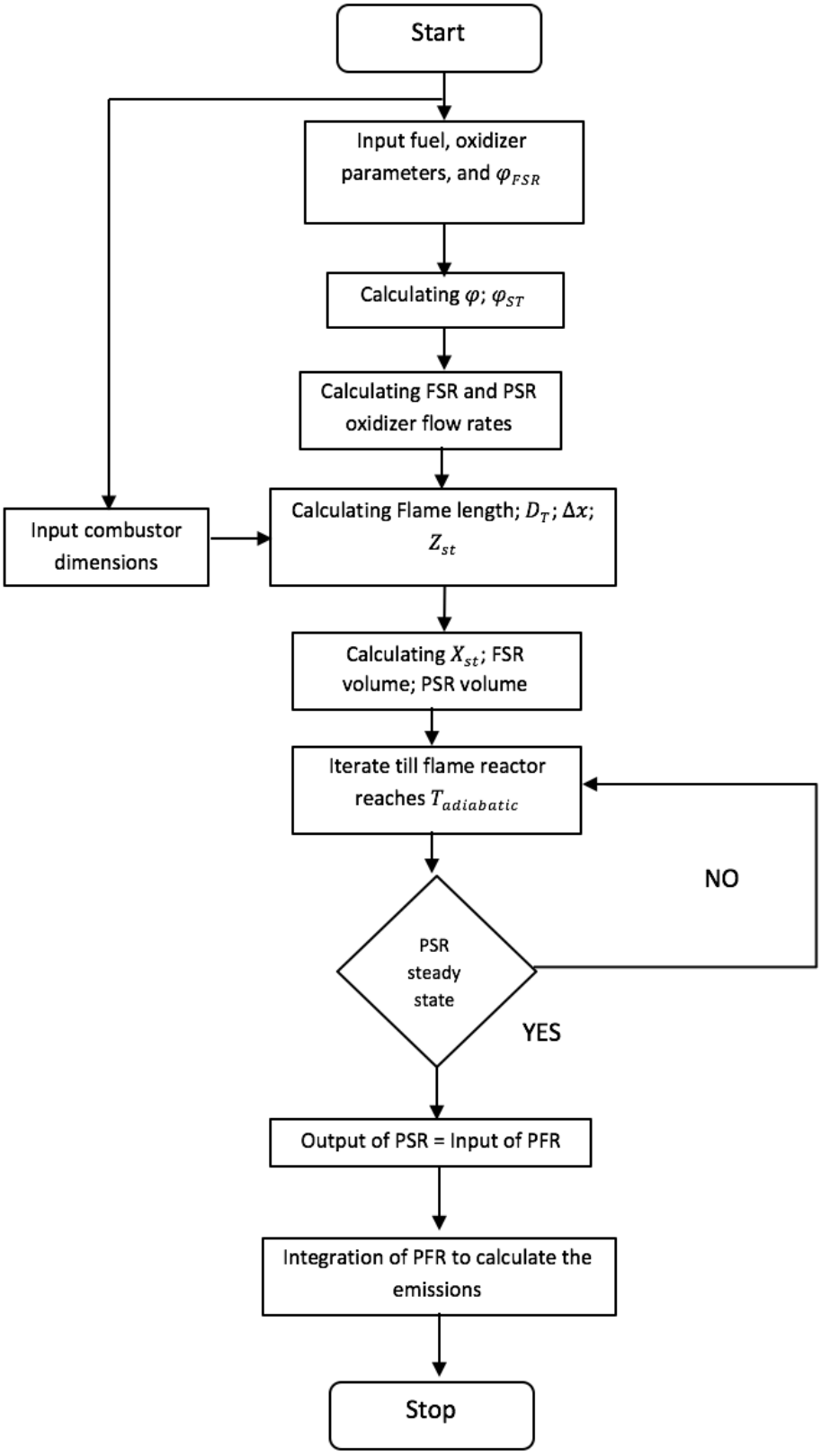


Figure 3.10: Flow chart to simulate the model in Cantera

### 3.4.2. Volume factors

Volume factors are calculated to divide the combustor volume between the FSR, PSR and the PFR. The following Equation is used to create the FSR volume factor inside the combustor:

$$FSR\ \ volume\ \ factor = \frac{V_{FSR}}{Volume\ \ of\ \ combustor} \tag{3.13}$$

Since emissions are calculated from the output of PFR, 50% of the combustor is used to define the PFR volume, (i.e.) PFR volume factor = 0.5. The rest of the combustor is divided between the PSRs.

$$PSR\ \ volume\ \ factor = 1 - (FSR\ \ volume\ \ factor + PFR\ \ volume\ \ factor) \tag{3.14a}$$

$$V_{PSR} = PSR\ \ volume\ \ factor * Volume\ \ of\ \ combustor \tag{3.14b}$$

$$Volume\ \ of\ \ each\ \ PSR, V_{PSRn} = \frac{V_{PSR}}{Number\ \ of\ \ PSRs} \tag{3.14c}$$

### 3.4.3. Initial assumptions

The following assumptions are taken into account while modelling the CRN:

- Mixing time is smaller than the chemical reaction time ($\tau_{mixing} < \tau_{chemical}$).
- All mixtures are ideal gas mixtures and modeled with ideal gas reactors.
- Adiabatic combustion is assumed and that there is no heat loss or cooling air in the dilution zone to reduce the temperature.
- Molecular transport of species, momentum and thermal energy is neglected compared to turbulent transport.
- The combustion that takes place inside the FSR is modelled to have achieved the highest adiabatic flame temperature.

Taking all of these assumptions into account, a CRN network is developed and used to understand the NOx emissions of a gas turbine for a diffusion flame.

### 3.4.4. Splitting the combustor volume in volume factors

The combustor volume was split based on initially the FSR volume factor and the PFR volume factor as given in Equation 3.13 and 3.14a. Whatever the volume of the PSR that was found, it was divided equally between PSR postflame and PSR recirculation. The flame, post-flame and recirculation zone which determines the intense mixing and turbulence effects, will be represented by the PSRs. The downstream zone where only radial mixing takes place and not axial mixing is represented by a PFR. This splitting of the flame in the combustor between PSR and PFR was proposed also by V.Prakash[13]. The splitting of the combustor volume has been shown as the final CRN model and can be seen in Figure 3.7.

The flame zone is mainly covered by the FSR and the PSR. The flame zone comprises of the flame sheet which is modelled using FSR, where the stoichiometric flame contour is formed. For modelling the stoichiometric flame contour, a perfectly stirred reactor is used and this specific PSR is called as the flame sheet reactor(FSR). The immediate post-flame zone and the recirculation zone is modelled using the PSR as the information from the FSR is passed on to PSR while computing the zones. The parameters involved in creating the CRN model has been carefully chosen. These choices have been validated in section 4.1 using an industrial furnace case study.

### 3.4.5. Air distribution between FSR and PSR

The air distribution between the FSR and PSR is one of the main functions that this model does. Equivalence ratio is the base at which the air is distributed among the FSR and the PSR. First the fuel to air ratio is found at stoichiometry, this will give the air required to burn the incoming fuel at stoichiometry. To calculate the air required to burn the oxidizer in FSR, Equation 2.34 is rearranged:

$$\dot{m}_{air,FSR} = \frac{\dot{m}_F}{\phi_{FSR} * F_{st}} \quad @(\phi_{FSR} = 1) \tag{3.15}$$

After the required air flow rate is calculated to burn at stoichiometry, rest of the air is divided equally among the PSRs. From Figure 3.7 it can be understood that the FSR is burnt at equivalence ratio of 1, and as the rest of the air is distributed equally. The combustion that takes place becomes leaner at post-flame PSR and then leaner at recirculation PSR. After reaching it's prescribed equivalence ratio, the information is passed from the PSR postflame to the PFR.

### 3.4.6. Initial settings for the CRN network

After setting the volumes of the reactors, each reactor is connected to each other by a mass flow controller. The post-flame PSR is connected to an exhaust reservoir defined in the model by using a valve. This is done so that a constant combustor pressure is maintained which can be seen from Figure 3.11

The igniter is a reservoir which is filled with H radicals. This igniter is used to combust the fuel-oxidizer mixture and is numerically modelled as a gaussian time varying mass flow of H radicals. Once the combustion is self-sustained the model makes the stream to die out after a certain period. The igniter does not alter composition of the emission but it can rather be seen as a starter for the flame to sustain. The igniter is modelled using the following Equation:

$$\dot{m}_{igniter}(t) = Ae^{\frac{4log(2)}{fwhm^2}(t-t_0)^2} \tag{3.16}$$

Table 3.1 displays the initial conditions set for the flame reactor, the convergence critieria, and the initial setting used to model the flame in cantera. The values of the valve coefficient and the igniter amplitude are chosen based on trial and error method and also by reducing the stiffness problem in the code.

Table 3.1: Initial settings given to the code in cantera

| Input | Unit | Value |
|---|---|---|
| Chemical Mechanism | - | GRI-Mech 3.0 |
| Convergence criteria | K | $T_{t+\Delta t}$-$T_t$ = 0.02 |
| Fuel | - | Natural Gas |
| Valve coefficient | kg/s-Pa | 1E-5 |
| Igniter amplitude | - | 0.01 |
| PFR volume factor | - | 0.5 |

### 3.4.7. CRN model

The way cantera compiles the whole CRN model can be seen in Figure 3.11. This figure is the same as Figure 3.7, but it just shows the different streams from the reservoirs that flow into the FSR, PSR post-flame and PSR-recirculation. There is a feedback loop provided between the PSR postflame and PSR recirculation that can be controlled by the USER(0% to 100%). The emissions are calculated and taken from the PFR.

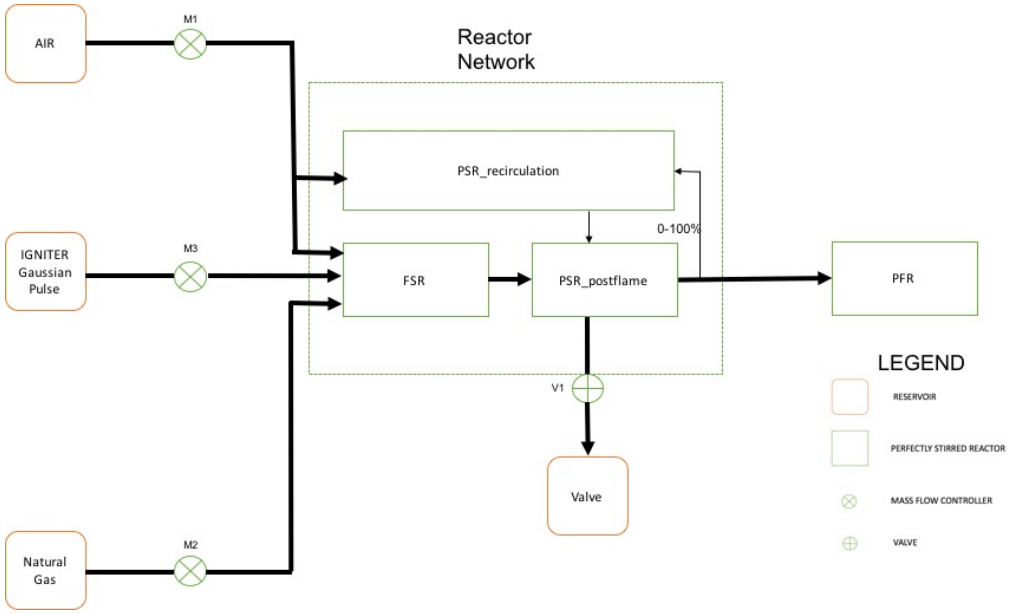


Figure 3.11: Reactor network model as seen by cantera

The CRN model was modified to implement water/steam injection and the updated CRN model can be seen from Figure 3.12. A new reservoir which contains water either in it's liquid phase or vapour phase is created. The amount of water to be injected into FSR is controlled by the USER (0% to 100%) and the rest of the water is equally distributed between PSR postflame and PSR recirculation. The USER has the ability to toggle between injecting water in it's liquid phase or vapor phase(Steam).

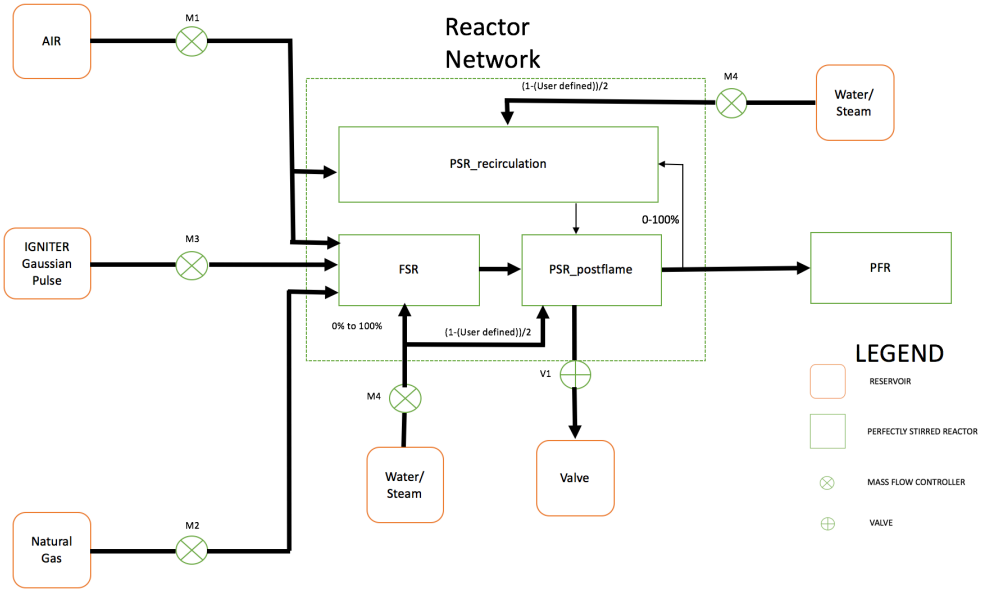


Figure 3.12: Reactor network model incorporating water/steam injection as seen by cantera

# 4

# Validation

This chapter discusses on how different experimental and technical data which was available in the combustion community validates the developed CRN model. This gives the model more robustness, which will allow the user to simulate different combustion scenarios in gas turbines. The composition of natural gas that was used for the purpose of validation can be seen from Table 4.1

Table 4.1: Composition of Natural Gas

| Compound | Mole fraction % |
|---|---|
| $CH_4$ | 96.5% |
| $C_2H_6$ | 1.7% |
| $C_3H_8$ | 0.2% |
| $CO_2$ | 0.3% |
| $N_2$ | 1.3% |

## 4.1. Case-I: BERL 300kW Industrial Gas Burner (S.Orsino and R.Weber)

This technical paper was primarily used to scale the natural gas flames to improve burner design to reduce the NOx emissions. As shown in Figure 3.7, the schematics of the burner and the furnace were adapted from Orsino et al[24] and Silva[19]. This was used by DeToni et al[18] to model a CRN for a BERL 300kW inustrial gas furnace(Figure 4.1) based on the experimental and CFD results of the furnace and presents a parametric NOx analysis.

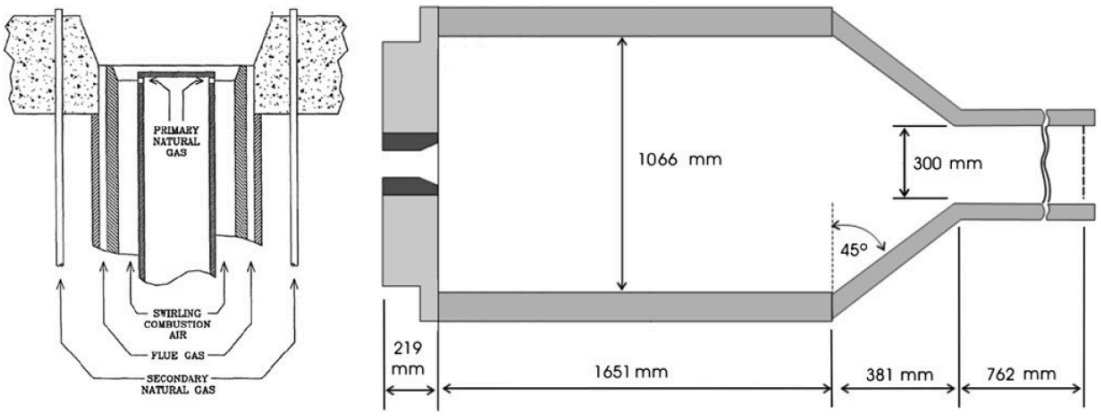


Figure 4.1: Burner and Furnace of the Berl 300kW test [19, 24]

The technical CRN model paper by De toni et al[18] describes a furnace that uses non-premixed combustion and provides all the available data required to simulate the model. Table 4.2 displays all the operational parameters that was used to simulate the model. The combustor dimensions are taken from Figure 4.1.

Table 4.2: Operational parameters for BERL-300kW, [18].

| Parameters | Units | Value |
|---|---|---|
| **Combustor parameters** | | |
| Diameter of combustor | meter | 1.066 |
| Length of combustor | meter | 2.016 |
| Pressure | Pa | 1E5 |
| **Fuel parameters** | | |
| Fuel | - | Natural gas |
| Diameter of fuel inlet | meter | 0.144 |
| Inlet temperature | Kelvin | 308.15 |
| Fuel flow rate | kg/sec | 0.00637 |
| **Oxidizer parameters** | | |
| Oxidizer | - | Air |
| Diameter of oxidizer inlet | meter | 0.174 |
| Inlet temperature | Kelvin | 312.5 |
| Air flow rate | kg/sec | 0.13022 |

The CRN model data results and the experimental data was compared and can be found in Table 4.3. This concludes that the developed CRN model can simulate emissions which gives values very close to the experimental ones.

Table 4.3: Comparison of experimental data to the model data results

| Quantity | Experimental data | CRN model data |
|---|---|---|
| Flame temperature (Kelvin) | 1945.0 | 1935.0 |
| External recirculation zone temperature (Kelvin) | 1350.0 | 1395.0 |
| NOx emission (g NOx /kg NG ) | 1.3 | 1.6 |

The model data values were compared with experimental values and also the results from different mechanisms. Figure 4.2 shows the comparison of different mechanisms with the experimental data. It can be seen that the NOx emission is a bit higher compared to the experimental data. This can be because of the mechanism GRI mech 3.0 that was used to solve the emission. Even though Konnov 4.0 gives results closer to the experimental values, GRI-mech 3.0 is still used. This was done because GRI-mech 3.0 follows the same trend and the mechanism was easy to use and load in cantera.

Using the same combustor of the industrial furnace all the sensitivity analysis was performed on the developed CRN model to understand the influence of each parameter on the NOx emission. This is to show that the developed CRN model can give acceptable and appreciable results.

### 4.1.1. Formation of NOx

NOx formation was first understood using the developed CRN model. Figure 4.3 shows how majority of the NOx was formed at the FSR. The highest temperature was recorded at the FSR and gradually reduces as it exits the combustor. As the program is simulated through the whole CRN network, the NOx that was recorded by the PFR at the combustor exit is only 35% of the total NOx formed.

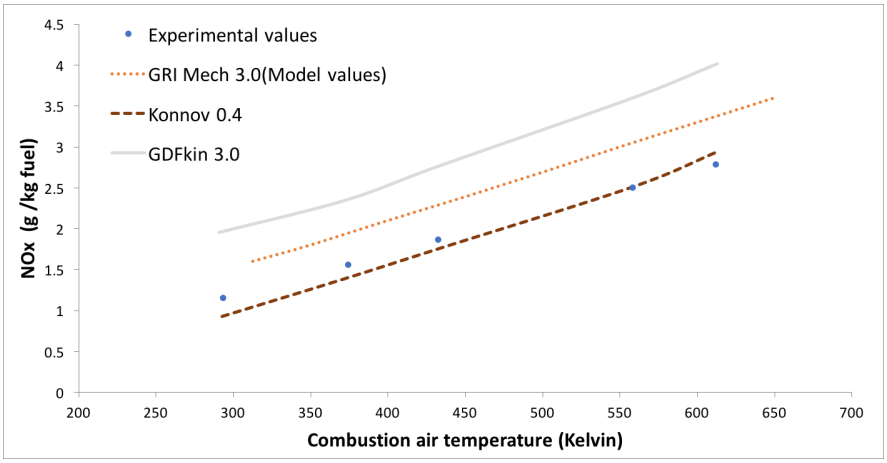


Figure 4.2: NOx levels: Experiment vs Model,[18].

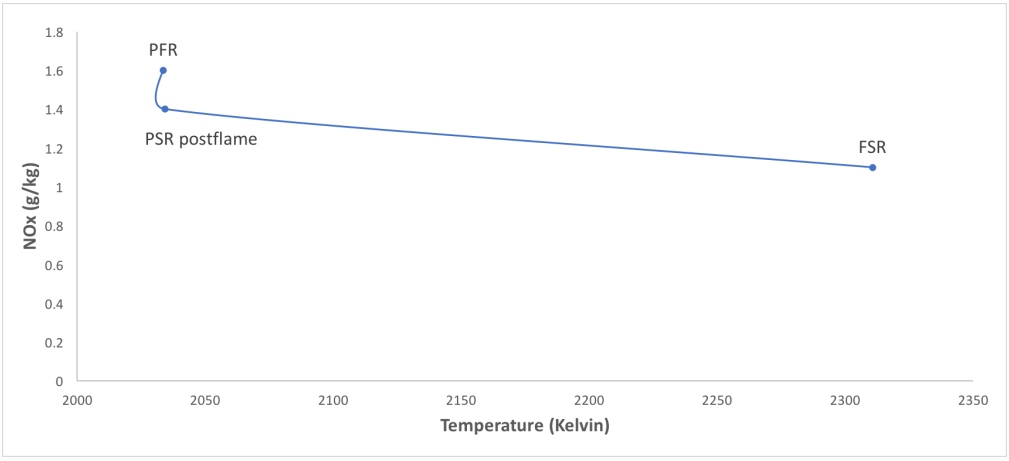


Figure 4.3: Evaluation of NOx through CRN

Figure 4.4 shows the reaction path of Nitrogen element since the start of the combustion to the combustor exit (i.e) from FSR to PFR. The reaction path shows how the 'N' as a radical breaks and then attaches with 'O' radical to form different compounds. When the arrow is thicker and darker, it represents more contribution to forming that radical or compound. The figure shows that the most contribution towards formation of NO is from 'N' radical. Equation 2.35c shows the thermal NOx chemical reaction. This concludes that the model can simulate thermal NOx mechanisms.

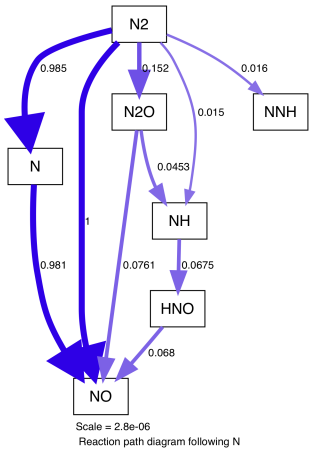


Figure 4.4: Reaction path of Nitrogen

### 4.1.2. Sensitivity analysis of combustor splitting

The combustor volume is equally split between the PSRs(FSR, PSR post-flame, PSR recirculation) and the PFR. However, a sensitivity analysis is done to understand the influence of splitting the combustor volume on the NOx emission. The sensitivity analysis was compared to that of the experimental values of the BERL-300kW test which can be seen in Figure 4.5. It was noticed that the closest trendline to the NOx values was with the PSRs having 30% of the combustor volume and PFR having 70% of the combustor volume. Nevertheless, the outcome of the sensitivity analysis shows us that the trend is the same. This allows the CRN model to use the 50-50 combustor volume split.

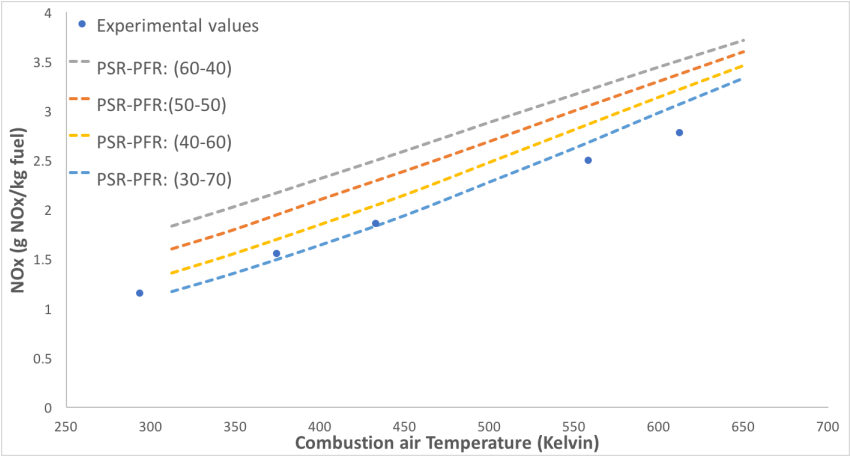


Figure 4.5: Effect of splitting the combustor between PSR and PFR on NOx emissions

### 4.1.3. Sensitivity analysis of FSR volume

Since most of the NOx is formed in the FSR, the volume of the FSR had to undergo a sensitivity analysis on it's influence on NOx emissions. Figure 4.6 shows the increase of the FSR volume to twice it's original calculated volume. The volume of the PSR also depends on the volume of the FSR, so the sensitivity analysis first took place by varying the FSR volume alone from -50% to +100%. However, while performing this analysis the PSR volume was kept constant. It was observed that as the volume of FSR increases the NOx emissions also increases. So the NOx emissions do also depend on the FSR volume.

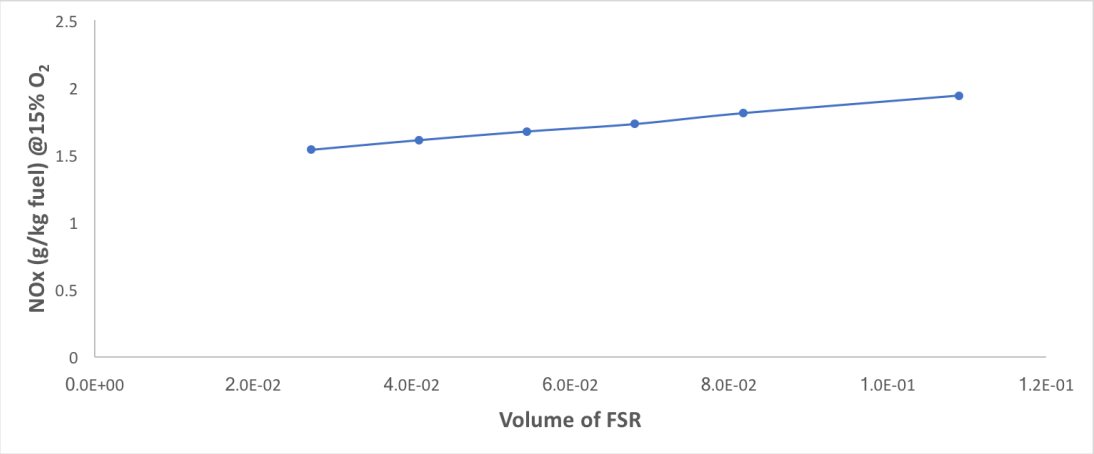


Figure 4.6: Varying FSR volume from -50% to +100% and it's effect on NOx

The FSR volume was then varied while it was also varying the PSR volume. From Figure 4.7 it can be seen again that there is influence on the NOx emissions by varying the FSR volume from -50% to +100% of the calculated FSR volume. The analysis shows the dependence of NOx on the FSR volume and how important FSR volume is in controlling the NOx emissions.

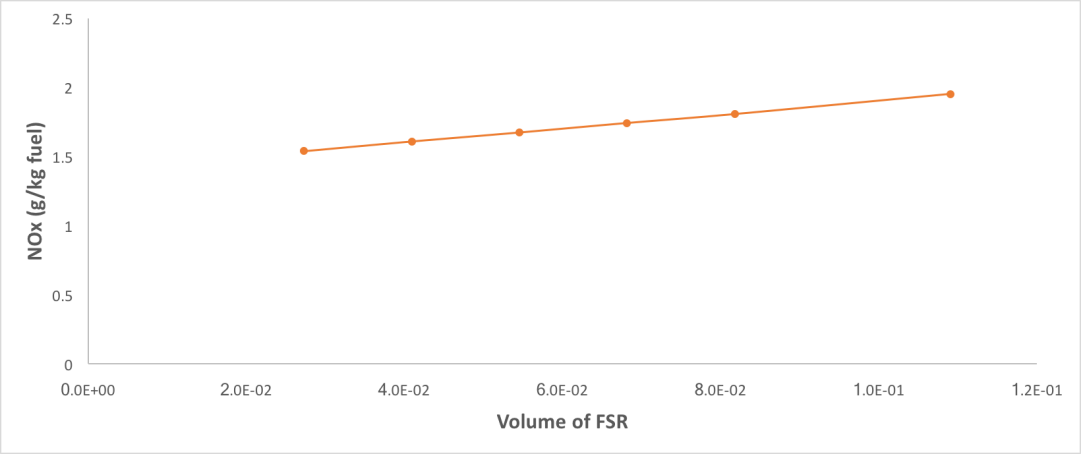


Figure 4.7: Varying FSR volume and PSR volume from -50% to +100% and it's effect on NOx

### 4.1.4. Sensitivity analysis with the recirculation between the PSRs

The percentage of recirculation between PSR post-flame and PSR recirculation was increased. Due to this the NOx emission also reduced gradually. This was because the combusted products were able to react with the oxidizer coming into PSR recirculation. As more combusted products reacted with the oxidizer in the PSR recirculation, different chemical pathways were formed thus reducing emissions. Thus validating that the recirculation between PSR-postflame and PSR-recirculation can be used to reduce NOx emissions. This can be seen as recreating the recirculation zone inside the combustor.

After carefully analyzing the sensitivity of each parameter the final CRN model was created(Figure 3.7). The gas turbine conducted researches were used to validate the developed CRN model. Using this model, the parametric analysis has been performed for a gas turbine to determine the impact of NOx on gas turbines when using EGR-oxydizer.

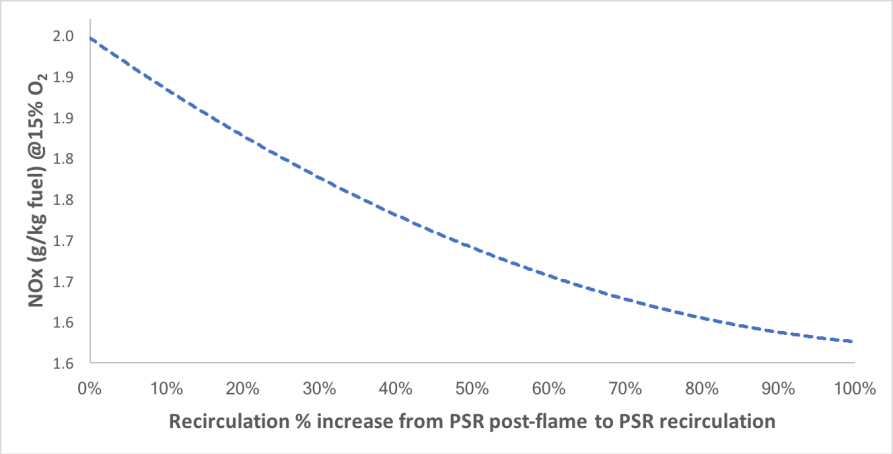


Figure 4.8: Effect of NOx emission when increasing Recirculation from 0% to 100%

### 4.1.5. Sensitivity analysis of Exhaust temperature vs $CO_2$%

The primary objective of this thesis research was to check the influence of exhaust gas recirculation on NOx. Oxygen was replaced with $CO_2$ and a sensitivity analysis was performed. Figure 4.9 shows the change in flame temperature and exit temperature with increasing $CO_2$ content in oxidizer. The replacement of $O_2$ with $CO_2$ led to a reduction in NOx as $CO_2$ is an inert gas altering the reaction kinetics.

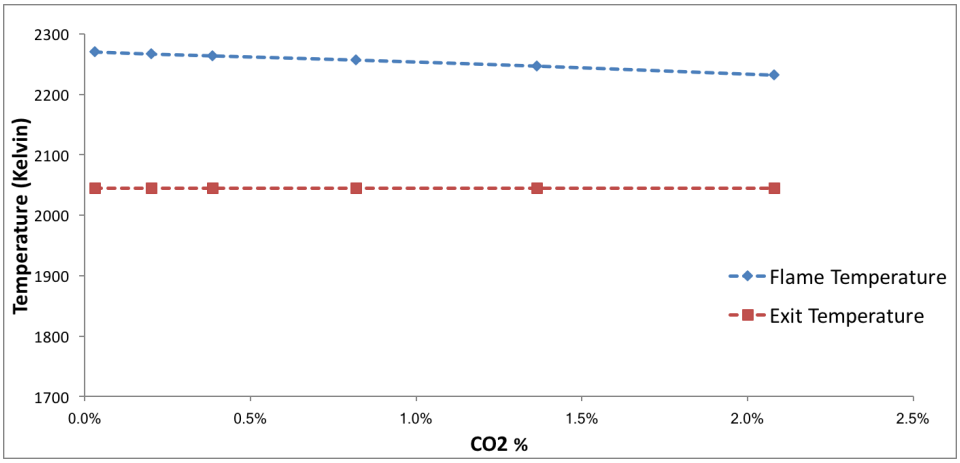


Figure 4.9: Effect of $CO_2$% on exhaust and stoichiometric flame temperature

The increase in $CO_2$% led to an obvious reduction in NOx emission as seen in Figure 4.10. The stoichiometric fuel to air ratio reduces as there is an increase in $CO_2$ content thereby increasing the amount of oxidizer to be burnt with the fuel at stoichiometry. Thus, the NOx formation reduces as the flame temperature reduces.

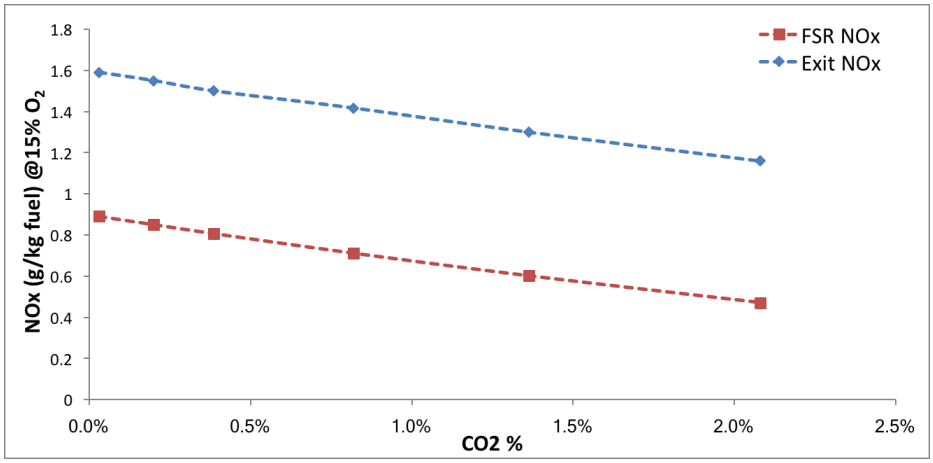


Figure 4.10: Effect of $CO_2$% on NOx

Figure 4.11 shows as stoichiometric flame temperature reduces so does the NOx production. The NOx production calculated at both the FSR and the PFR shows a reduction along with stoichiometric flame temperature reduction. This shows that the developed CRN model can incorporate EGR in it's oxidizer and can thus reduce NOx emissions.

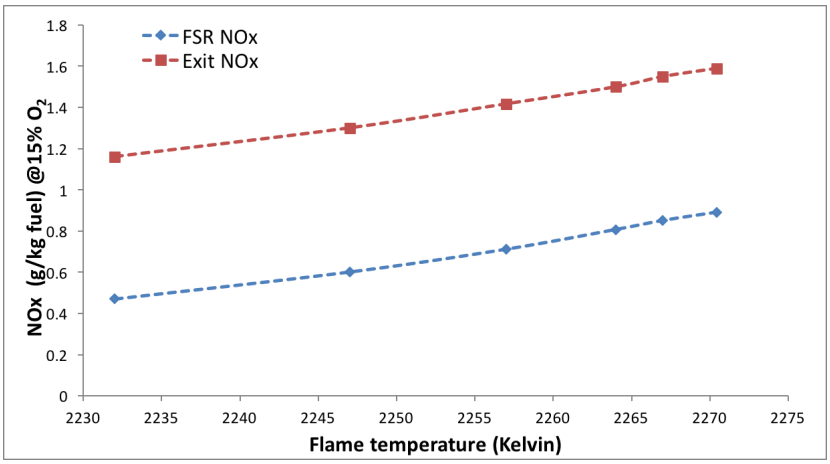


Figure 4.11: Flame temperature vs NOx

## 4.2. Case-II: Direct fuel injection burner for Gas Turbines (Terasaki et al)

An experiment was conducted using a Direct fuel-injection burner for gas turbine combustors by Terasaki et al to understand the NOx emission [25]. They used a unique double swirler burner and compared it to the traditional small-hub swirl and a large-hub swirl burner. Since, the double-hub swirl burner swirls the incoming oxidizer flow twice, it is assumed that it would be a premixed flame. As this research covers only non-premixed combustion, the model data was compared to the data obtained from a non-premixed small-hub swirl burner.

The incoming oxidizer temperature was varied between 650 Kelvin and 950 Kelvin with an inlet oxidizer velocity of 10m/sec. Keeping the incoming air flow rate constant and using Equation 2.34, the fuel flow rate was found for different equivalence ratios. The operational parameters that was used to obtain the emissions are given in Table 4.4 and the schematic diagrams of the combustor and burners (double swirler and small-hub swirler) can be seen from Figure 4.12.

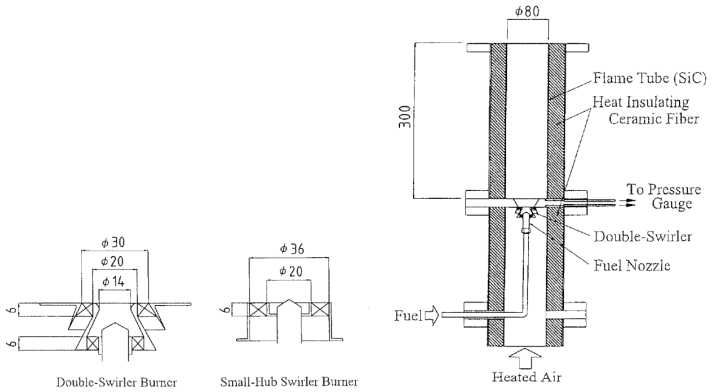


Figure 4.12: Schematic diagram of the experimental burner [25]

Table 4.4: Operational parameters of the Direct fuel injection burner for GT,[25]

| Parameters | Units | Value |
|---|---|---|
| **Combustor parameters** | | |
| Diameter of combustor | meter | 80E-3 |
| Length of combustor | meter | 0.3 |
| Pressure | Pa | 1E5 |
| **Fuel parameters** | | |
| Fuel | - | Natural gas |
| Diameter of fuel inlet | meter | 20E-3 |
| Inlet temperature | Kelvin | 300 |
| Fuel flow rate | kg/sec | 0.00617 |
| **Oxidizer parameters** | | |
| Oxidizer | - | Air |
| Diameter of oxidizer inlet | meter | 36E-3 |
| Inlet temperature | Kelvin | 650/950 |
| Air flow rate | kg/sec | 0.11399 |

Figure 4.13 shows the comparison of the experimental data obtained from the paper to that of the CRN model that was simulated. The trend shows that as the fuel flow rate increases, NOx emissions also increases. There is especially steep increase in NOx after equivalence ratio of 0.5 with an inlet air temperature of 950 Kelvin. Although, the data values between the experimental and model varies, the trend appears to be the same. This variation in data can be due to the type of burner that was used while performing the experiment. The model doesn't take into account different types of swirl burners that are used in gas turbines and only a general overview of the recirculation zone caused due to a swirl induced combustion.

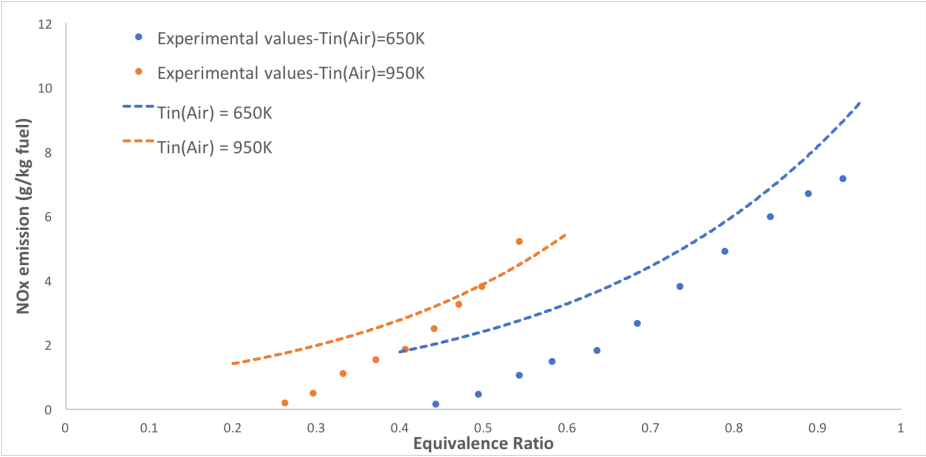


Figure 4.13: Comparison of experimental data vs model data

The correlation between the experimental data and model data was made to understand the strength of the relation between the variables. Table 4.5 and 4.6 show the correlation for air inlet temperature 650 Kelvin and 950 Kelvin respectively. As the correlation between the variables are closer to +1, it means that they are strongly related to each other. That is if one parameter increases, then the other parameter strongly increases along with it or it means that both the parameters strongly depend on each other.

Table 4.5: Correlation between experimental data and model data for Air inlet temperature of 650 Kelvin

| | Experimental phi | Experimental NOx | Model phi | Model NOx |
|---|---|---|---|---|
| **Experimental phi** | 1 | | | |
| **Experimental NOx** | 0.9786 | 1 | | |
| **Model phi** | 0.9959 | 0.9598 | 1 | |
| **Model NOx** | 0.9392 | 0.9186 | 0.9414 | 1 |

Table 4.6: Correlation between experimental data and model data for Air inlet temperature of 950 Kelvin

| | Experimental phi | Experimental NOx | Model phi | Model NOx |
|---|---|---|---|---|
| **Experimental phi** | 1 | | | |
| **Experimental NOx** | 0.9946 | 1 | | |
| **Model phi** | 0.9997 | 0.9939 | 1 | |
| **Model NOx** | 0.9987 | 0.9902 | 0.9987 | 1 |

## 4.3. Case-III: Study of MS5002 gas turbine combustor (Feitelberg et al)

A laboratory diffusion flame combustor was developed similar to that of the MS5002 gas turbine combustor[27]. This is to understand the difference in the NOx emitted between the standard MS5002 combustor and the laboratory developed combustor. The experiment was performed with two different air flow rates. The air flow rates were 5.4 kg/sec and 3.3 kg/sec at 5 bar and 3.1 bar respectively.

The NOx emission was plotted with respect to the combustor exit temperature. Since, the fuel flow rates weren't provided, using a simple energy balance Equation(Equation 4.1) the fuel flow rates were calculated.

$$\dot{m}_F * LHV_F = (\dot{m}_O + \dot{m}_F) * Cp * \Delta T \tag{4.1}$$

The combustor dimensions were taken from [26], but the fuel inlet diameter wasn't specified. The dimensions were estimated based on the standard fuel injectors for MS5002 GT. The operational parameters can be seen in Table 4.7. Figure 4.14 shows the dimensions of the combustor and the schematic diagram of laboratory MS5002 combustor test stand.

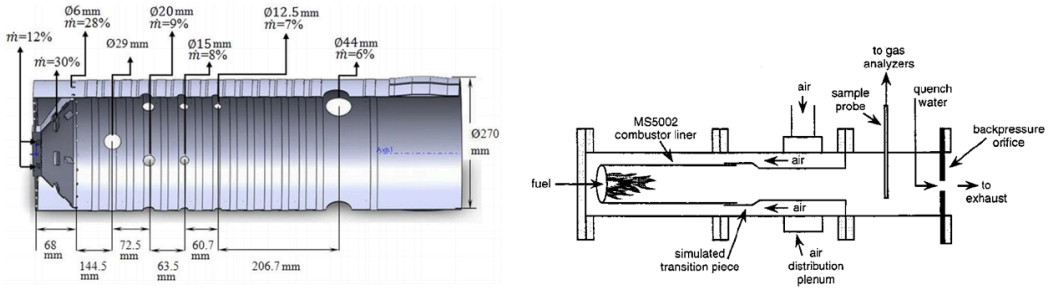


Figure 4.14: Schematic diagram of MS5002 combustor(left) [26], and the laboratory test stand(right) [27]

Table 4.7: Operational parameters used for MS5002 GT, [27].

| Parameters | Units | Value |
|---|---|---|
| **Combustor parameters** | | |
| Diameter of combustor | meter | 40.5E-2 |
| Length of combustor | meter | 112E-2 |
| Pressure | Pa | 3.1E5/5.0E5 |
| **Fuel parameters** | | |
| Fuel | - | Natural gas |
| Lower heating value | kJ/kg | 53,700 |
| Diameter of fuel inlet | meter | 4.4E-2 |
| Inlet temperature | Kelvin | 300 |
| **Oxidizer parameters** | | |
| Oxidizer | - | Air |
| Diameter of oxidizer inlet | meter | 27E-2 |
| Inlet temperature | Kelvin | 573 |
| Air flow rate | kg/sec | 3.3/5.4 |

Figure 4.15 displays the experimental data for a standard MS5002 combustor compared to that of the model data. The trend between the experimental results and the results obtained from simulating the CRN model seems to be the same. Since the trend is validated, the CRN model is considered to be a working model.

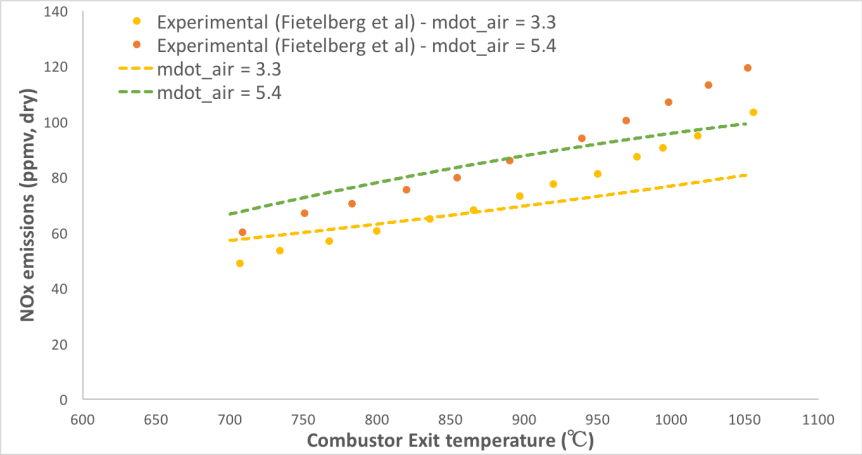


Figure 4.15: Comparison of experimental data vs model data for MS5002 GT combustor

A correlation between the experimental data and model data was analyzed to understand how strongly the two data are related to each other. This can be seen in Tables 4.8 and 4.9 for air flow rate of 3.3 kg/sec and 5.4 kg/sec respectively.

Table 4.8: Correlation between experimental data and model data for air flow rate of 3.3 kg/sec

| | Experimental temperature | Experimental NOx | Model temperature | Model NOx |
|---|---|---|---|---|
| **Experimental temperature** | 1 | | | |
| **Experimental NOx** | 0.9925 | 1 | | |
| **Model temperature** | 0.9866 | 0.9938 | 1 | |
| **Model NOx** | 0.976 | 0.984 | 0.993 | 1 |

Table 4.9: Correlation between experimental data and model data for air flow rate of 5.4 kg/sec

| | Experimental temperature | Experimental NOx | Model temperature | Model NOx |
|---|---|---|---|---|
| **Experimental temperature** | 1 | | | |
| **Experimental NOx** | 0.9934 | 1 | | |
| **Model temperature** | 0.9858 | 0.9908 | 1 | |
| **Model NOx** | 0.9903 | 0.9856 | 0.9953 | 1 |

The correlation for the data lies between +1 and -1. The closer the correlation lies to +1, it means that the two variables are strongly related to each other. Which means if both the parameters are closer to +1, then if one parameter increases, then the other parameter will also increase. If the parameters are closer to -1, then if one reduces then the other will also definitely reduce.

## 4.4. Case-IV: $H_2$ enriched flames in diffusion combustors (Cozzi et al)

An experiment was conducted to understand the influence of hydrogen enriched combustion in a diffusion combustor [28]. In a co-flow configuration the fuel was burnt at ambient temperature and pressure. A fuel mixture of natural gas and volumetric fraction of hydrogen ranging from 0% to 100% was used. The operational parameters used for the model can be seen in Table 4.10. Figure 4.16 shows the schematic diagram of the laboratory developed combustor.

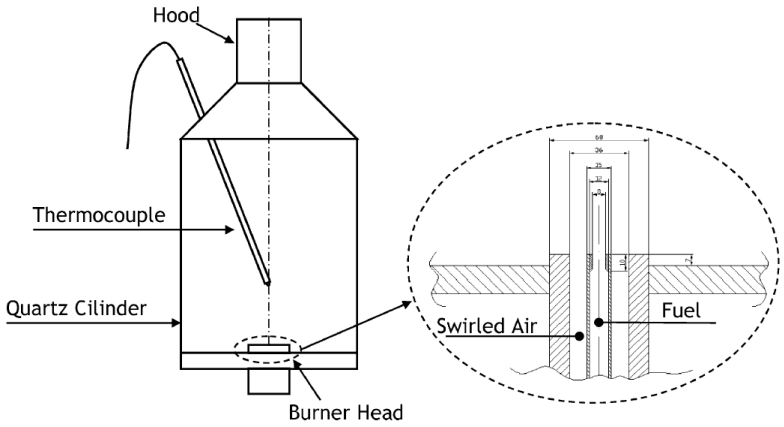


Figure 4.16: Schematic diagram of the combustor, dimensions are in millimeters [28]

Table 4.10: Operational parameters for the $H_2$ enriched GT combustor,[28].

| Parameters | Units | Value |
|---|---|---|
| **Combustor parameters** | | |
| Diameter of combustor | meter | 0.192 |
| Length of combustor | meter | 0.3 |
| Pressure | Pa | 1E5 |
| **Fuel parameters** | | |
| Fuel | - | Natural gas/$H_2$ |
| Fuel flow rate | kg/sec | 0.425E-3 |
| Diameter of fuel inlet | meter | 8E-3 |
| Inlet temperature | Kelvin | 300 |
| **Oxidizer parameters** | | |
| Oxidizer | - | Air |
| Diameter of oxidizer inlet | meter | 36E-3 |
| Inlet temperature | Kelvin | 300 |
| Air flow rate | kg/sec | 9.48E-3 |

The hydrogen volume fraction was increased in the model and at the same time equally reducing the volume fraction of natural gas. The experiments were carried out at different equivalence ratios for different volume fraction of $H_2$. Figure 4.17 shows the comparison between the experimental results that were conducted to that of the results given by the CRN model simulation.

It is seen that when the hydrogen content in the fuel mixture reached 80%, there was a maximum NOx emission that was attained. Cozzi et al explained that even though temperature along the burner axis was reduced, the mean temperature that was measured near the burner head showed a blue flame zone. This blue flame zone increased by 50% when hydrogen was added to the fuel mixture which justifies the higher NOx(thermal) that was produced. This CRN model that was developed was used to check the validation of $H_2$ as a fuel as it can be a future fuel replacement source. The model data

seem to follow the experimental data trend, but there is still a difference in the values. This can be because GRI mech-3.0 mechanism was used, but further study needs to be performed with different chemical mechanisms to bring the values closer to each other.

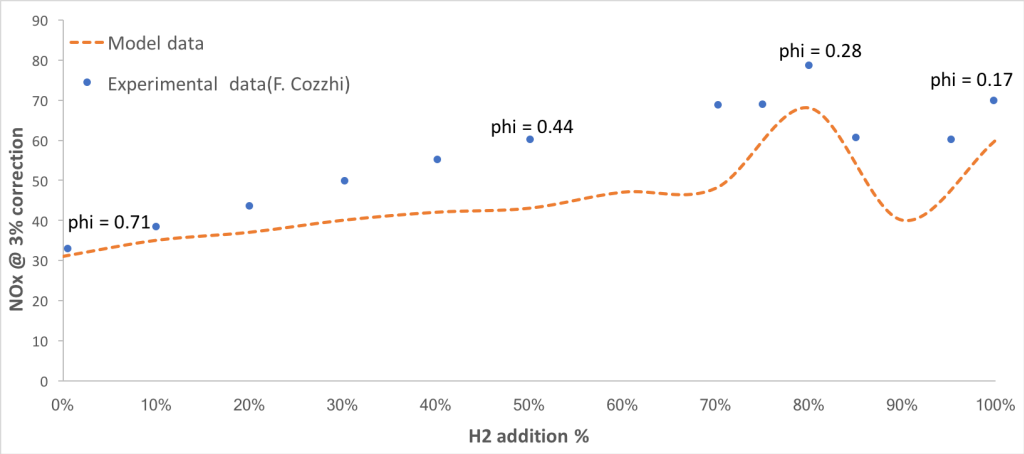


Figure 4.17: Comparison of experimental data vs model data for $H_2$ enriched non-premixed combustion

A correlation data for this study can be seen in Table 4.11 to understand the strength of the relationship between the variables from experimental data and the model data.

Table 4.11: Correlation between experimental data and model data

| | Experimental temperature | Experimental NOx | Model temperature | Model NOx |
|---|---|---|---|---|
| **Experimental $H_2$%** | 1 | | | |
| **Experimental NOx** | 0.8802 | 1 | | |
| **Model $H_2$%** | 0.9921 | 0.8287 | 1 | |
| **Model NOx** | 0.7796 | 0.8232 | 0.7716 | 1 |

## 4.5. Case-V: Validation of water injection for a LM2500 Gas Turbine:

Injecting water or steam allows the reduction of flame temperature and therefore also assists in reducing NOx. This method is widely used especially in non-premixed combusted gas turbines to keep NOx below the required level. LM2500 gas turbine is used in Akzo Nobel and it uses a non-premixed combustor (also known as SAC combustor). The data required to validate this study was obtained from Akzo Nobel with the help of Prof. Dr. Ir. S. A. Klein. While performing this validation study, the CRN model from Figure 3.12 was used. Figure 4.18 shows the schematic diagram of the combustion chamber. There are a total of 30 fuel injectors/air swirler combinations which can also be seen from Figure 4.19. The operational parameters for each combustor that was used to validate this study can be seen from Table 4.12.

Table 4.12: Operational data that was used to validate the case study, Source:[Akzo Nobel]

| MW | Air flow rate (kg/sec) | Fuel flow rate (kg/sec) | Water injection (kg/sec) | Pressure (bars) | Air inlet temperature (° C) | Fuel inlet temperature (° C) |
|---|---|---|---|---|---|---|
| 19.19 | 1.77 | 0.047 | 0.0205 | 17.02 | 446 | 60 |
| 19.74 | 1.8 | 0.0482 | 0.028 | 17.23 | 449 | 60 |
| 19.79 | 1.81 | 0.049 | 0.037 | 17.46 | 454 | 60 |
| 15.2 | 1.64 | 0.038 | 0.0092 | 15.3 | 434 | 60 |
| 15.09 | 1.65 | 0.039 | 0.023 | 15.5 | 436 | 60 |

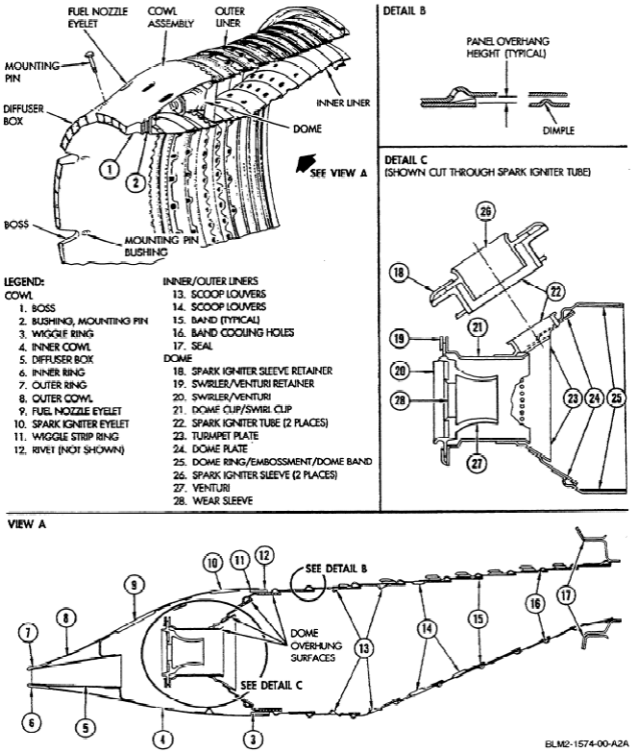


Figure 4.18: Schematic of a LM2500GT combustion chamber, Source:[Akzo Nobel].

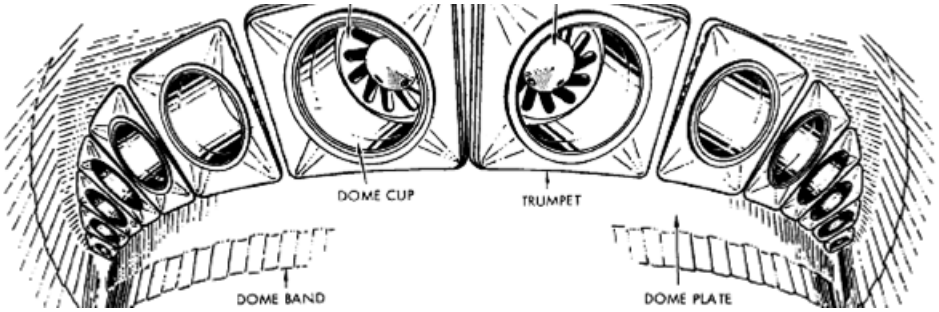


Figure 4.19: Schematic of the fuel injection/air swirler, Source:[Akzo Nobel].

Table 4.13 shows the combustor dimensions that was used in calculating the volume of the chamber. The diameter of the air and fuel nozzle weren't available, so based on the schematics that were shown above it was intuitively guessed and incorporated into the model.

Table 4.13: Combustor dimensions

| **Parameters** | **Unit** | **Value** |
|---|---|---|
| Length of the combustor | meter | 1 |
| Internal diameter of the combustor | meter | 0.2 |
| Overall diameter of the combustor | meter | 0.5 |
| Diameter of the air nozzle | meter | 0.08 |
| Diameter of the fuel nozzle | meter | 0.007 |

Experimental data and the values obtained from the model data were plotted together and can be seen from Figure 4.20. Since, the combustor fuel nozzle and air nozzle diameter were intuitively estimated, the volume of the FSR was accordingly modified along with the amount of water to be injected into the FSR. This was done so that the model data curve can come as close as possible to the experimental data curve.

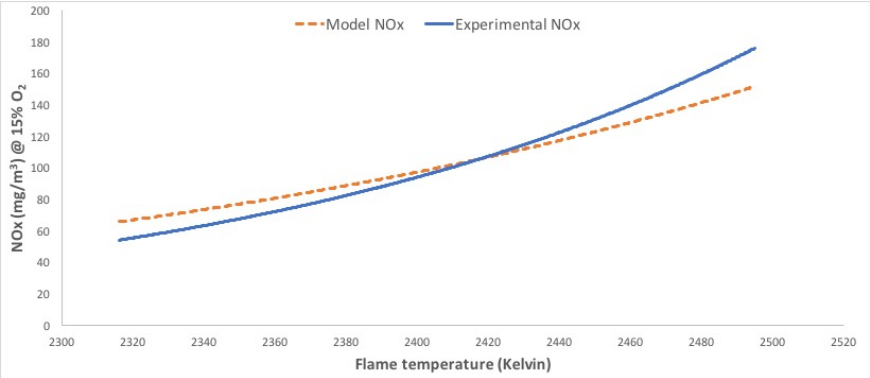


Figure 4.20: Comparison of Experimental data Vs Model data for 19 MW and 15 MW load

To understand the robustness of the model and how much fuel can be saved using EGR an analysis was performed. This analysis shows how the water injection can be saved and thus saving fuel. The NOx emissions were kept at a set reference value of 75 mg/m$^3$. At this newly set NOx value, the water injection was calculated when EGR-oxydizer was used and compared to that when air was used. It was noticed that as the $CO_2$ levels increased in the oxidizer, the amount of water required to bring the NOx levels down below 75 mg/m$^3$ reduced as well and this can be seen from Figure 4.21. When 14% of EGR was recirculated ( $CO_2$% at 1.3% in the oxidizer), 3% of the fuel was saved due to the reduction of water injection into the combustor for 19 MW and 15 MW load.

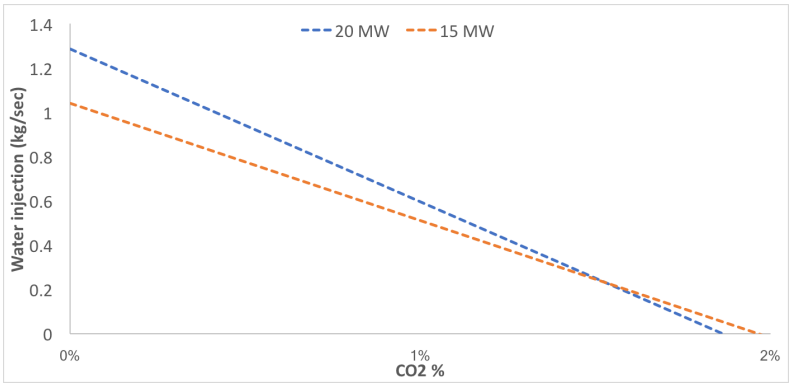


Figure 4.21: Amount of water required with respect to $CO_2$% to bring the NOx levels below 75 mg/m$^3$

# 5

# Parametric study and Results

To understand the influence of EGR on emissions, the combustor dimensions from MS5002 gas turbine(Section 4.3) is used for the parametric analysis. The combustor dimensions are given in Table 4.7 and the schematic diagram for the combustor can be seen in Figure 4.14. The composition of natural gas that was used for this parametric analysis is the same as which was used for validation of the model(Table 4.1).

## 5.1. Part load operations

To maintain a set turbine inlet temperature and at the same time reduce emissions, EGR is used in the oxidizer when gas turbines operate at part load. For every part load operation, the oxidizer composition changes to accommodate the EGR composition so that the required turbine inlet temperature is generated. This study analyses the NOx and CO emitted by the gas turbine at part load compared to it's full load operation. Table 5.1 gives all the data that was used in the model to calculate the emissions.

Table 5.1: Parameters for exhaust gas recirculation at different part load operations

| **GT load** | **Unit** | **100%** | **91%** | **83%** | **75%** | **68%** | **64%** | **63%** | **54%** |
|---|---|---|---|---|---|---|---|---|---|
| **Fuel and air input parameters** | | | | | | | | | |
| **Fuel flow** | kg/s | 2.36E-03 | 2.20E-03 | 2.08E-03 | 1.96E-03 | 1.87E-03 | 1.81E-03 | 1.79E-03 | 1.67E-03 |
| **Air flow** | kg/s | 1.24E-01 | 1.17E-01 | 1.12E-01 | 1.07E-01 | 1.03E-01 | 9.98E-02 | 9.90E-02 | 9.50E-02 |
| **TiT** | Kelvin | 1377.5 | 1377.5 | 1377.5 | 1377.5 | 1377.5 | 1377.5 | 1377.5 | 1354.55 |
| **P combustor inlet** | bar | 11.56 | 10.96 | 10.48 | 10.04 | 9.66 | 9.376 | 9.307 | 8.883 |
| **T combustor inlet** | Kelvin | 618.75 | 633.65 | 648.65 | 664.65 | 678.75 | 689.15 | 691.65 | 701.55 |
| **Composition of oxidizer** | | | | | | | | | |
| **Mole percent of $N_2$** | % | 77.29 | 77.02 | 76.7 | 76.29 | 75.74 | 75.16 | 74.99 | 73.9 |
| **Mole percent of $O_2$** | % | 20.74 | 19.98 | 19.05 | 17.87 | 16.32 | 14.66 | 14.16 | 11.05 |
| **Mole percent of $CO_2$** | % | 0.03 | 0.3755 | 0.796 | 1.33 | 2.031 | 2.784 | 3.01 | 4.42 |
| **Mole percent of $H_2O$** | % | 1.009 | 1.697 | 2.534 | 3.597 | 4.993 | 6.491 | 6.94 | 9.747 |
| **Mole percent of Ar** | % | 0.9309 | 0.9276 | 0.9237 | 0.9187 | 0.9122 | 0.9052 | 0.9031 | 0.89 |

### 5.1.1. NOx study

NOx emissions were calculated at the end of every gas turbine load. Figure 5.1 shows how much the NOx reduces when introducing EGR-oxydizer during part load operations. One of the major reasons behind NOx emission in non-premixed combustion is due to the high temperature. This shows that the replacement of oxygen with EGR composition lowers the stoichiometric flame temperature.

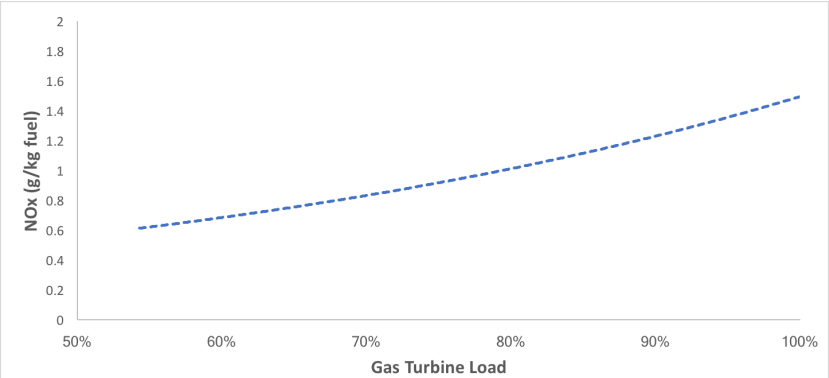


Figure 5.1: NOx changes with respect to gas turbine load

Introduction of EGR is suppose to maintain a good turbine inlet temperature while reducing the stoichiometric flame temperature. Figure 5.2 shows the changes in flame temperature and turbine inlet temperature as the gas turbine load increases. The heat energy which is released from combusting oxygen and fuel is reduced. This high heat energy breaks the 'N' triple bond to form NOx also known as Thermal NOx. Thermal NOx is the key mechanism in NOx production inside the gas turbine. Thus understanding that EGR reduces stoichiometric flame temperature but still maintains an acceptable TiT

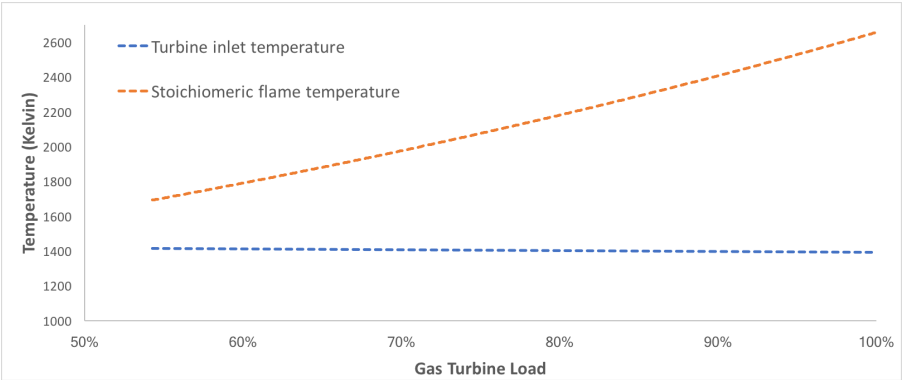


Figure 5.2: Stoichiometric flame and Turbine inlet temperature with respect to gas turbine load

The decrease in stoichiometric flame temperature during the part load operation limits the Thermal NOx mechanism. Figure 5.3 shows the decrease of NOx as there is a decrease in flame temperature. So, NOx is linearly proportional to the stoichiomeric flame temperature.

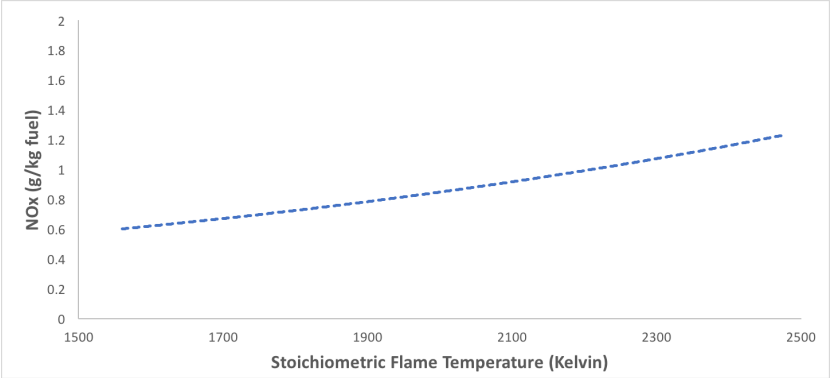


Figure 5.3: NOx emission with respect to the stoichiometric flame temperature

The impact of replacing oxygen with EGR in combustion is looked into. Figure 5.4 shows how the stoichiometric fuel to air ratio increases with increase in the gas turbine load. The stoichiometric fuel to air ratio increases with the reduction in gas turbine load. As the oxygen levels reduces and the amount of $CO_2$% increases in the oxidizer, the absence of oxygen leads to requiring more oxidizer to complete stoichiometric combustion. Thus introducing part load operations with EGR-oxydizer results in requiring more oxidizer to complete stoichiometric combustion.

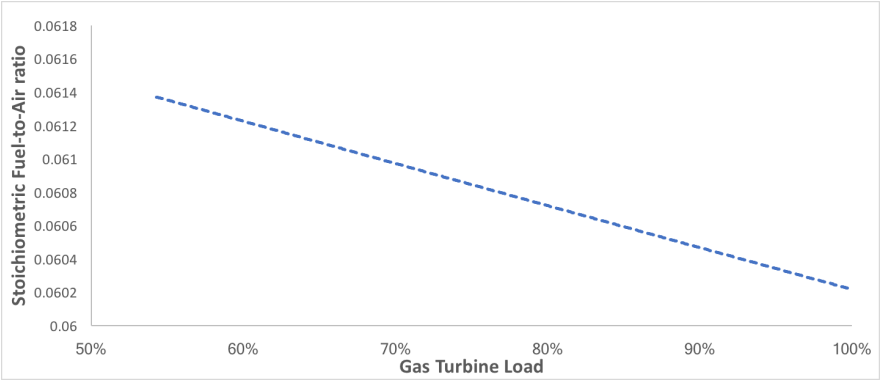


Figure 5.4: Stoichiometric Fuel-to-Air ratio with respect to gas turbine load

### 5.1.2. CO study

The impact of using part load operation in gas turbine on CO levels was studied. Figure 5.5 shows the comparison of CO levels and CO equilibrium levels with respect to that of the gas turbine load. As the EGR % increases in the oxidizer, the amount of CO levels increases proportionally. CO emission increases due to the availability $CO_2$ in the oxidizer and equally due to the absence of $O_2$ as well. CO emission levels at equilibrium represents infinite residence time. The time to reach equilibrium for CO is insufficient during part load. Thus concluding that using part load operations with EGR-oxydizer leads to a decrease in NOx levels as the stoichiometric flame temperature reduces. While at the same time the introduction of EGR causes an increase in CO levels too.

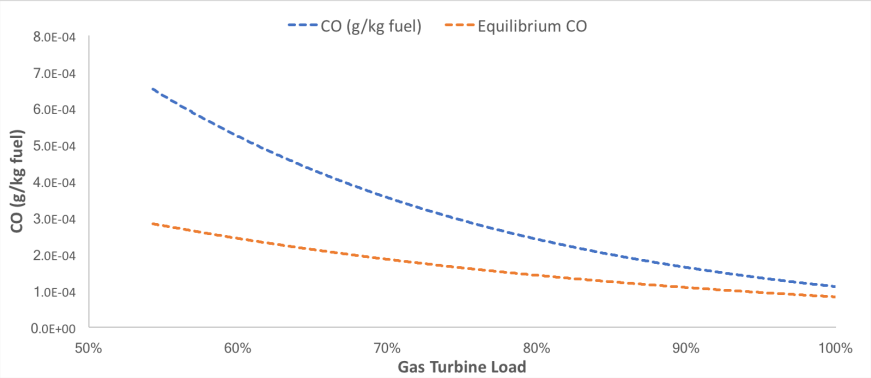


Figure 5.5: CO emission levels and CO emission level at equilibrium with respect to gas turbine load

## 5.2. Comparison between IGV and EGR

Inlet guide vanes are located at the first stage of the compressor of the gas turbine and is useful to control the amount of air into the compressor. This increases the efficiency of the gas turbine at part load and is very useful when it comes to part load operations of the gas turbine. A comparison was derived to understand which part load technique gives the least NOx emission while still retaining it's output efficiency. Table 5.2 shows the parameters that were used to calculate the emissions for IGV and draw the comparison between EGR and IGV.

Table 5.2: Parameters for inlet guide vane at different part load operations

| GT load | Unit | 100% | 91% | 81% | 71% | 61% | 51% | 41% |
|---|---|---|---|---|---|---|---|---|
| **Fuel and air input parameters** | | | | | | | | |
| **Fuel flow** | kg/s | 2.34E-03 | 2.16E-03 | 2.00E-03 | 1.81E-03 | 1.62E-03 | 1.44E-03 | 1.25E-03 |
| **Air flow** | kg/s | 1.24E-01 | 1.11E-01 | 1.02E-01 | 1.02E-01 | 1.02E-01 | 1.02E-01 | 1.02E-01 |
| **TIT** | Kelvin | 1371.15 | 1373.65 | 1371.75 | 1303.05 | 1232.85 | 1160.85 | 1086.55 |
| **P combustor inlet** | bar | 11.53 | 10.34 | 9.539 | 9.277 | 9.005 | 8.72 | 8.419 |
| **T combustor inlet** | Kelvin | 618.25 | 595.45 | 587.55 | 583.95 | 580.05 | 575.85 | 571.25 |
| **Composition of oxidizer** | | | | | | | | |
| **Mole percent of N2** | % | 77.29 | 77.29 | 77.29 | 77.29 | 77.29 | 77.29 | 77.29 |
| **Mole percent of O2** | % | 20.74 | 20.74 | 20.74 | 20.74 | 20.74 | 20.74 | 20.74 |
| **Mole percent of CO2** | % | 0.03 | 0.03 | 0.03 | 0.03 | 0.03 | 0.03 | 0.03 |
| **Mole percent of H2O** | % | 1.009 | 1.009 | 1.009 | 1.009 | 1.009 | 1.009 | 1.009 |
| **Mole percent of Ar** | % | 0.9309 | 0.9309 | 0.9309 | 0.9309 | 0.9309 | 0.9309 | 0.9309 |

### 5.2.1. NOx study

NOx emissions were calculated and compared for both of the part load operations to understand the difference in the emissions. Figure 5.6 shows NOx levels reduce more when using EGR than using IGV. Only up to 80% of the part load operation uses IGV and thereafter turbine inlet temperature is reduced. Air was used in the oxidizer and the air flow rate was kept constant from 81% part load operation in the gas turbine. So, the only major difference in both the part load operations was the oxidizer composition. This factor evidently plays an important role in reducing NOx emissions.

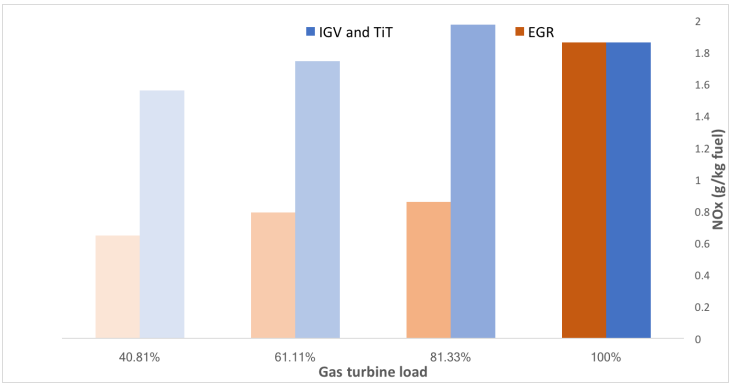


Figure 5.6: Contribution to NOx emissions by using IGV and EGR at loads 100%, 81%, 61% and 41%

Stoichiometric flame temperature was then compared between IGV and EGR. Figure 5.7 shows the trend on how the stoichiometric flame temperature reduces very little while using IGV compared to that of EGR. Stoichiometric flame temperature depends on the composition of the oxidizer. For IGV the oxidizer used was air, thus a very low drop in the flame temperature.

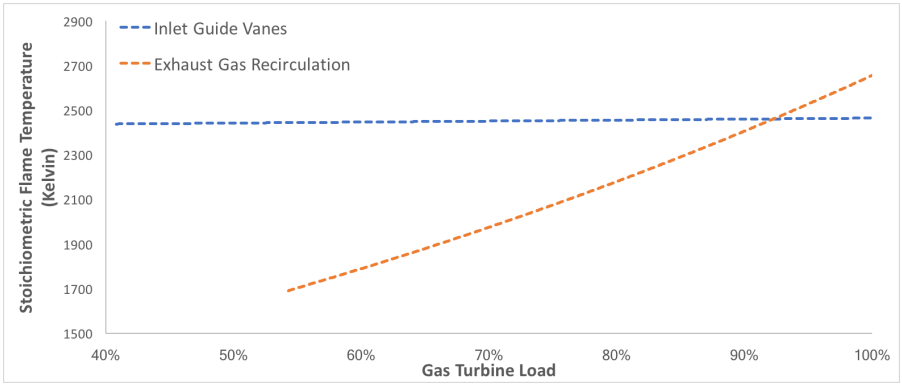


Figure 5.7: Stoichiometric flame temperature of IGV and EGR with respect to gas turbine load

From Figure 5.8 for EGR the NOx values reduce proportionally with the stoichiometric flame temperature. As for IGV part load operation, the NOx reduces but not much as the stoichiometric flame temperature is almost the same as IGV uses air in it's oxidizer. Thus providing the information that EGR-oxydizer plays a vital role in reducing NOx emissions.

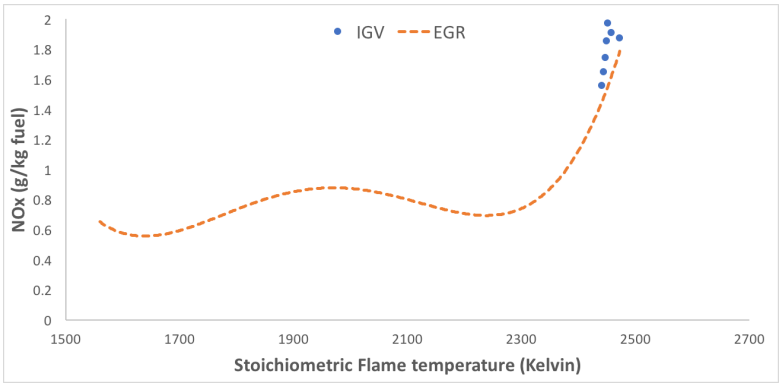


Figure 5.8: NOx emissions for IGV and EGR with respect to stoichiometric flame temperature

The thermodynamic property specific heat capacity of both the part load operations was then calculated and compared which can be seen from Figure 5.9. The specific heat capacity of IGV as a part load operation reduces when compared to it's counterpart which increases. The oxidizer is kept constant, while the fuel flow rate reduces in the case of IGV. While in EGR also the fuel flow rate reduces but the composition changes with respect to the gas turbine load. From this, it is understood that using air as an oxidizer is one of the main attribute contributing to a high stoichiometric flame temperature thus high NOx emissions.

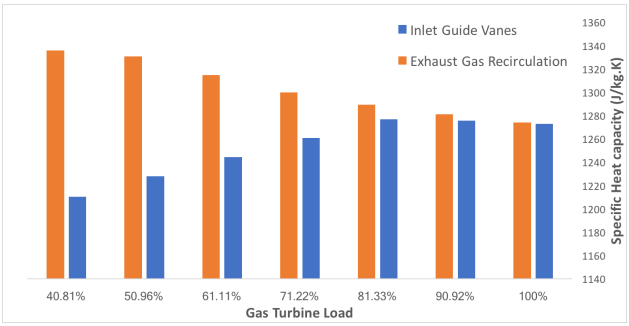


Figure 5.9: Heat capacity of IGV and EGR with respect to gas turbine load

### 5.2.2. CO study

The CO levels were compared as well to give a broader perspective on the difference in using both these part load operations. The results to the CO emissions from using these part load operations can be seen from Figure 5.10. Since inlet guide vanes contain almost 0% of $CO_2$ content, the CO levels are lower than the EGR operation. Thus confirming that introducing higher amounts of $CO_2$ in the oxidizer will lead to increase in CO levels.

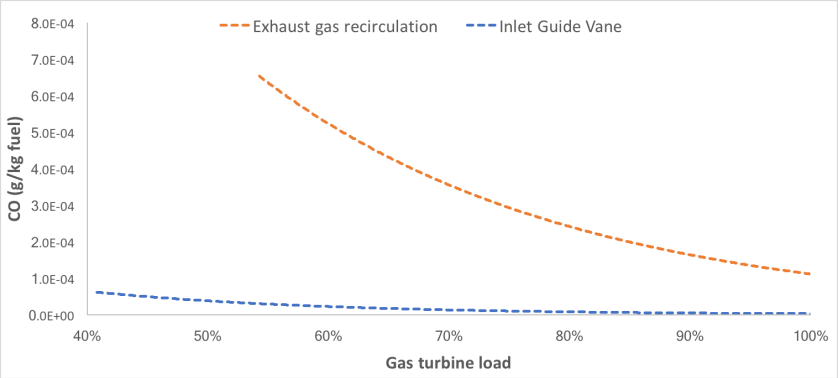


Figure 5.10: CO levels of IGV and EGR with respect to gas turbine load

## 5.3. Influence of $CO_2$ content

To understand the influence of EGR-oxydizer in the combustor during non-premixed combustion, an analysis on the influence of $CO_2$ on the emissions was studied. To study this, all the parameters that was used in the 100% load operation of Table 5.1 were kept constant throughout. The fuel flow rate was only reduced thus reducing the turbine inlet temperature. This keeps the stoichiometric flame temperature constant for each oxidizer composition. Table 5.3 shows the composition of EGR-oxydizer in molar fraction that was used in this study.

Table 5.3: Composition in mole fraction of air and different $CO_2$% used in the oxidizer

| | $N_2$ | $O_2$ | $CO_2$ | $H_2O$ | Ar |
|---|---|---|---|---|---|
| **Air** | 77.29% | 20.74% | 0.03% | 1.009% | 0.9309% |
| **$CO_2$ @ 1%** | 76.29% | 17.87% | 1.33% | 3.597% | 0.9187% |
| **$CO_2$ @ 2%** | 75.74% | 16.32% | 2.031% | 4.993% | 0.9122% |
| **$CO_2$ @ 3%** | 74.99% | 14.16% | 3.01% | 6.94% | 0.9031% |
| **$CO_2$ @ 4%** | 73.9% | 11.05% | 4.42% | 9.747% | 0.89% |

### 5.3.1. NOx study

Figure 5.11 shows the dependence of NOx on the stoichiometric flame temperature. It can be clearly observed as the $CO_2$ content inside the oxidizer increases, the flame temperature reduces and this also reduces the NOx emissions as well. $CO_2$ being an inert gas alters the chemical kinetics inside the combustion chamber greatly. These altered chemical kinetics changes the chemical pathways which limits the NOx production. This shows that adding $CO_2$ in the oxidizer reduces the stoichiometric flame temperature.

With $CO_2$ being the inert species, the reaction kinetics which lead to the formation of NOx is reduced greatly. Due to the reduction of 'O' radical in the reaction during combustion, the NOx formation is reduced which can be understood mainly from the following equation:

$$N_2 + O \rightleftharpoons NO + N \tag{5.1}$$

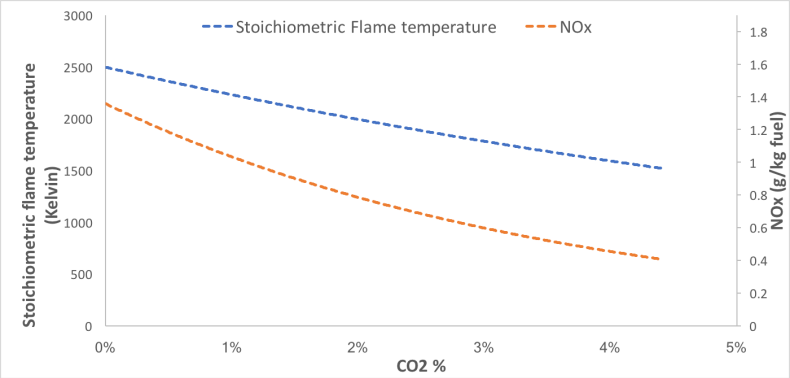


Figure 5.11: Stoichiometric flame temperature and NOx emission change with respect to $CO_2$% in the oxidizer.

The formation of NOx was studied with respect to the TiT. Figure 5.12 shows how NOx changes at different $CO_2$% in the oxidizer compared to that of air. This analysis was performed with constant pressure of 11.53 bar. As $CO_2$ content in the oxidizer increases, the NOx emission reduces. At 4% $CO_2$, the NOx is completely low compared to that with air as an oxidizer. Due to having a constant stoichiometric flame temperature for each oxidizer composition the respective NOx doesn't reduce much. At each oxidizer composition the stoichiometric flame temperature drops. As little as introducing 1% of $CO_2$, the NOx drops a lot since the stoichiometric flame temperature drops. This shows that thermal NOx mechanism plays a vital role in NOx production. Thus understanding how much the presence of $CO_2$ in the oxidizer influences the formation of NOx during combustion.

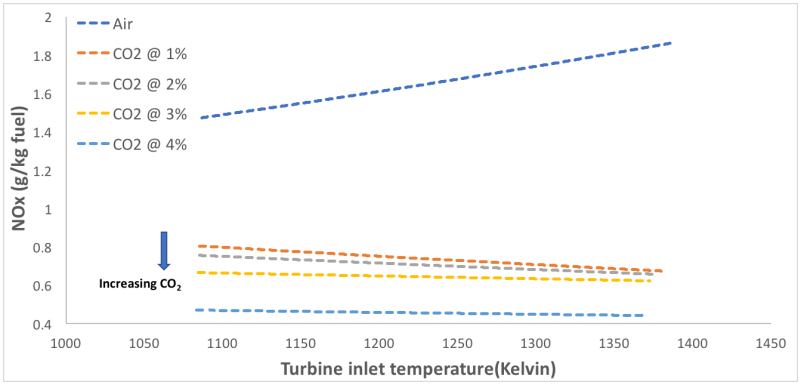


Figure 5.12: NOx levels for different $CO_2$ content in oxidizer with respect to Turbine inlet temperature @ p=11.53 bar

The change in oxidizer content also influences the heat capacity which can be seen in Figure 5.13. The depletion of oxygen leads to requiring more fuel to produce the same heat energy. Thus the increase in heat capacity and reduction in flame temperature. The absence of oxygen in the oxidizer can limit the NOx reaction kinetics. This concludes that, adding controlled amounts of $CO_2$ inside the oxidizer enhances the reduction of NOx.

### 5.3.2. CO study

Due to the increase in heat capacity of the fluid, a higher amount of fuel is required which can lead to low residence time and thus incomplete combustion. Figure 5.14 shows how CO levels increase with increase in $CO_2$ content in the oxidizer. This shows the limitation of using EGR-oxydizer as a part load operation in a gas turbine. $CO_2$ in the oxidizer effects the equilibrium reaction between CO and $CO_2$ and may favour the formation of CO [13]. At higher $CO_2$% more CO is formed. The dissociation of

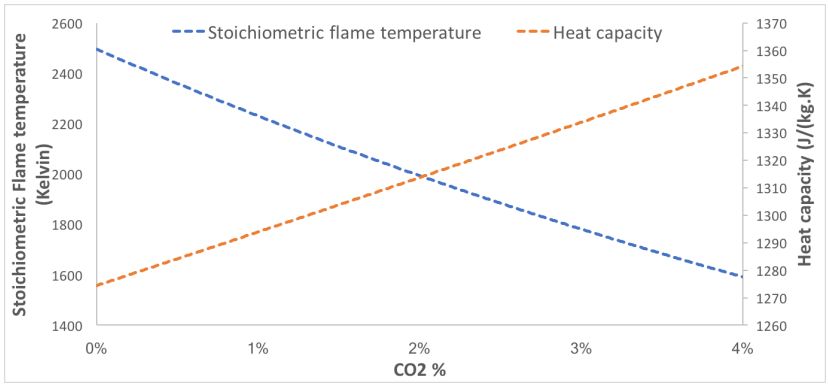


Figure 5.13: Stoichiometric flame temperature and heat capacity change with respect to $CO_2$% in the oxidizer.

$CO_2$ when reacted with hydrogen radical forms CO which can be seen from Equation 5.2. Le Chatelier's principle states that increasing the concentration of the reactants will drive the reaction to the products and vice versa which can be noticed from the figure below.

$$CO_2 + H \rightleftharpoons CO + OH \tag{5.2}$$

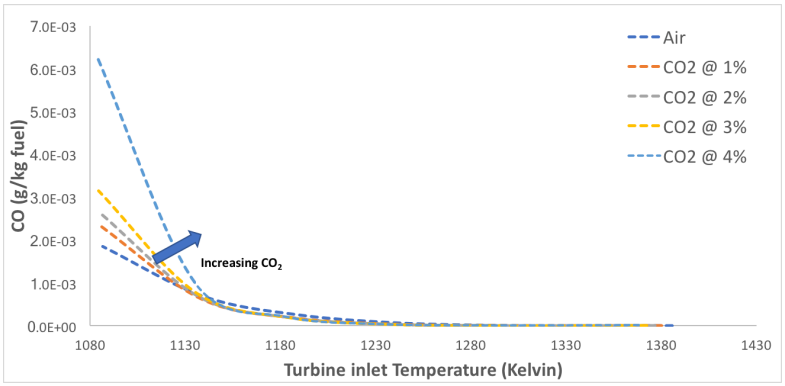


Figure 5.14: CO levels with respect to $CO_2$% in the oxidizer.

To understand the reason behind the influence of CO emission with respect to $CO_2$% in the oxidizer, CO levels at equilibrium were calculated and compared. The comparison was plotted at each $CO_2$% which is 1%, 2%, 3% and 4% inside the oxidizer. It is considered that at infinite residence time the CO levels would be at equilibrium.

From the figures that were plotted, the equilibrium CO levels are lower than the CO levels calculated at each $CO_2$% content inside the oxidizer. Since, the residence time of the combustion process inside the combustor is for a finite amount of time and limited, the calculated CO levels are higher. This study thus concludes that the CO levels increase due to insufficient residence time and it also increases with increase in $CO_2$ content in the oxidizer. Thus showing that the presence of $CO_2$ substantially reduces the NOx levels due to a drop in stoichiometric flame temperature but at the same time increases the CO levels.

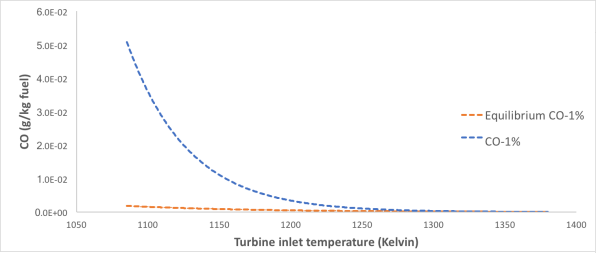


Figure 5.15: CO levels calculated vs Equilibrium CO levels at 1% $CO_2$

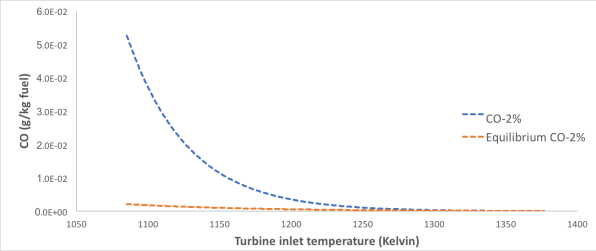


Figure 5.16: CO levels calculated vs Equilibrium CO levels at 2% $CO_2$

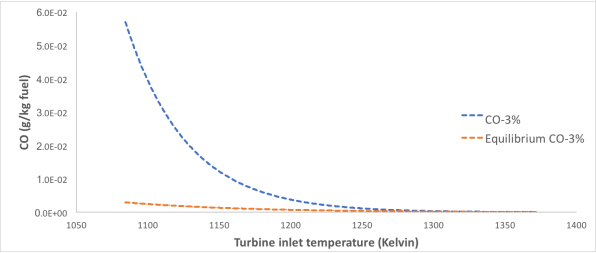


Figure 5.17: CO levels calculated vs Equilibrium CO levels at 3% $CO_2$

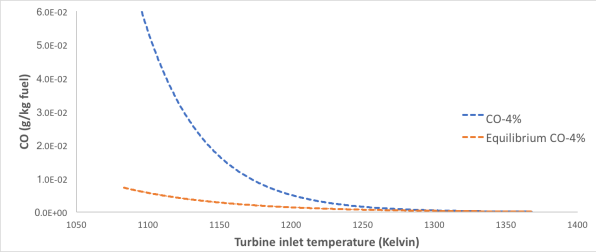


Figure 5.18: CO levels calculated vs Equilibrium CO levels at 4% $CO_2$

### 5.3.3. Influence of $CO_2$ at constant turbine inlet temperature

The influence of $CO_2$ in the combustion process was also analysed by keeping the turbine inlet temperature constant and calculating the NOx and CO levels. This was done to understand a different approach while analysing the NOx emissions and also make a correlation between these parameters. Figure 5.19 shows how NOx and CO levels change when keeping turbine inlet temperature constant and keeping pressure constant at 11.53 bar.

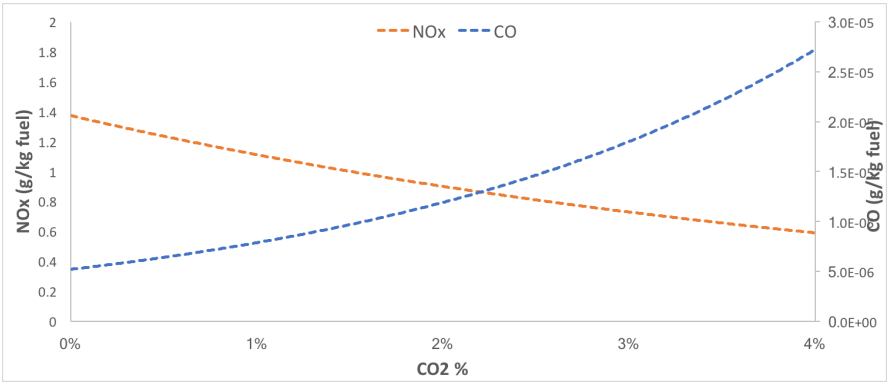


Figure 5.19: NOx and CO levels with respect to $CO_2$% at P=11.53 bar and TiT = 1385 K

A correlation was analysed between $CO_2$% in the oxidizer, CO and NOx emission data. This is to understand the strength in the relationship between the parameters and this can be noticed in Table 5.4.

Table 5.4: Correlation between $CO_2$%, CO emission and NOx emission

| | $CO_2$% | CO emission | NOx emission |
|---|---|---|---|
| **$CO_2$%** | 1 | | |
| **CO emission** | 0.9914 | 1 | |
| **NOx emission** | -0.782 | -0.706 | 1 |

From the correlation results that were analyzed, $CO_2$ was strongly related to CO emission. This means that as $CO_2$% increases there is a high and strong probability that CO emission will also increase. The dependence of CO emission on NOx emission is less. Thus giving the idea that how much ever CO level increases, the NOx level decreases. It is not as strongly dependent as between CO and $CO_2$. Figure 5.20 shows stoichiometric flame temperature and NOx emissions were also calculated and plotted in the same graph.

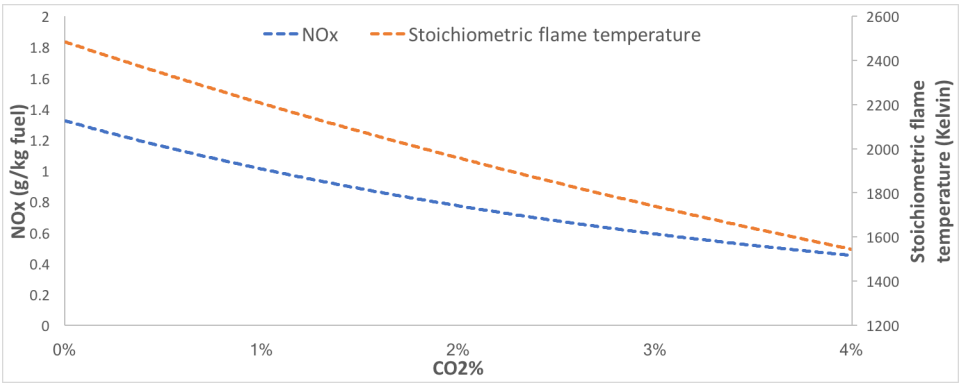


Figure 5.20: Stoichiometric flame temperature and NOx with respect to $CO_2$% at P=11.53 bar and TiT = 1385 K

A correlation was formed and analysed between $CO_2$, NOx and flame temperature to understand the dependency on each other. This can be seen form Table 5.5.

Table 5.5: Correlation between $CO_2$%, flame temperature and NOx emission

| | $CO_2$% | Stoichiometric flame temperature | NOx emission |
|---|---|---|---|
| **$CO_2$%** | 1 | | |
| **Stoichiometric flame temperature** | -0.998 | 1 | |
| **NOx emission** | -0.782 | 0.81 | 1 |

The correlation shows that $CO_2$ has a higher impact on stoichiometric flame temperature than the NOx emissions. So as $CO_2$% increases in the oxidizer the stoichiometric flame temperature will strongly reduce. As $CO_2$ content increases, there is a strong probability that NOx emissions will reduce as well. This concludes that $CO_2$ has a big influence on NOx emissions and the stoichiometric flame temperature. At the same time $CO_2$'s increase in the oxidizer also strongly increases CO emission.

## 5.4. Influence of EGR-oxydizer and air

From the previous section the importance of EGR in a part load operation was understood. The comparison between EGR-oxydizer and air is then studied. Table 5.6 shows the composition in mole fraction of EGR and air that was given to the oxidizer. The EGR-oxydizer that was used to perform this study was from the part load operation of 91%. This was done to understand the little difference the oxidizer composition can cause in pollution emissions. This analysis was performed by keeping all the parameters constant that was used in the 100% load operation of Table 5.1. Only the fuel flow rate was reduced thus reducing TiT. This keeps the stoichiometric flame temperature constant for each oxidizer composition.

Table 5.6: Composition in mole fraction of Air and EGR used for the study

| | $N_2$ | $O_2$ | $CO_2$ | $H_2O$ | Ar |
|---|---|---|---|---|---|
| **Air** | 77.29% | 20.74% | 0.03% | 1.009% | 0.9309% |
| **EGR** | 77.02% | 19.98% | 0.3755% | 1.697% | 0.9276% |

### 5.4.1. NOx study

NOx emissions were calculated using both EGR-oxydizer and air in the oxidizer. The results were plotted and compared against each other and can be seen in Figure 5.21. The difference in NOx emission between EGR-oxydizer and air is at least 0.4 g/kg fuel. Thus showing the influence of a little amount of EGR in the oxidizer.

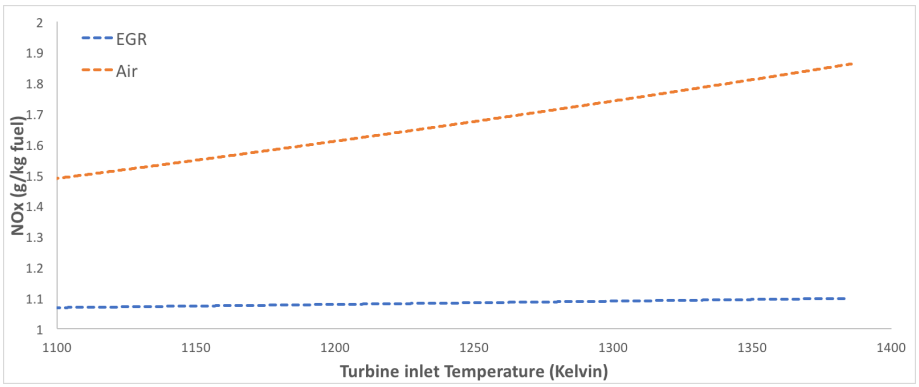


Figure 5.21: NOx levels for EGR and air composition with respect to Turbine inlet temperature @ p=11.53 bar

The stoichiometric flame temperature was 2472 Kelvin for air and 2417 Kelvin for EGR-oxydizer. At a constant stoichiometric flame temperature, the reduction in NOx for both air and EGR-oxydizer was less. This showed that NOx depended mostly on flame temperature. At the same time the addition of EGR-oxydizer lead to making the inert gases such as $CO_2$ to reduce the reaction kinetics. As little as 0.38% of $CO_2$ presence in the oxidizer can lead to almost 10% reduction in NOx emission. As the turbine inlet temperature was increased in the case of air, the NOx emission also increased. When comparing this to EGR-oxydizer, the NOx remains almost the same when the turbine inlet temperature increases. From this it can be understood that oxygen content in the oxidizer plays a vital role in the formation of NOx. The concentration of 'O' radical drops when using EGR-oxydizer thus inhibiting the formation of oxides of nitrogen (Equation 5.1).

Using the reaction path tool in cantera, the reaction pathways after combustion following $N_2$ was plotted. Figure 5.22 and 5.23 shows the reaction path following '$N_2$' for air and EGR-oxydizer respectively. If the arrow path is darker and thicker, it shows the amount of contribution to the formation of that specific compound or radical. The scale(at the bottom of the Figure) represents the rate of formation. Due to the introduction of EGR-oxydizer, the rate of formation of NO is slower compared to when using air. This is because EGR suppresses the formation of NO by forming other compounds such as NNH and resisting the compounds to further break to form NO or NH.

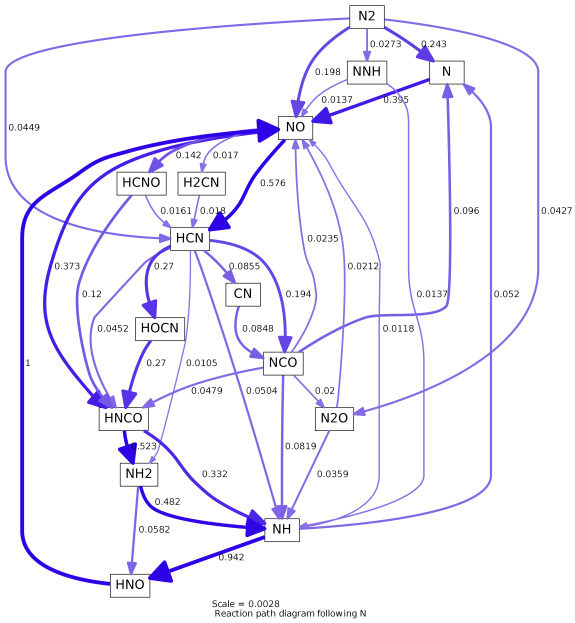


Figure 5.22: Reaction path diagram using Air

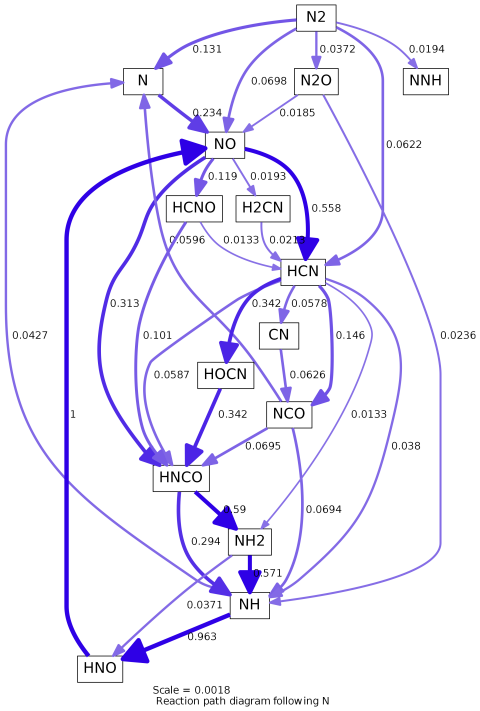


Figure 5.23: Reaction path diagram using EGR-oxydizer

## 5.4.2. CO study

When comparing EGR to air with respect to TiT, the CO levels were almost the same at higher temperatures. Figure 5.24 shows the CO levels that were calculated at a constant pressure(11.53bar). At lower temperatures, CO emission due to EGR was about 0.3% lower than that of the emission calculated when air was used. Replacing oxygen with a small amount of $CO_2$ can lead to an increase in CO levels. The formation of $CO_2$ after combustion is inhibited due to the replacement of $O_2$. Thus introduction of a small amount of EGR leads to a larger decrease in NOx. For CO levels the increase is less compared to the amount of NOx that is reduced. Thus concluding that EGR is a preferable oxidizer while operating gas turbines.

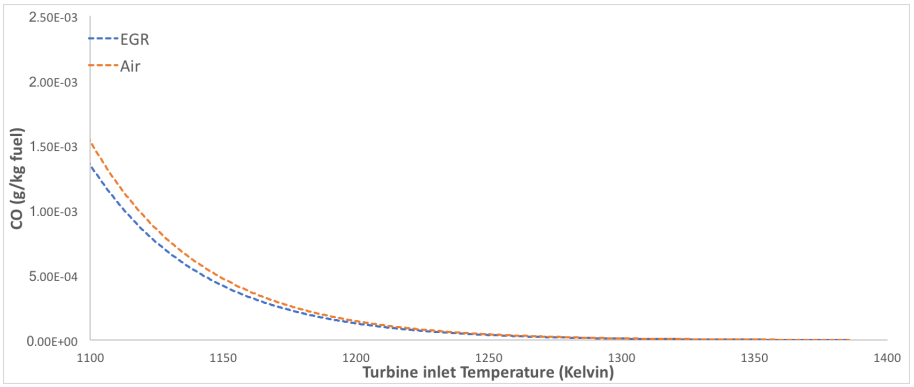


Figure 5.24: CO levels for EGR and air composition with respect to Turbine inlet temperature @ p=11.53 bar

## 5.5. Influence of pressure

The influence of pressure on the NOx emissions for a given EGR was studied and compared with that of air in the oxidizer. The emissions were calculated at 1 bar, 5 bar, 10 bar and 15 bar of pressure. The composition that was used in the oxidizer is given in Table 5.7. All the parameters that was used in the 100% load operation of Table 5.1 were kept constant throughout. Only the fuel flow rate was reduced thus reducing TiT. This keeps the stoichiometric flame temperature constant for each oxidizer composition.

Table 5.7: Composition in mole fraction of Air and EGR used for the study

| | $N_2$ | $O_2$ | $CO_2$ | $H_2O$ | Ar |
|---|---|---|---|---|---|
| **Air** | 77.29% | 20.74% | 0.03% | 1.009% | 0.9309% |
| **EGR** | 77.02% | 19.98% | 0.3755% | 1.697% | 0.9276% |

### 5.5.1. NOx study

The figures below display the NOx emissions that were calculated. As pressure increases, so does the NOx emission for both EGR and air. Although the NOx levels increases while using EGR in the oxidizer, it still remains to be lower than the NOx level when using air as an oxidizer.

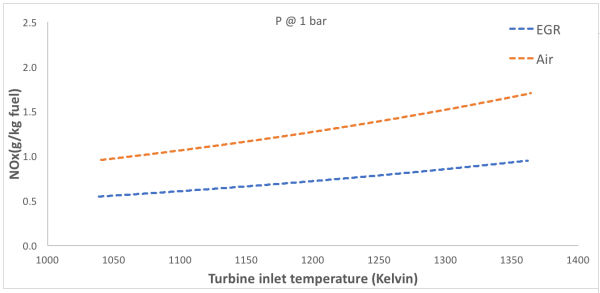


Figure 5.25: NOx emission @ P=1bar

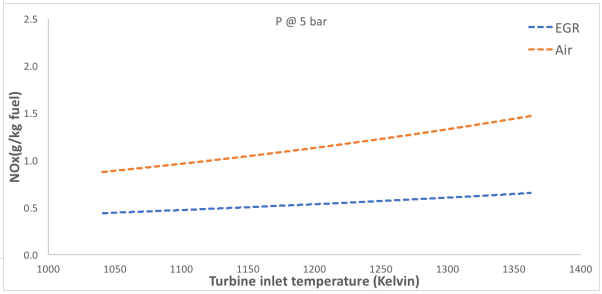


Figure 5.26: NOx emission @ P=5bar

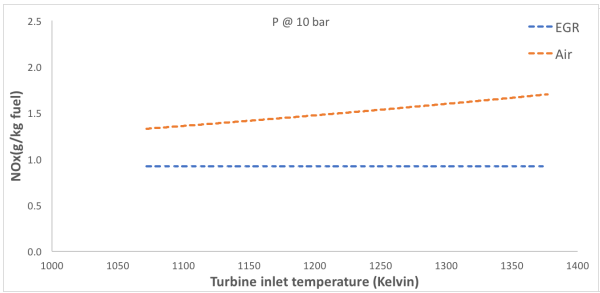


Figure 5.27: NOx emission @ P=10bar

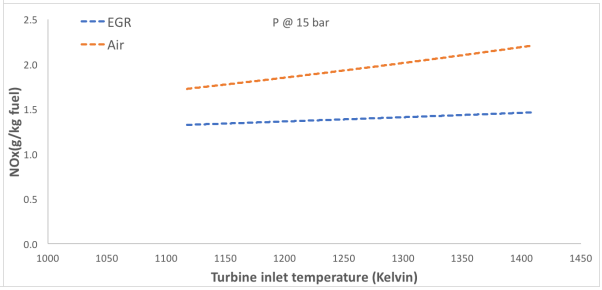


Figure 5.28: NOx emission @ P=15bar

At lower pressures (@ P=1 bar) there appears to be a huge difference in the NOx emission between EGR and air. As the pressure increases the difference in the NOx emission between EGR and air reduces. At higher temperatures the NOx emissions are due to thermal NOx and are dependent on pressure [51]. So, at higher pressures the reaction rates towards thermal NOx are accelerated. So, this implies that at higher pressures, the role of inert gases is less in limiting the NOx emissions.

The difference in the amount of NOx that is reduced can be seen from Figure 5.29. At pressure of 1 and 5 bar there is a high percentage of NOx reduction for EGR-oxydizer. At pressures of 10 bar and 15 bar, the amount of NOx that is reduced due to the EGR-oxydizer becomes less. This can be useful for boilers as they operate at low pressure unlike gas turbines.

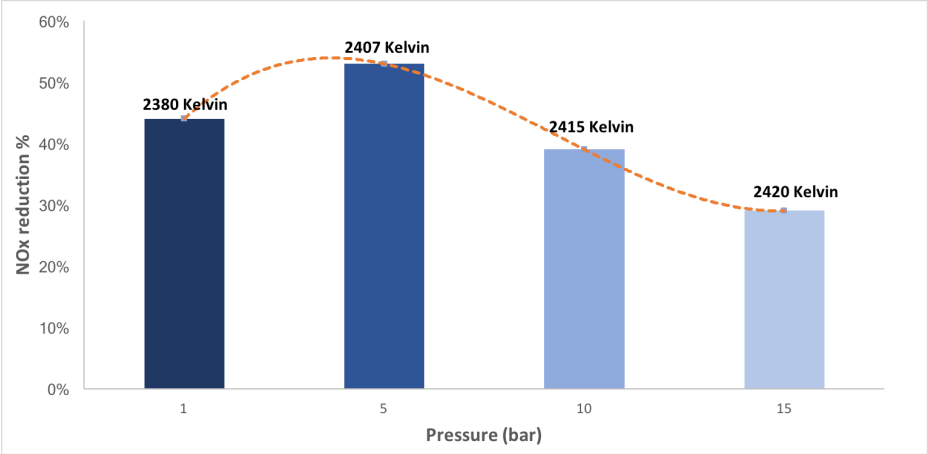


Figure 5.29: Percentage of NOx reduction at different pressures when using EGR-oxydizer

### 5.5.2. CO study

The figures below show the CO levels that were calculated at different pressures with respect to the TiT. At a pressure of 1 bar and at lower turbine inlet temperature, the CO level given out by EGR is more. This is because at lower pressure the $CO_2$ dissociation occurs easily and rapidly. As the temperature increases the formation of $CO_2$ is again favoured due to the increasing consumption of oxygen at higher temperatures. This goes for both EGR and air that act as an oxidizer.

As the pressure increases, the chemical dissociation of $CO_2$ is limited. As EGR has more $CO_2$ content in the oxidizer, the equal proportion of CO that should be emitted is also limited. For air as an oxidizer, as the pressure builds up, oxygen tends to readily react and combust to form $CO_2$. This also eventually dissociates to form CO compoiund. As per Le Chatelier's principle, as the pressure increases, the reaction shifts towards the side which has lesser number of moles of gas which can be understood from the following Equation:

$$CO_2 \rightleftharpoons CO + 0.5\,O_2 \tag{5.3}$$

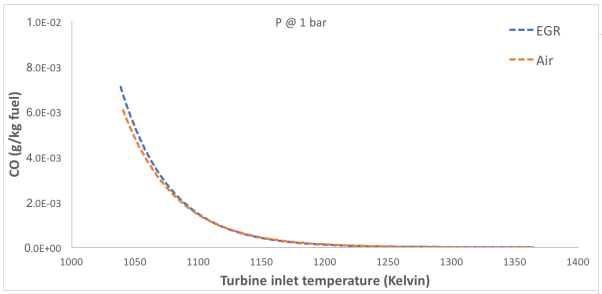


Figure 5.30: CO emission @ P=1bar

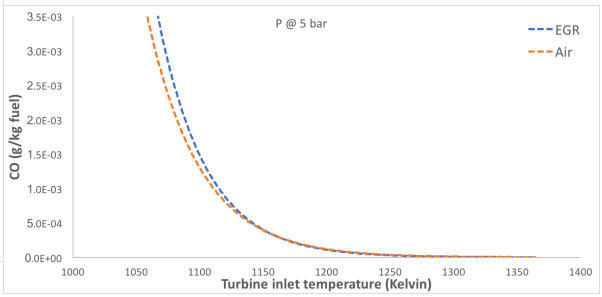


Figure 5.31: CO emission @ P=5bar

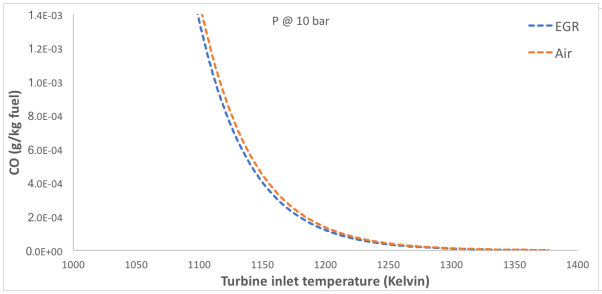


Figure 5.32: CO emission @ P=10bar

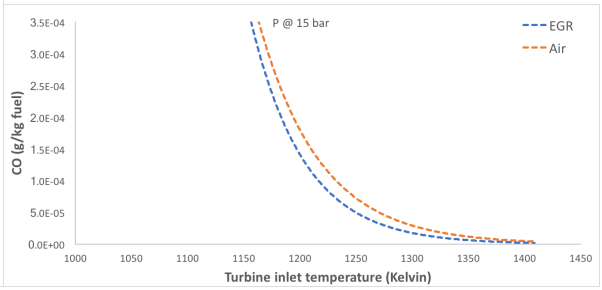


Figure 5.33: CO emission @ P=15bar

As discussed before the CO levels which were calculated were above their equilibrium levels due to insufficient residence time. Figures 5.34 and 5.35 show the difference between actual CO levels and equilibrium CO levels at pressure of 5 bar and 15 bar respectively. As the pressure increases, the actual CO levels come closer their equilibrium levels. This shows that there is even a higher suppression of $CO_2$ dissociation at high pressures.

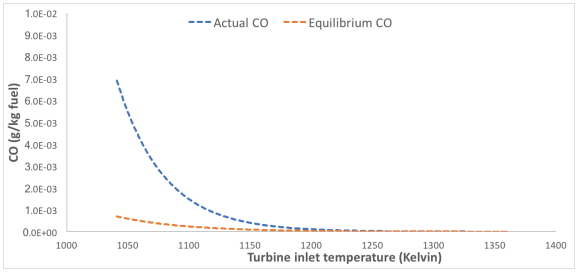


Figure 5.34: Actual CO levels vs Equilibrium CO levels at p = 5 bar

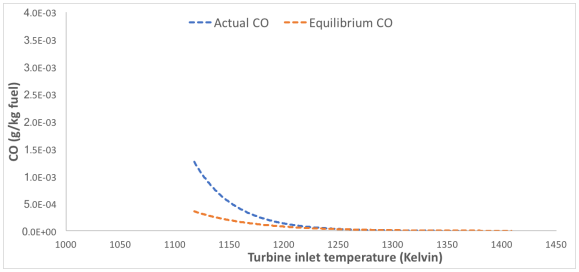


Figure 5.35: Actual CO levels vs Equilibrium CO levels at p = 15 bar

These results conclude that at higher pressures where gas turbines are favorable to operate on, using EGR-oxydizer gives appreciable and lower CO levels. Even though the amount of NOx reduced is lower at high pressures compared to that of lower pressures, using EGR-oxydizer still favours NOx reduction, more than that of CO reduction.

## 5.6. Influence of $H_2$ in the fuel

The concept of introducing a blend of $H_2$ and hydrocarbon fuel is introduced to limit the instability which can cause in the flame due to the loss in the reactivity. Mixing $H_2$ in the fuel can widen the flammability limits due to the high reactivity factor in $H_2$. This boosts the reaction rate. Wider flammability limits and higher flame speeds of $H_2$ as compared to natural gas should be able to sustain non-premixed combustion under very lean conditions[28, 52]. This study performs analysis of $H_2$ with EGR to sustain non-premixed combustion at high EGR ratios.

Table 5.8 and 5.9 shows the composition of the oxidizer and blend of $H_2$ and NG in molar fraction respectively. In oxidizer, the EGR composition that is used consists of 0.38% of $CO_2$ to understand the sensitivity due to the presence of small amount of EGR. The study was carried out with reducing fuel flow rate, while the rest of the parameters were kept constant. The oxidizer flow rate, pressure, and the inlet temperature values were taken from the 100% gas turbine load of Table 5.1.

Table 5.8: Composition in mole fraction of Air and EGR used for the study

| | $N_2$ | $O_2$ | $CO_2$ | $H_2O$ | Ar |
|---|---|---|---|---|---|
| **Air** | 77.29% | 20.74% | 0.03% | 1.009% | 0.9309% |
| **EGR** | 77.02% | 19.98% | 0.3755% | 1.697% | 0.9276% |

Table 5.9: Composition in mole fraction of natural gas and hydrogen blend used for the study

| | $CH_4$ | $C_2H_6$ | $C_3H_8$ | $CO_2$ | $N_2$ | $H_2$ |
|---|---|---|---|---|---|---|
| **Natural gas-100%** | 96.5% | 1.7% | 0.2% | 0.3% | 1.3% | - |
| **Natural gas-80%; $H_2$-20%** | 77.2% | 1.36% | 0.16% | 0.24% | 1.04% | 20% |
| **Natural gas-75%; $H_2$-25%** | 72.375% | 1.275% | 0.15% | 0.225% | 0.975% | 25% |

### 5.6.1. NOx study

Figure 5.36 and 5.37 shows the amount of NOx that was calculated when introducing $H_2$ in the fuel for air and EGR acting as oxidizer. The solid line shows the NOx levels emitted when only natural gas is used as fuel during combustion.

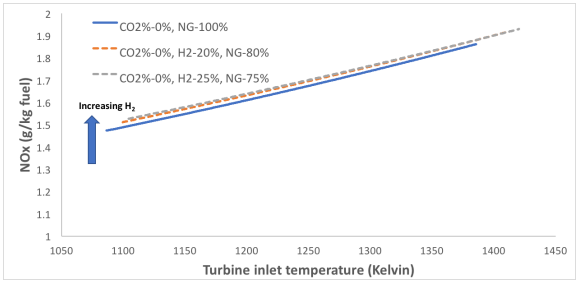


Figure 5.36: NOx emission with AIR as oxidizer

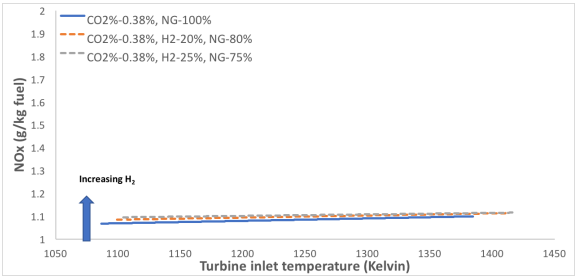


Figure 5.37: NOx emission with EGR-oxydizer

The blend with highest content of $H_2$ shows higher NOx emission for both EGR-oxydizer and air. The chemical kinetics of NOx is altered when combusting under the presence of $H_2$. This is because $H_2$ has high reactivity. EGR is used to slowdown these kinetics which is counteracted due to the existence of $H_2$ during combustion. Due to hydrogen's ability to have a stable flame, results in a sTable flame front. This will lead to a temperature increase and thus activating thermal NOx.

Figures 5.38 and 5.39 show the change in stoichiometric flame temperature and NOx emission with respect to increasing $H_2$ content in the fuel for air and EGR respectively. It can be noticed that the addition of $H_2$ in the fuel mixture leads to an increase in the stoichiometric flame temperature. This activates the thermal NOx mechanism, thus increasing the NOx levels. Therefore showing that adding $H_2$ into the fuel would result in an increase in NOx emission.

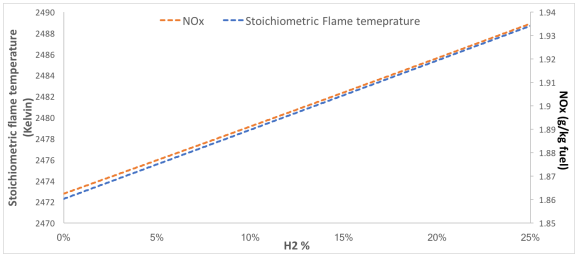


Figure 5.38: Stoichiometric flame temperature and NOx emission with respect to $H_2$ content in fuel with AIR as oxidizer

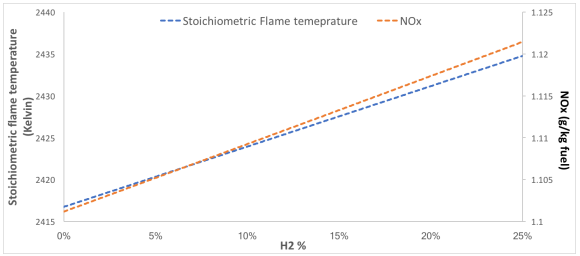


Figure 5.39: Stoichiometric flame temperature and NOx emission with respect to $H_2$ content in fuel with EGR-oxydizer

## 5.6.2. CO study

The CO levels were calculated for air and EGR and the results can be seen in Figures 5.40 and 5.41. The solid line indicates the CO emission from using only natural gas as fuel. Results indicate that CO emission does not favour the addition of $H_2$ gas in the fuel. This indicates that due to a better flame stability since the addition of hydrogen, CO emission has been reduced. When $H_2$ is combusted, the following reactions occur:

$$H_2 + O_2 \rightleftharpoons OH + O \tag{5.4a}$$

$$CO + OH \rightleftharpoons CO_2 + H \tag{5.4b}$$

When hydrogen reacts with oxygen, it breaks to form an hydroxyl radical and an oxygen radical(Equation 5.4a). This hydroxyl radical reacts with CO to form $CO_2$ (Equation 5.4b). Also due to the fact that there is a decrease in carbon content in the fuel due to the replacement with $H_2$, CO levels might have reduced. Thus, blending hydrogen in the fuel along with natural gas sees a decrease in carbon monoxide but also a slight increase in NOx emissions.

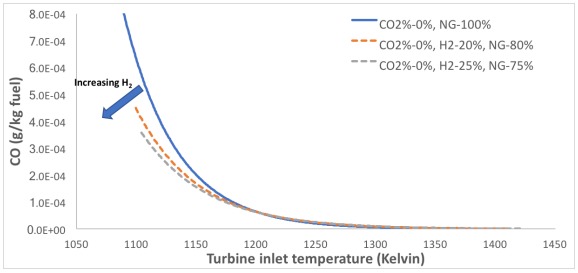


Figure 5.40: CO emission with AIR as oxidizer

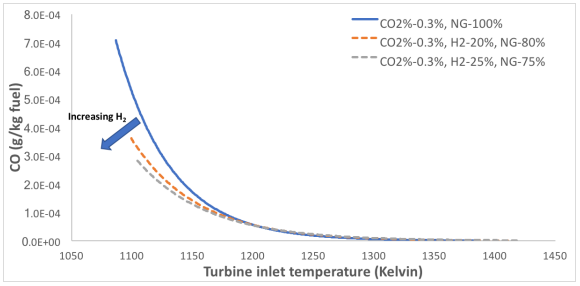


Figure 5.41: CO emission with EGR as oxidizer

# 6

# Conclusion

This thesis enlightened an approach on modelling non-premixed combustion using a CRN and understanding the NOx and CO formations for a MS5002 gas turbine combustor. All the Research questions that were formulated at the beginning is re-introduced. This thesis is concluded by providing answers to all those questions.

- **How can non-premixed combustion in a gas turbine be modelled using a Chemical Reactor Network?**

  1. The modelling of the combustor was done using a CRN method and invoking the GRI-mech 3.0 mechanism to understand the chemistry of combustion. The CRN uses two main reactors which is a perfectly stirred reactor and a plug flow reactor. The combustor volume is split equally between the PSR and PFR to model the flame. The first half of the combustor where intense mixing and high temperature occurs is modelled using three PSRs (FSR, PSR post-flame and PSR recirculation). The second half of the combustor where only radial diffusion and non-axial interaction occurs is modelled using a PFR. The PSR models the flame sheet reactor along with the post-flame zone and also the recirculation zone of the combustor. Residence time is imposed on these reactors by imposing the right volume for each reactor in this model. Flame sheet reactor models the stoichiometric combustion of the flame where most of the NOx is released. When the fuel and oxidizer are combusted at stoichiometry inside the flame sheet reactor, this will produce the highest temperature inside the combustor which activates thermal NOx. FSR volume is modelled by understanding the mixture fraction gradients inside the combustor.
  2. The mixture fraction at stoichiometry describes the point where the fuel and oxidizer reacts with each other to undergo complete combustion. This mixing field is described by the scalar dissipation rate. The scalar dissipation rate describes the rate of mixing of fuel and oxidizer inside the combustor after combustion. This scalar dissipation rate is used to estimate the stoichiometric mixing field and therefore impose a flame sheet reactor volume inside the combustor. Since, this model is used to validate turbulent combustion, molecular transport of species, momentum and thermal energy is neglected compared to turbulent transport. When assuming turbulent Lewis number, Prandtl number and Schmidt number to be unity, turbulent momentum diffusivity becomes equal to turbulent mass diffusivity and thermal diffusivity. Here, the turbulent momentum diffusivity is taken to be the eddy viscosity which is an extension of the mixing length hypothesis for the constant density jet. After imposing the flame sheet reactor volume, the rest of the first half of the combustor volume is divided equally between the PSRs. The output from the FSR is given to the PSR post-flame which then is given to a recirculation PSR on a feedback loop. Recirculation is done to recreate the recirculation zone inside the combustor. After using the stoichiometric amount of oxidizer in the FSR, the rest of the oxidizer which is available is divided equally between both the PSRs.

3. Combustion is the most complex phenomenon and cannot be uniquely modelled and predicted with precision especially by using only a CRN model. The adiabatic assumption integrated on the CRN model may not give the exact results and the results might be over or under predicted. This model was developed to understand the trend when different parameters are changed. This CRN model gives an overview of the NOx emissions. The model was validated by a number of different combustors. The results that were computed with the model was then compared with the experimental. The trendline showed to be the same and when the model and experimental data were correlated with each other, it was found that the parameters between both the data were strongly related to each other.

- **What are the emission(NOx and CO) characteristics in a non-premixed combustion in a gas turbine with Exhaust Gas Recirculation?**

1. The influence of EGR was studied for part load operations in gas turbines. It was found that due to the introduction of EGR in the oxidizer, the NOx emission was reduced by at least 40%. As the gas turbine load reduced, the EGR-oxydizer composition in the oxidizer increased. Due to the replacement of of $O_2$ with $CO_2$, the stoichiometric flame temperature reduced. Stoichiometric fuel to air ratio reduced as gas turbine load increased, this was because the oxidizer molecular weight reduced. Thus requiring more oxidizer flow to combust at stoichiometry. This gives a lower stoichiometric flame temperature and thus lowering the NOx emissions. Studying the CO levels for part load operations showed an increase in the emission. The calculated CO levels was more than the equilibrium CO levels. This shows that the increase in CO levels was due to insufficient residence time inside the combustor.
2. The EGR results were compared with the results when using IGV as a part load operation. NOx released when using EGR was less due to drop in stoichiometric flame temperature when compared to using IGV and reducing TiT. This is because IGV uses only air as it's oxidizer and has a constant oxidizer flow rate after 80% gas turbine load. IGV and EGR had an increase in heat capacity with reduction in gas turbine load. EGR required more amount of fuel to burn at the same temperature due to $O_2$ depletion. CO levels with IGV operation was much lower than that of EGR. The major difference between both the operations was the oxidizer composition. This concludes that compared to IGV that used only air in it's oxidizer, using EGR results in a lower NOx emission but higher CO emission levels.
3. It can be concluded that most of the NOx that is released is due to the thermal NOx activation. As the presence of inert gases increase in the oxidizer, the reaction kinetics that produce NOx are changed as well. A small presence of EGR in the oxidizer leads to a large reduction in NOx and a small increase in CO emission levels. Therefore EGR can be said that it is a useful part load technique to reduce NOx levels in gas turbine.

- **How sensitive are the emissions (NOx and CO) to parameters such as amount of $CO_2$ in the oxidizer, pressure, blend of $H_2$ and natural gas?**

1. A study was performed to understand influence of $CO_2$ in the oxidizer. This was done by keeping all the parameters constant and changing only the oxidizer composition and reducing the fuel flow. This gives a constant stoichiometric flame temperature at each oxidizer composition. As the $CO_2$% increased in the oxidizer, it was found that the NOx levels reduced. The least NOx was produced with highest content of $CO_2$ in the oxidizer. As the $CO_2$% increased, the stoichiometric flame temperature dropped. At each oxidizer composition, due to constant flame temperature, the NOx levels were almost the same. This showed the influence of thermal NOx mechanism in non-premixed combustion. As the $CO_2$ content increased in the oxidizer, the CO levels also increased. The CO levels were also higher than their equilibrium levels which is due to insufficient residence time in the combustor. It was found through correlation that at constant TiT, an increase in $CO_2$ content showed a strong increase in CO levels. Even though the NOx emission levels would reduce, it looked like the formation of CO was more favourable than the reduction of NOx emission. Thus, it is concluded that adding controlled amounts of $CO_2$ in the oxidizer would give a reduction in NOx but also an increase in CO levels.

2. An analysis was performed for pressures of 1 bar, 5 bar, 10 bar, and 15 bar. It was shown that as the pressure increased, the amount of NOx levels increased for both EGR and air. At pressure of 15 bar the amount of NOx reduced was less with EGR-oxydizer compared to pressure at 5 bar. At higher pressures, thermal NOx is directly dependent on pressure which favours NOx emission levels. At higher temperatures and pressures, the reaction rates towards thermal NOx is accelerated. So at higher pressures the role of EGR in limiting the NOx emissions is less. When studying the CO levels, at lower pressure EGR had higher CO levels as there is more $CO_2$ content in EGR. When looking at higher pressures, the rate of dissociation of $CO_2$ is suppressed. Even when comparing the actual CO levels to the equilibrium CO levels, at pressure of 15 bar, both were coming close to each other. This makes EGR to emit lower CO levels at high pressures. This study concluded that while using EGR-oxydizer at high pressures the amount of NOx reduced is less, but it still produced lower NOx than air. EGR-oxydizer also produced less CO, making it the most effective part load operation for gas turbines that always operate at high pressures.
3. When studying the impact of mixing NG with $H_2$ at different blends, it was found that the NOx levels increased with an increase of $H_2$ in the blend. It was also noticed that $H_2$ allowed an increase in stoichiometric flame temperature temperature due to high reactivity ability of $H_2$. This led to an increase in thermal NOx emission. It was also shown that due to lesser number of carbon atoms in the fuel, less CO levels were emitted. When $H_2$ reacts with oxygen it forms a hydroxyl radical which supports the formation of $CO_2$ from CO. Therefore this study showed that NOx levels and CO levels are still lower for EGR-oxydizer than air. Thus concluding that a mixture of $H_2$ in the fuel would increase the NOx levels but at the same time reduce the CO levels for both EGR-oxydizer and air.

This thesis research concluded that non-premixed combustion can be modelled using a CRN. The results of this model only gives an overview or trend or an understanding on the emissions. Performing parametric analysis on MS5002 gas turbine combustor concluded that EGR is definitely a very effective part load operation to reduce NOx emissions.

# 7

# Further Recommendations

This chapter will discuss all the recommendations that can improve this research work.

## 7.1. Implementing the model for counter-flow diffusion flame

Modelling counter-flow diffusion flame can be helpful in understanding the burners which incorporate this type of diffusion flame. One dimensional diffusion flames are essentially represented by the counter flow flames. The CRN model in this research is created for a co-flow diffusion flame. Most of the jets, use counter-flow combustion where oxidizer and fuel are injected at opposite directions to each other. The mixing and turbulence is far greater than co-flow diffusion flames. The scalar dissipation rate is calculated using the strain rate of the diffusion flame. This strain rate is caused due to the interaction between the oxidizer and fuel when coming in contact with each other and forms a stagnation point. This strain rate provides an important information about the extinction and ignition of the flame.

## 7.2. Implementing heat loss in the model

This model incorporates adiabatic combustion, which means that it does not take into the effects of heat loss are any other cooling effects. This isn't true in reality when it comes to combustion inside gas turbines. So, the turbine inlet temperature that is obtained using this model in reality is less when taking heat loss into consideration. When convective and radiative heat losses are implemented, there would be a difference in the local temperature inside the combustor and thus giving changes in NOx emissions that is recorded at the PFR. Heat loss can be implemented by creating a wall in cantera between the PFR and the outside environment(modelled as a resevoir). When defining the heat transfer coefficient between the wall PFR and the wall, the heat is extracted from the PFR and given to the environment. Fractional heat loss can be defined to know how much of the heat should be extracted. Implementing this would give a much better prediction of the NOx emissions by the model.

## 7.3. Creating a hybrid CFD-CRN model

In the current model, the flow field is only assumed and chemical reactors are split based on mixture fraction gradients and residence times. As explained in the literature, creating a hybrid CFD-CRN model will give a better NOx emission values. CFD can be used to extract the flow field information during combustion and also implement turbulence. This information can then by given as as input to the CRN model. The CRN model applied all the reduced and simplified chemistry to calculate the NOx emissions. The size of the grid and the computed velocities can provide information of local combusted zones which can be modelled as PSRs. This could lead to a large increase in computation time, but it can improve the accuracy of NOx emissions as well substantially.

# A

# First CRN Design

There were two different CRN layouts that was drafted initially based on the combustor and program settings. The final layout has been discussed in Chapter-3. Both the CRN layouts showed promising results, but only one of them was finalized due to it's affinity to model the recirculation zone of the flame. In the first layout that was initially modeled, recirculation (modelling the recirculation zone) was done by making the products of the final PSR given a reverse direction back to the initial PSR as seen in Figure A.1. This was done to understand how cantera solved the CRN model. To understand if each PSR would take the product of it's subsequent PSR as an incoming reactant or just add the incoming reactant along with the combusted product which is present inside the reactor. Recirculation through swirling results in the formation of toroidal recirculation zones. Recirculation also reduces combustion lengths by producing high rates of entrainment of the ambient fluid and fast mixing, especially near to the boundaries of recirculation zones.

It was seen that cantera did not recognise the incoming products being given as an input to each PSR. Instead the recirculation was recognised as an addition to the combusted product and not complete mixing. Increasing the recirculation, increased the NOx production and then after 20% recirculation the NOx coming out of each PSR dropped but the final NOx recorded at PFR stayed steadily high which did not make sense. This led to finalizing the second layout.

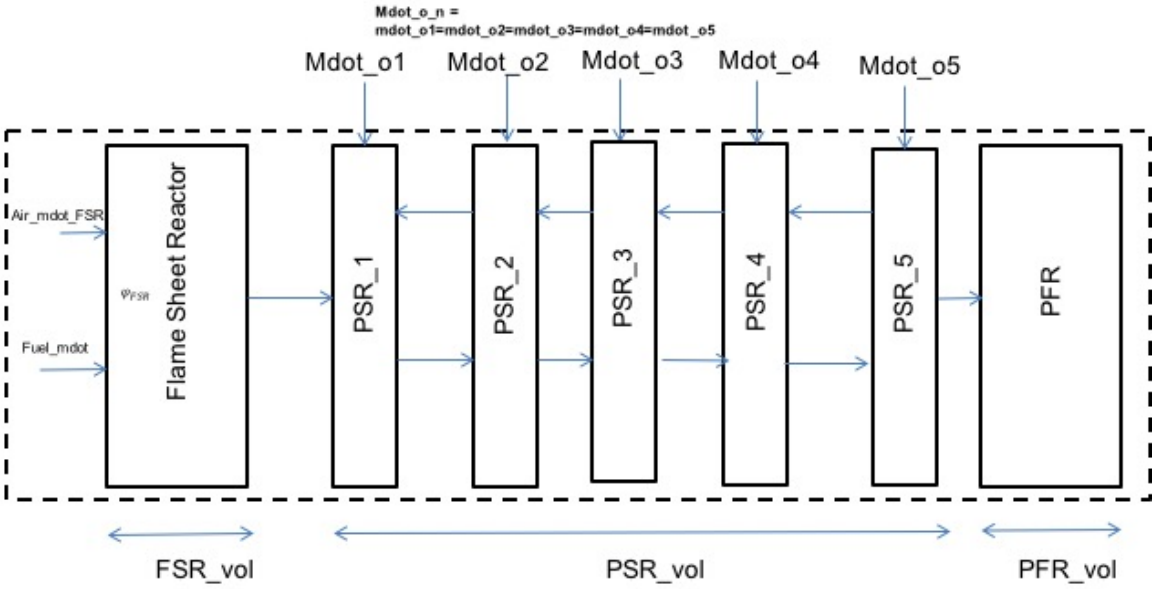


Figure A.1: The first CRN layout created

Figure A.2 shows the results of increasing the recirculation between the PSRs. When the recirculation increased, the NOx increased coming out of each PSR upto the point of 20% apart from the NOx coming out of the FSR. After that as the recirculation increased, the NOx reduced as well other than that of the NOx coming out of the PFR. There was a large difference in the NOx coming out each PSR and to the one recorded at PFR. This made the fact that the recirculation zone cannot be regulated using this layout and should be kept always at 100%. Even though the CRN layout at 100% recirculation showed promising NOx results and most of it was from the FSR. This CRN layout was not chosen as the final layout to perform the parametric analysis, but can still be used to calculate NOx emissions.

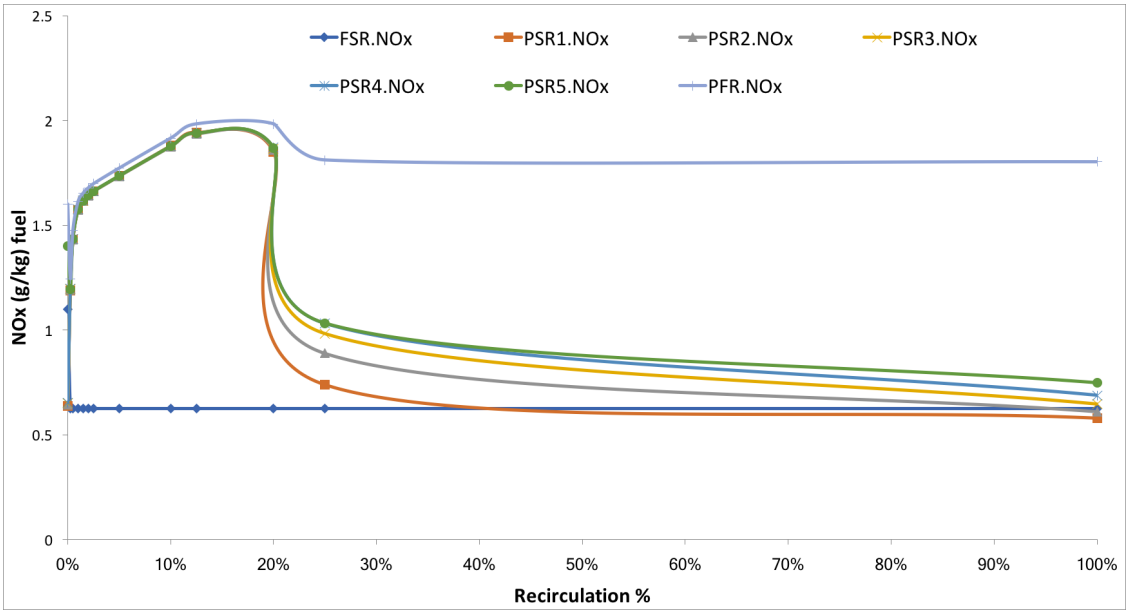


Figure A.2: The results of the recirculation using the first CRN layout

# B

# Turbulent diffusion scaling

To understand the turbulent diffusion rate for non-premixed combustion at macro-scale or micro-scale, a scaling analysis can be performed to relate each parameter of the eddies to the diffusion rate. The scaling analysis is done for an axis-symmetric turbulent jet flow. The mixing length hypothesis helps in understanding eddy viscosity ($\nu_{turb}$) which is Prandtl's hypothesis [53]. For a given turbulent flow, the turbulent viscosity is proportional to the product of the fluid density and a characteristic kinematic eddy viscosity [53] (i.e.):

$$\mu_{turb} = \nu_{turb} * \rho \tag{B.1}$$

A simple dimensional analysis shows that the eddy viscosity relates to the length over which there is high interaction of vortices in a turbulent flow field [53],

$$\nu_{turb} \sim l_m * U_{turb} \tag{B.2}$$

where, $U_{turb}$ is the turbulent velocity of the fuel jet.

In an one Equation model, the turbulent kinetic energy can be expressed as:

$$k = \frac{1}{2}(\overline{u^2} + \overline{v^2} + \overline{w^2}) \tag{B.3}$$

So, the above Equation can be scaled and related to the turbulent viscosity giving the following relation of turbulent viscosity to turbulent kinetic energy,

$$\nu_{turb} \sim l_m * \sqrt{k} \tag{B.4}$$

Now turbulent viscosity is expressed in terms of the turbulent kinetic energy, so a PDE is developed for turbulent kinetic energy which makes the turbulent stress and turbulent fluxes as functions of the kinetic energy,

$$\frac{\partial \rho k}{\partial \tau} + \frac{\partial \rho U_j k}{\partial x_j} = -\rho\overline{u_i u_j}\frac{\partial \rho U_i}{\partial x_j} - \beta g_i \rho \overline{u_i t} \ldots\ldots\ldots\ldots (P_k + G_k) \tag{B.5}$$

$$-\frac{\partial}{\partial x_j}\left(\frac{1}{2}\rho\overline{u_i^2 u_j} + \overline{pu_j} - \mu\frac{\partial k}{\partial x_j}\right) \ldots\ldots\ldots\ldots (D_k) \tag{B.6}$$

$$-\mu\overline{\frac{\partial U_j}{\partial x_j}\frac{\partial U_j}{\partial x_j}} \ldots\ldots\ldots\ldots (\epsilon_k) \tag{B.7}$$

where, $\epsilon_k$ is the turbulent dissipation rate, and from dimensional analysis we obtain,

$$\epsilon = \mu\overline{\frac{\partial U_j}{\partial x_j}\frac{\partial U_j}{\partial x_j}} \sim \frac{k^{\frac{3}{2}}}{l_m} \tag{B.8}$$

By, rearranging Equation B.4 in terms of turbulent kinetic energy, eddy viscosity can be scaled with turbulent dissipation rate.

$$\epsilon \sim \frac{1}{l_m}(\frac{\nu_{turb}}{l_m})^3 \sim \frac{(\nu_{turb})^3}{l_m^4} \tag{B.9}$$

Now, after relating the mixing length and eddy viscosity to the turbulent dissipation rate, next step is to define the mixing length with relation to the free flowing axis-symmetric turbulent jet. For a wide variety of flows, the mixing length functions are given by Launder et al [54]. For a free axis-symmetric jet, mixing length is defined by [15] as,

$$l_m = 0.075\delta_{99\%} \tag{B.10}$$

where, $\delta_{99\%}$ is the half-width measured from the jet-centerline to the radial location where the maximum axial velocity is decayed by 1% of it's centerline value. Since, $\delta_{99\%}$ grows with increasing axial distance from the centre of the fuel nozzle, the mixing length can be known as a function of the axial distance as well and can be scaled to the axial distance from the origin.

$$l_m \sim x \tag{B.11}$$

where x is defined as the axial distance at every point from the origin. Stephen R Turns derives the eddy viscosity for an axis-symmetric turbulent jet and defines it as [15],

$$\nu_{turb} = 0.0285 U_{turb} R \tag{B.12}$$

where, R is the radius of the fuel nozzle. By scaling all of this to the turbulent dissipation rate we get the following relation:

$$\epsilon \sim \frac{(U_{turb}R)^3}{x^4} \tag{B.13}$$

With this relation, it is evident that the turbulent dissipation rate reduces as the axial distance from the origin of the jet increases which can be seen in Figure B.1

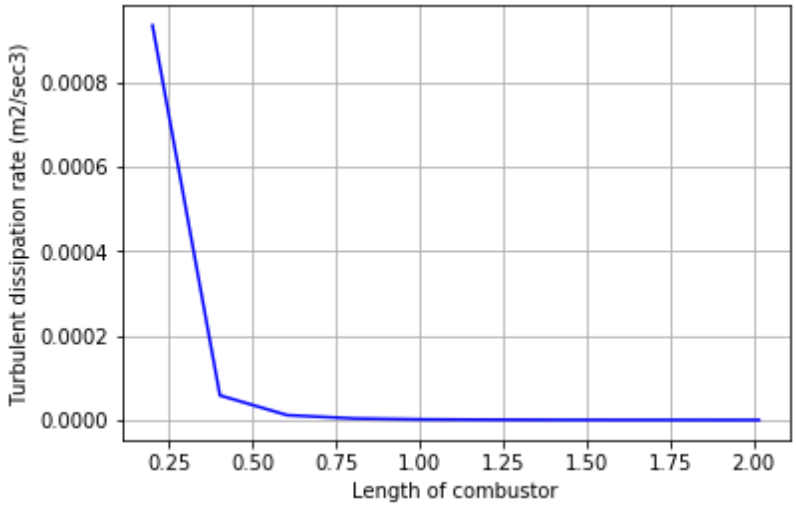


Figure B.1: Turbulent dissipation rate along the length of the combustor

From Figure B.1 the turbulent dissipation rate drops exponentially as the distance from the centre of the fuel inlet nozzle is increased. So, the turbulent dissipation rate is calculated at 10% of the length of the combustor which is used to find the scalar dissipation rate at stoichiometry. This can be understood as the highest turbulent diffusion occurs near the inlet of the combustor as the fuel and oxidizer mix instantaneously.

# C

# PFR model in cantera

In cantera the plug flow reactor is modelled in two ways:

1. **Flowreactor( )**: There is a built-in module inside cantera that can simulate steady state plug flow reactor. This can be done only with a fixed cross sectional area. Along the length of the combustor time integration is applied and is a part of the module. This module cannot implement mass flow controllers and valves and therefore can sustain pressure loss. This would violate the assumption of 100% combustor efficiency.
2. **PSRs in series**: In cantera PFR can be modelled also by using PSRs in series. As explained in the Chapter-2, PFR assumes that there is only radial diffusion and not axial diffusion. Using this assumption, the PFR volume is spatially discretized as a series of 1000 PSRs (the number can be changed) and then it is integrated individually. The output of the PSR is given as an input to the next subsequent PSR. All these PSRs are placed according to the PFR length which is described by the USER based on the combustor length. This way of creating PFR has been also used and recommended by Vaibhav Prakash [13] and Rosati[44] in their respective thesis. This way of integrating the PFR into cantera has been proved to produce good results and thus has been used in this thesis as well. Figure C.1 shows how the PFR is discretized as a series of PSRs.

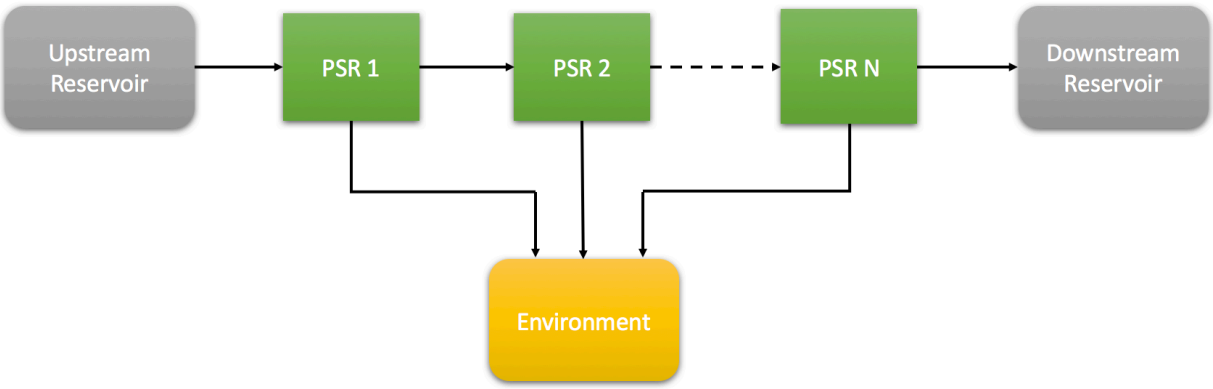


Figure C.1: PFR represented as series of PSRs

# Bibliography


[1] EIA, *EIA projects world energy consumption will increase 56% by 2040 - Today in Energy - U.S. Energy Information Administration (EIA),* .

[2] P. Jansohn, *Overview of gas turbine types and applications,* Modern Gas Turbine Systems , 21 (2013).

[3] *Improving the Flexibility and Efficiency of Gas Turbine-Based Distributed Power Plants - Power Engineering,* .

[4] J. Steimes, S. A. Klein, and M. Persico, *Enabling efficient and low emissions deep part load operation of combined cycles and combined heat and power plants with external Flue Gas Recirculation,* Proceedings of Global Power and Propulsion Society forum 18 (Submitted GPPS-2018-0013) , 10 (2018).

[5] T. Poinsot and D. Veynante, *Theoretical and Numerical Combustion,* Combustion and Flame , 81 (2005), arXiv:arXiv:1011.1669v3 .

[6] A. Mameri and F. Tabet, *Numerical investigation of counter-flow diffusion flame of biogas–hydrogen blends: Effects of biogas composition, hydrogen enrichment and scalar dissipation rate on flame structure and emissions, International Journal of Hydrogen Energy,* **41** (2015).

[7] J. Greenberg, *The Burke-Schumann diffusion flame revisite—With fuel spray injection,* Combustion and Flame **77**, 229 (1989).

[8] S. P. Burke and T. E. W. Schumann, *Diffusion Flames,* Industrial & Engineering Chemistry **20**, 998 (1928).

[9] N. Peters, *Turbulent Combustion,* Measurement Science and Technology **12**, 2022 (2001), arXiv:arXiv:1011.1669v3 .

[10] H. Pitsch and H. Steiner, *Scalar mixing and dissipation rate in large-eddy simulations of non-premixed turbulent combustion,* Proceedings of the Combustion Institute **28**, 41 (2000).

[11] D. Anderson, *Effects of Equivalence Ratio and Dwell Time on Exhaust Emissions From an Experimental Premixing Prevaporizing Burner,* in *Volume 1B: General* (ASME, 1975) p. V01BT02A007.

[12] J. Bluestein, *Nox controls for gas-fired industrial boilers and combustion equipment: A survey of current practices. topical report, march-october 1992,* .

[13] V. Prakash, *Parametric Emission Prediction Model in Gas Turbines with Exhaust Gas Recirculation Vaibhav Prakash,* Thesis: Delft (2017).

[14] V. Fichet, M. Kanniche, P. Plion, and O. Gicquel, *A reactor network model for predicting NOx emissions in gas turbines,* Fuel **89**, 2202 (2010).

[15] S. R. Turns, *An Introduction to Combustion*, 2nd ed. (McGraw-Hill Book Co-Singapore, 2000).

[16] J. E. Broadwell and J. E. Lutz, *A turbulent jet chemical reaction model: {NO}_x production in jet flames,* Combust. Flame **114**, 319 (1998).

[17] L. S. Pedersen, P. Breithauptb, K. Dam-Johansen, and R. Weber, *COMBUSTION SCIENCE AND TECHNOLOGY Residence Time Distributions in Confined Swirling Flames,* COMBUSTION SCIENCE AND TECHNOLOGY **127**, 251 (1997).

[18] A. De Toni, T. Hayashi, and P. Schneider, *A reactor network model for predicting NOx emissions in an industrial natural gas burner,* Journal of the Brazilian Society of Mechanical Sciences and Engineering **35**, 199 (2013).

[19] O. Silva, *Numerical simulation of the reactive flow in a combustion chamber.*, Ph.D. thesis, University of Evora (2003).

[20] A. B. Lebedev, A. N. Secundov, A. M. Starik, N. S. Titova, and A. M. Schepin, *Modeling study of gas-turbine combustor emission,* Proceedings of the Combustion Institute **32 II**, 2941 (2009).

[21] A. Andreini and B. Facchini, *Gas Turbines Design and Off-Design Performance Analysis With Emissions Evaluation,* Journal of Engineering for Gas Turbines and Power **126**, 83 (2004).

[22] H. Schlichting and K. Gersten, *Boundary-layer theory* (Springer, 2000) p. 799.

[23] M. Delichatsios, *Transition from momentum to buoyancy-controlled turbulent jet diffusion flames and flame height relationships,* Combustion and Flame **92**, 349 (1993).

[24] S. Orsino and R. Weber, *IFRF Combustion Journal Article Number*, Tech. Rep. (2000).

[25] T. Terasaki and S. Hayashi, *The effects of fuel-air mixing on NOx formation in non-premixed swirl burners,* Symposium (International) on Combustion **26**, 2733 (1996).

[26] E. Poursaeidi, M. Arablu, M. A. Yahya Meymandi, and M. R. Mohammadi Arhani, *Investigation of Choking and Combustion Products' Swirling Frequency Effects on Gas Turbine Compressor Blade Fractures,* Journal of Fluids Engineering **135**, 061203 (2013).

[27] G. R. S. Alan S. Feitelberg, Michael D. Starkey, Richard B Schiefer, Roointon E. Pavri, Matt Bender, John L Booth, *Performance of a Reduced NOx Diffusion Flame Combustor for the MS5002 Gas Turbine,* , 10016 (2018).

[28] F. Cozzi and A. Coghe, *Behavior of hydrogen-enriched non-premixed swirled natural gas flames,* International Journal of Hydrogen Energy **31**, 669 (2006).

[29] *Chapter Climate Change 2014 Synthesis Report Summary for Policymakers Summary for Policymakers*, Tech. Rep.

[30] *Adoption of the Paris Agreement*, Tech. Rep. (UNFCC, Paris, 2015).

[31] E. Directive, *Directive of the European Parliament and of the Council of 25 November 2015 on the limitation of emissions of certain pollutants into the air from medium combustion plants (MCP Directive) European Commission DG Environment*, Tech. Rep.

[32] D. R. B. Arthur H Lefebvre, *Gas Turbine Combustion; Alternative Fuels and Emissions*, 3rd ed. (CRC Press, 2010) pp. 218–222.

[33] S. R. Turns, *Understanding NOx formation in nonpremixed flames: Experiments and modeling,* Progress in Energy and Combustion Science **21**, 361 (1995).

[34] R. W. Bilger, *The Structure of Diffusion Flames,* Combustion Science and Technology **13**, 155 (1976).

[35] *Flame D,* .

[36] J. F. Driscoll, R.-H. Chen, and Y. Yoon, *Nitric oxide levels of turbulent jet diffusion flames: Effects of residence time and damkohler number,* Combustion and Flame **88**, 37 (1992).

[37] J. M. Seitzman, *Quantitative applications of fluorescence imaging in combustion (Book, 1991) [WorldCat.org]*, Ph.D. thesis, Stanford university (1991).

[38] D. G. Nicol, P. C. Malte, and R. C. Steele, *Simplified Models for NOx Production Rates in Lean-Premixed Combustion,* in *Volume 3: Coal, Biomass and Alternative Fuels; Combustion and Fuels; Oil and Gas Applications; Cycle Innovations* (ASME, 1994) p. V003T06A037.

[39] S. M. CORREA, *A review of nox formation under gas-turbine combustion conditions, Combustion Science and Technology - COMBUST SCI TECHNOL*, **87**, 329 (1993).

[40] J. W. Bozzelli and A. M. Dean, *O + NNH: A possible new route for NOX formation in flames,* International Journal of Chemical Kinetics **27**, 1097 (1995).

[41] P. C. MALTE and D. T. PRATT, *The role of energy-releasing kinetics in nox formation: Fuel-lean, jet-stirred co-air combustion, Combustion Science and Technology - COMBUST SCI TECHNOL*, **9**, 221 (1974).

[42] M. Talboom, *Chemical Kinetic Study of the Hybrid Combustion System*, Ph.D. thesis (2016).

[43] I. V. Novosselov, *Chemical Reactor Networks for Combustion Systems Modeling,* Phd Dissertation (2006).

[44] B. Rosati, *Prediction of emissions from combustion sys- tems using 0D and 1D reacting flow models Chemical Reactor Network modeling Prediction of emissions from combustion systems using 0D and 1D reacting flow models,* , 153 (2015).

[45] C. M. Madrid, *Chemical Reactor Network for LDI Combustor. CRN development and Analysis of Different Fuels,* (2017).

[46] R. Pankaj Sampat, *Automatic Generation of Chemical Reactor Networks for Combustion Simulations*, Ph.D. thesis (2018).

[47] D. G. Goodwin, H. K. Moffat, and R. L. Speth, *Cantera: An object-oriented software toolkit for chemical kinetics, thermodynamics, and transport processes,* `http://www.cantera.org` (2017), version 2.3.0.

[48] G. P. Smith, D. M. Golden, M. Frenklach, N. W. Moriarty, B. Eiteneer, Goldenberg Mikhail, C. T. Bowman, R. K. Hanson, S. Song, W. C. Gardiner Jr, V. V. Lissianski, and Z. Qin, *GRI-Mech 3.0,* .

[49] S. Bragg, *Application of reaction rate theory to combustion chamber analysis,* Aeronautical Research council Pub **131**, 1629 (1953).

[50] A. T. Evulet, A. M. ELKady, A. R. Branda, and D. Chinn, *On the Performance and Operability of GE's Dry Low NOx Combustors utilizing Exhaust Gas Recirculation for PostCombustion Carbon Capture,* Energy Procedia **1**, 3809 (2009).

[51] J. R. Maughan, A. Luts, and P. J. Bautista, *A Dry Low NOx Combustor for the MS3002 Regenerative Gas Turbine,* in *Volume 3: Coal, Biomass and Alternative Fuels; Combustion and Fuels; Oil and Gas Applications; Cycle Innovations* (ASME, 1994) p. V003T06A010.

[52] M. Ditaranto, H. Li, and T. Løvås, *Concept of hydrogen fired gas turbine cycle with exhaust gas recirculation: Assessment of combustion and emissions performance,* International Journal of Greenhouse Gas Control **37**, 377 (2015).

[53] L. Prandtl, *Bemerkungen über die Entstehung der Turbulenz,* ZAMM - Zeitschrift für Angewandte Mathematik und Mechanik **1**, 431 (1921).

[54] J. Hunt, *Mathematical Models of Turbulence. By B. E. L AUNDER and D. B. S PALDING . Academic Press, 1972. 169 pp. £2.50 or $7.50,* Journal of Fluid Mechanics **57**, 826 (1973).